ABSTRACT

YANG, CHEN. Preform Design for Forging and Tube Hydroforming Processes. (Under the direction of Dr. Gracious Ngaile.)

In the metal forming process, preforming is widely used to deform the work piece into a suitable shape that can form the required product successfully without forming defects and excessive waste of material in the final process. A proper preforming stage can improve the product quality, reduce forming stages and minimize manufacturing cost. Preform design problems are encountered in various metal forming processes. However, this research focuses on the preforming problems in the forging process and Tube Hydroforming process.

Preform Design in Forging Process: Preform design is critical for multi-stage forging processes to ensure the production of defect-free parts. Moreover due to the geometry and material flow complexities in forging processes, finding the optimal preform shapes could be difficult and time consuming.

An efficient design methodology based on geometrical resemblance is proposed for the preform design in forging process. The premise of this methodology is such that the initial and subsequent simulations are carried out by constructing a slightly larger part which geometrically resembles the desired part. Initial FEA simulation of the larger part is performed with reasonably guessed preform shape which may allow the occurrence of forming defects or flash formation. Then a series of intermediate resembling parts between the largest part and the desired part are constructed. The undeformed shape corresponding to the intermediate part could be obtained by backward tracing of material flow from the simulation results of the larger part. This undeformed shape is then taken as the preform shape of the intermediate part. The procedure is repeated until the intermediate part is geometrically close to the desired part, which leads to the preform shape. In order to verify this preform design methodology, several case studies on

forging and extrusion processes have been carried out. The methodology has been proven to be computationally efficient since it requires fewer numbers of iterations.

Preform Design in Tube Hydroforming Processes: In the last decade, the tube hydroforming process has received increased attention in the automotive and aerospace industries owing to its advantages such as part consolidation, weight reduction, and better part quality over stamped and welded assemblies. However, an incoming straight tube may need to be preformed due to the shape complexity of the tubular part and material flow limitation. One such preforming process, axial crushing, is used to accumulate the material in the die cavity by forming axisymmetric wrinkles on the tube. However, the knowledge of how to axially crush the tube in the tube hydroforming process is still limited.

In this research, a two-stage preforming process based on the wrinkle formation is developed for the Tube Hydroforming process to accumulate material in the forming zone so that the thinning rate can be reduced and formability can be improved. In preforming stage one, the wrinkle onset is triggered with limited axial compression. In preforming stage two, the wrinkle grows stably and uniformly to a certain height. Then the preformed wrinkles are flattened to conform to the die shape in the final tube hydroforming process. An analytical model based on the bifurcation analysis and post-buckling analysis of the elastic-plastic circular cylinder under internal pressure and axial compression is used to study wrinkle evolution characteristics. The analytical results offer guidance to the process design of the two-stage preforming process. To validate this methodology, preform die sets for three axisymmetric parts were designed and tube bulging experiments were carried out on SS 304 tubing and Al 6061 tubing. Through this methodology, expansion rates of the bulging process are significantly improved.

Preform Design for Forging and Tube Hydroforming Processes

by
Chen Yang

A dissertation submitted to the Graduate Faculty of
North Carolina State University
in partial fulfillment of the
requirements for the degree of
Doctor of Philosophy

Mechanical Engineering

Raleigh, North Carolina

2011

APPROVED BY:

_____	_____
Dr. Gracious Ngaile Committee Chair	Dr. Gregory Buckner
_____	_____
Dr. Jeffrey W. Eischen	Dr. Tiegang Fang

DEDICATION

Dedicated to

my wife Hua

for her endless love, encouraging and understanding

to my daughter Xu

for bringing me smiles and joys

to my parent

for unconditional support.

BIOGRAPHY

Chen Yang was born in Changzhou, Jiangsu province of China in 1976. He graduated from Wujin high school in 1995. Then he received Bachelor degree in the Mechanical & Electrical Engineering from Nanchang Institute of Aeronautic Technology in 1999. After completing his undergraduate degree, he joined the graduate school of Nanjing University of Aeronautics and Astronautics and received Master degree in the Aerospace Manufacturing Engineering in 2003. From 2003 to 2006, he worked as a mechanical engineer in the 14^{th} Institute of China Electronics Technology Group Corporation. In 2007, he was a visiting scholar in North Carolina State University, where he conducted researches on Tube Hydroforming Process. In the spring of 2008, he joined Mechanical Engineering program of North Carolina State University to pursue PhD degree. Since then, he has been working on the researches on metal forming process with focus on preform design for forging and tube hydroforming processes.

ACKNOWLEDGMENTS

First and foremost, I would like to thank my advisor, Dr. Gracious Ngaile for his patent guidance, enthusiastic encouragement and generous support throughout my study and research at NC State University. Especially, his insight into the research and his insistence of pursuing excellence in my research work has influenced me greatly, and surely my future academic career will benefit much from that.

I would like to thank my committee members, Dr. Gregory D. Buckner, Dr. Jeffrey W. Eischen, and Dr. Tiegang Fang for their generous help and suggestions in completing this work. I would also like to express my appreciation to Dr. Jingyan Dong for accepting to be the graduate representative for both my PhD oral exams and final defense.

I would like to acknowledge the National Science Foundation, through which this work was funded under Project No. DMI-0448885. Any opinions, findings, and conclusions or recommendations expressed in this material are those of the author and do not necessarily reflect the views of the National Science Foundation

I would like to express my appreciation to all my colleagues in the Advanced Metal Forming & Tribology Lab, especially Angshuman Ghosh, for providing me help in the researches and experiments.

Last but not the least, my gratitude goes to my family for their endless love and continuous encouragement. I wouldn't have been what I am without you all.

TABLE OF CONTENTS

PHASE I: PREFORM DESIGN IN FORGING PROCESS

LIST OF FIGURES

LIST OF TABLES

LIST OF SYMBOLS

$\bar{\sigma}$, σ_e : effective stress

$\bar{\varepsilon}$, ε_e : effective strain

P_i (i=a, b, c, d……): preform shape of billet

X_i (i= a, b, c, d……) : deformed shape of the billet

L_s: longitudinal span of the tube hydroforming die cavity

R, t, L: tube radius, tube thickness and tube length

E: Young's modulus

V: Poisson ratio

σ_y: yielding stress

n*: plastic hardening parameter

K: strength coefficient

n: strain hardening exponent

σ_c: critical axial stress of wrinkle onset

ε_c: critical strain

λ_c: half wave length of wrinkle onset

Δ : axial compression rate

σ_x: axial stress,

ε_x: axial strain

σ_θ : hoop stress

N_x: axial stress resultant

N_θ: hoop stress resultant

C_{ij} (i,j=1,2): constitutive matrix element

W_0: imperfection factor

$\bar{w}$: geometrical imperfection

W: radial displacement

H_b : wrinkle height

p, p_1,p_2 : internal pressure

f_1, f_2 : axial feeding

ER: expansion rate

TR: thinning rate

N: wrinkle number

CHAPTER 1: INTRODUCTION

1.1 Introduction

Metal forming is a manufacturing process in which the shape of the desired part is obtained through the plastic deformation from an initial work piece of simple shape. The processes involved with the metal forming include rolling, forging, extrusion, drawing, sheet metal forming, tube hydroforming etc. During the metal forming process, the work piece experiences severe plastic deformation under the action of the tools and very less or no material is removed. The parts made from the metal forming process commonly have better mechanical properties than parts made from casting or machining due to the change in properties caused by severe plastic deformation.

1.2 Problem statement

In the metal forming process, material flow pattern can be affected by a number of process variables such as: geometrical complexity, friction conditions, temperature distributions, stress/strain, velocity gradient and material properties. Improper material flow pattern can result in forming defects. Therefore, the forming sequence needs to be carefully designed. Material flow characteristics and the associated forming defects will be highlighted in the next section for forging, extrusion and tube hydroforming.

Material flow in forging process. During the forging process, the material flow will take a path of least resistance. It is critical that die and preform shapes are designed in such a way that they create material flow paths which do not result in defective part. The common defects associated with material flow are under fill, lap/folding and piping.

Normally, under fill is caused by insufficient starting mass, poor lubrication or improper material fill patterns. Fig.1-1.b, c and d show the formation of the under-fill defect due to improper material flow pattern. When a billet is deformed by the finisher die without preforming, the upsetting-type material flow where material velocity is in the lateral direction is dominant under the compression stress σ_n and friction stress τ_f of the dies. Under this scenario, once the lateral material flow hits the die corner, the material flow is split into two, one becomes extrusion-type material flow which has a velocity field V_1 toward the rib top, and another keeps the original direction and has a velocity field V_2. Because of the excessive amount of material flow in the lateral direction, considerable amount of flash is formed, while insufficient material fill in the rib part results in the under-fill defect as shown in Fig.1-1d. The ideal flow pattern for avoiding under fill is the dominant extrusion-type material flow in the rib region, which can be realized by introducing a preformed billet shape (Fig.1-1e) to promote the material flow in the rib region and reduce the lateral material flow (Fig.1-1.f).

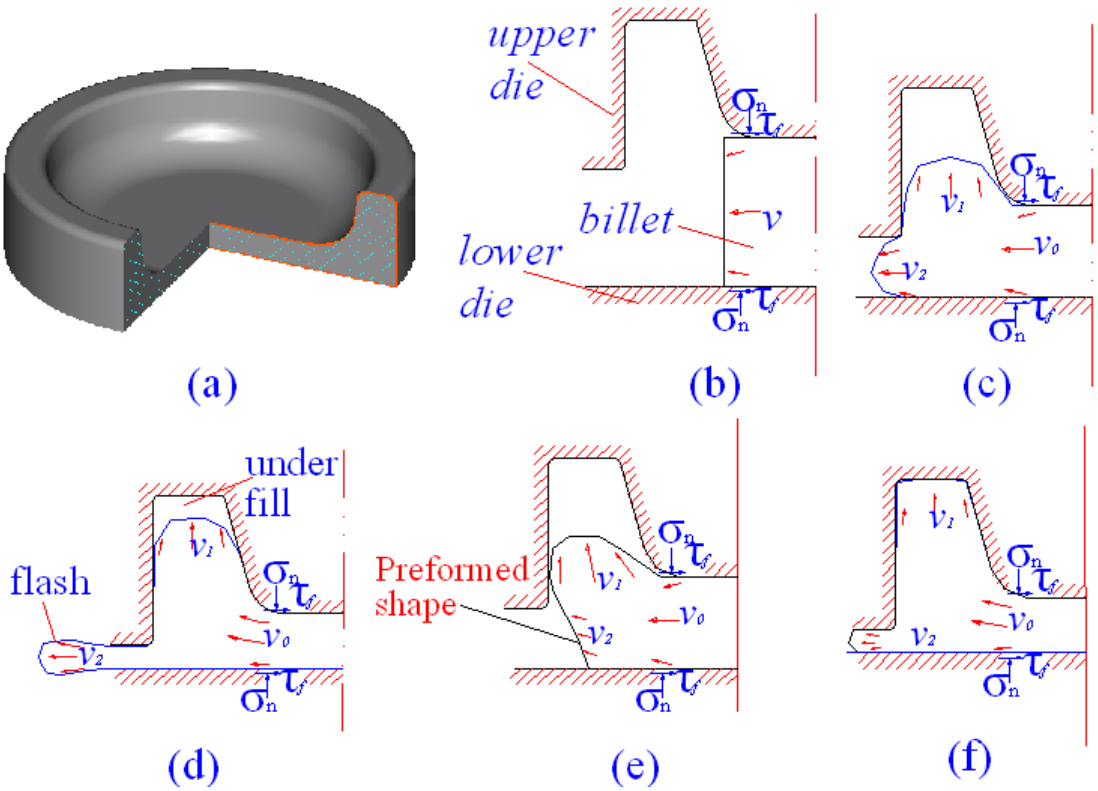

Fig.1- 1 Under fill in forging process and preform

Lap is material folding over a metal surface and is not metallurgically bonded together due to an oxide layer. Lap defects are usually formed due to improper progression of material flow in the die cavity. Fig.1-2 a,b shows a typical process of the lap formation. Due to the filling velocity gradient from the left side to the right side of the die cavity, the left side of the die cavity accumulates more material. Therefore, the left-side material hits the top of the cavity first and then bounces backwards to form a material flow (V_2) reversal to the right filling material (V_1). Because of the reversal material movement, material is folding over the metal surface and forms the lap as shown in Fig.1-2.b. The ideal material flow pattern for avoiding the lap formation is the proper progression of the material fill in the die cavity as shown in the Fig.1-2.c, which can be realized by a good preformed shape (Fig.1-2.c) or more generous die corner radius R (Fig.1-2d).

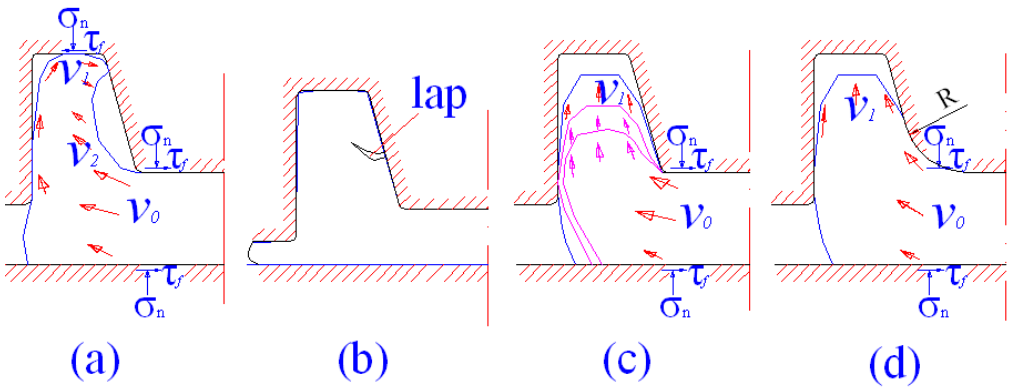

Fig.1- 2 Folding defect

In the forging of the web-rib (Fig.1-3a) part, the piping defect is also associated with the material flow pattern. When the upper die moves downwards, the material on the web region is compressed and flows into the rib region, which forms an extrusion-type material flow. During the advancing, both sides of the material flow are subject to the contact pressure σ_n and friction stress τ_f, resulting in a center-to-surface velocity gradient (V_0 to V_1 in Fig.1-3b) which draws more material from the web center to form a dimple on the opposite face. The piping defect can be eliminated by increasing the web thickness t or changing the aspect ratio (H/B). If both methods could not be done, a preformed protrusion shown in Fig.1-3.c can be used to counteract the extra material fill amount near the center.

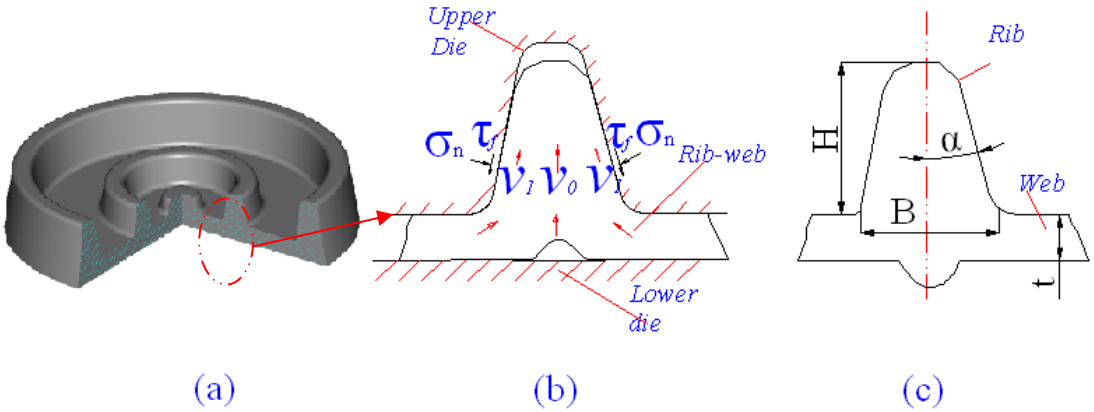

Fig.1- 3 Piping defect in the rib-web part forging

Other than the material flow associated defects, fracture may occur when the material experiences high effective strain and work hardening conditions. Under this circumstance, annealing is needed to remove the work hardening.

Material flow in extrusion process. In the extrusion process, the billet is pushed by the ram to pass through a die opening to realize section changing (Fig.1-4.a). When the material flows through the die opening, a dead zone of stagnant material flow will build up at the die corner due to friction force from the die. The dead zone acts as a rigid die surface and the material undergoes shear deformation along the interface of the dead zone. The size of the dead zone can be affected by the temperature gradient, punch speed, friction condition and extrusion ratio. Fig.1-4.b,c,d show three different material flow patterns at different friction conditions and temperature gradient. An ideal pattern without dead zone (Fig.1-4 b) can be observed with frictionless conditions at the container and die. The material properties of the extruded part are uniform in the longitudinal direction and transverse direction. When friction force is presented on the die and container surface, flow pattern with dead zone (Fig.1-4 c) can be found near the die surface. The material near the dead zone surface moves diagonally to the exit at slower velocity than the material at the center, forming the outer shell of the extruded part. This flow pattern can result in non-uniform material properties on the extruded part.

When the temperature gradient or inhomogeneous material properties is presented on the billet from center to surface, a flow pattern with more severe shear deformation and extended dead zone will develop as shown in Fig.1-4.d. This flow pattern will result in unacceptable gradient of the material properties on the extruded part. Normally, extra preforming stage or heat treatment is required to overcome these forming defects.

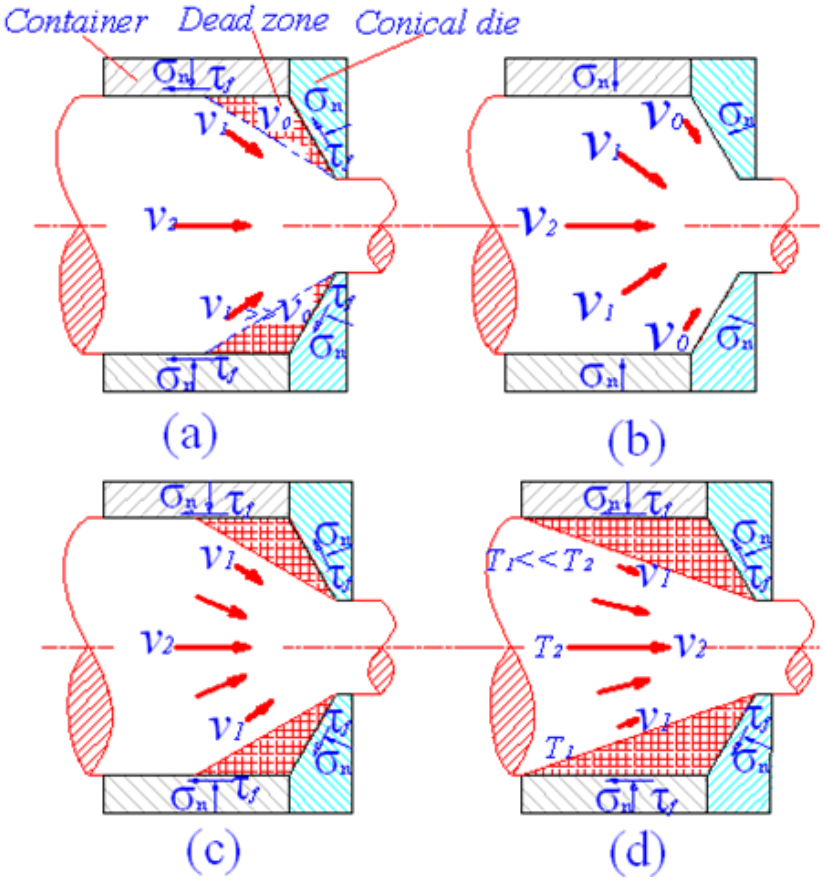

Fig.1- 4 Three types of flow patterns in the extrusion process

Material flow in the tube hydroforming process. Tube Hydroforming (THF) is the metal forming process that uses a pressurized fluid in place of a hard tooling to plastically deform a tube into a desired part, which offers advantages such as: part consolidation, weight reduction, fewer secondary operations, and improved structural strength and

stiffness over parts made by conventional stamping-weld technology. In the THF process, accurate material feed and internal pressure profile known as loading path is critical to avoid forming defects, such as buckling and fracture.

During the expansion of the tube, the material is subject to severe interface friction (Fig.1-5.b) due to high internal pressure. The interface friction hinders material from flowing into the die cavity and reduces the uniformness of the thinning distribution. When material is pushed to die cavity under internal pressure, the tube is subject to biaxial-tensile stress, which tends to make the tube thin out and burst. If the tube has axial compressive stress and circumferential tensile stress (Fig.1-5.c), the thinning due to hoop tensile stress can be compensated by axial compression deformation and higher expansion can be achieved.

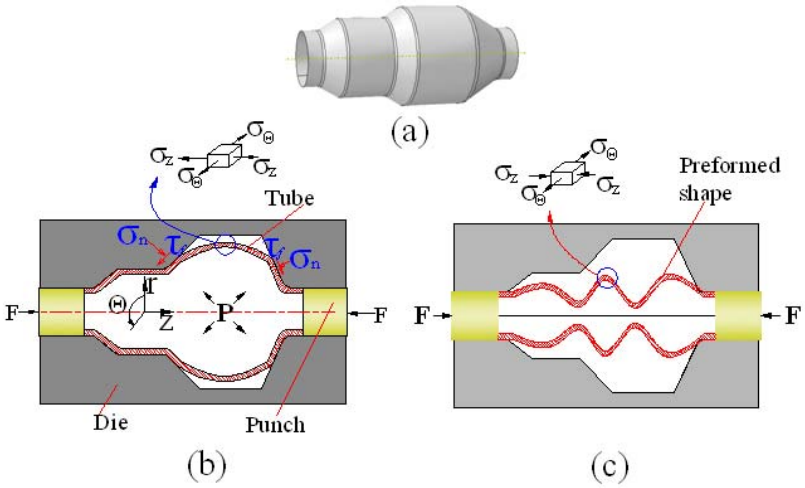

Fig.1- 5 THF process and preform

Depending on the shape complexity and formability of the material, the incoming straight tube may need to be preformed, such as pre-bending, crushing prior to the final Tube Hydroforming process. The pre-bending process is mostly used to bend the straight tube to fit the THF die cavity. For low formability materials, preforming by crushing is

often used to deform the tubes in such a way that a certain amount of material can be accumulated in the large expansion zone of the final THF process to avoid excessive thinning and bursting. However, how to preform the tube to accumulate material in the forming zone is still a very challenging task.

From the above discussions, the forming defects associated with material flow and it's possible solutions are identified in three metal forming processes. They are summarized and listed in the Tab.1-1 below.

Tab.1- 1 Forming problem and solution in the metal forming processes

	Forming problems	Metal forming process	Solutions
1	Under fill	Forging	Proper material fill sequence Or preform shape design
2	Laps	Forging	Proper progression of material flow or preform shape design
3	Piping	Forging	Optimization of the rib parameter or add preforming step
4	Fracture/Excessive work hardening	Forging	Heat treatment
5	Dead zone	Extrusion	Minimize the friction or reduce the temperature gradient
6	Inhomogeneous material properties	Extrusion	Minimize the friction or reduce the temperature gradient
7	Severe friction condition	Tube Hydroforming	Developing better lubricant
8	Thinning/Fracture	Tube Hydroforming	Proper preforming design
9	Buckling/Bursting	Tube Hydroforming	Proper loading path design

1.3 Research objectives

The main goal of this research is to develop a preform design methodology or preforming process to avoid the forming defects associated with the material flow and improve the formability of the forging and tube hydroforming processes.

The specific objectives pertaining to forging are:

a) Develop a preforming design methodology for the forging and extrusion processes
b) Verify the developed method by carrying out the FEA simulations for several cases.
c) Verify the developed method experimentally.

The specific objectives pertaining to tube hydroforming are

a) Model wrinkle formation in the Tube Hydroforming process
b) Develop preform design methodology for THF based on wrinkle generation
c) Study the effects of process variables on formability for THF with wrinkle based preforming.
d) Verify the wrinkle based preform design methodology experimentally.

CHAPTER 2: LITERATURE REVIEW

2.1 Preform design for forging process

2.1.1 Forging process and operations

Various forging parts usually have complex geometrical shapes which need intermediate passes to forge a sound part due to material flow limitation. In a common multistage process, a set of blocking dies are used to sequentially preform the initial billet into a proper shape suitable for the finisher forging. If the material of the billet could not be distributed properly in the blocking stage, forming defects such as under fill, laps and folding would occur in the final forging stage.

Normally, the forging-sequence design is carried out in a backward direction (Fig.2-1), which starts with the finished-part geometry and ends up with the preform shape design, die design and process parameters determination. During each phase of the process design, all the physics involved in the metal forming process such as plastic deformation, heat transfer, lubricant& interface friction, and microstructure evolutions need to be fully considered to determine the preform shape, forging equipment and die configuration. The overall design of the forging process requires (1) prediction of the preforming numbers (2) determination of the preform shape (3) determination and optimization of the process parameters of each stage.

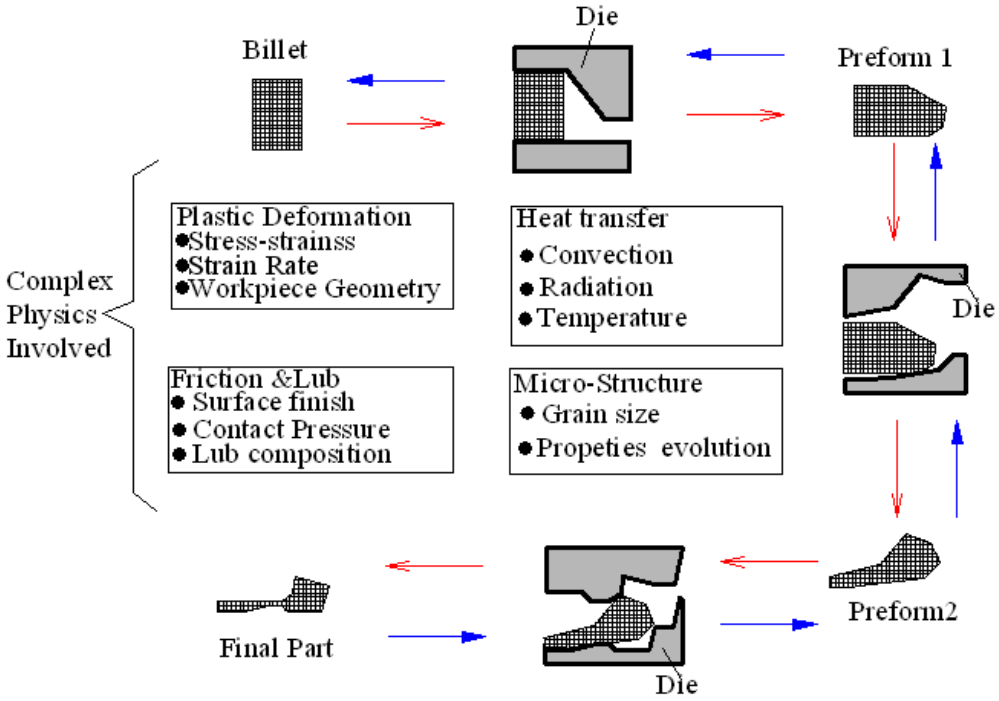

Fig.2- 1 Complex physics and forming sequence of the forging process

2.1.2 Preform design and optimization

In the forging industry, design of die performs has heavily relied on tryout, accumulated experience, and skill of the process designers. In the last few decades, expert-systems [1–14] based preform design methods have been developed in metal forming process to facilitate the forging process design. Most expert systems developed for determining forging sequences for cold- and hot-forged parts make use of rules and/or known progression sequences that can be retrieved from a database. For example, Kim and Im [5] developed an expert system that can produce the basic process design depending on the initial billet size, the material, or the order of upsetting and forwards extrusion. This system was also capable of process redesign based on either reduction of number of sequences by combining two stages into one, or reduction of deviations of the

distribution and the level of the required forging load by controlling the forming ratios. Bakhshi-Jooybari et al. [14] proposed an intelligent knowledge-based system for designing dies and forging processes, whereby the system compares new forging parts with those it had encountered previously. The comparison was based on weighting effects of process and geometrical parameters that significantly influence the success of the forging.

Owing to a multitude of variables involved in a forging operation, there may exist different forging sequences to produce a sound part. This may involve changing parameters such as the initial diameter of the billet or the intermediate forging progression steps, e.g. upsetting, forwards extrusion, or backwards extrusion. Kim and Im [11] proposed a search method to determine an optimal process sequence using the controlled variables of global effective strain and required forging load at each stage. In this expert system, the search was carried out after a tree of possible process sequences was established.

Because the expert systems are rule-based and use plasticity theories, empirical formulae, approximate load calculations, etc. an optimal forging sequence that will lead to a sound part may be hard to obtain, particularly if the forged part is complicated. For this situation, expert systems have widely been used to provide initial progression sequences of forging, which are later refined to ensure good material flow, complete die fill, and that other part defects associated with material flow are eliminated. Several researchers have incorporated finite element analysis (FEA) in expert systems as a verification tool for the established forging sequences [3, 4].

Much effort has been directed towards direct use of FEA in determining forging sequences, particularly for parts that require few progression sequences. Park et al. proposed a backwards tracing method in preform design of shell nosing [15]. In 1989, Kobayashi et al. systematically developed the backwards tracing method for preform

design in forging processes based on rigid visco-plastic finite element methods [16]. The preform shape can be computed by detaching boundary nodes from the die contact in an assumed sequence or based on some criterion. The method was successfully applied to the preform design of an axisymmetrical H-shaped forged part [17]. However, the validity of backwards tracing highly depends on the node-detach criteria for the deformation path. Zhao et al. [18, 19] proposed two detach criteria based on contact history and shape complexity. The detach criteria were, however, limited to specific forging parts. Chang and Bramley [20] proposed a methodology for detaching contact areas from the die surface by combining the upper-bound method with the finite-element (FE) procedure. The premise of this detach criterion was that during forwards simulation, the contact areas between work piece and dies increase along the cavities. This contacting sequence can thus be inverted in reverse simulation, i.e. nodes are detached along cavities from the deepest area. Although this method was successfully employed on a plane-strain problem, it was difficult to obtain smooth boundary shape via the FE procedures.

Researchers have attempted to optimize forging preforms by using sensitivity analysis. The objective function in the sensitivity analysis is to minimize under-fill, eliminate barreling, or decrease the deviation of the state variables, whereas the design variables are coordinates of the control points of shape edges. Badrinarayanan and Zabaras developed a sensitivity analysis for large deformation of hyper-elastic visco-plastic solids for optimization of extrusion die shape to achieve a more uniform distribution of the state variables on the extruded part [21]. Fourment and Chenot suggested a shape optimization method for the initial shape of the billet as well as the shape of preform die of a two-step forging operation [22]. Zhao et al. optimized the die preform shape to minimize the difference between actual forging shape and the desired final forging shape, based on sensitivity analysis [23]. Srikanth and Zabaras optimized the shape of the initial billet to minimize the barreling in open die forging by sensitivity analysis for the single-stage

problem [24]. Zabaras et al. developed a sensitivity method to optimize the die preform shape for multi-stage metal-forming processes [25]. Vieilledent and Fourment proposed that folding defects could be avoided by minimizing the sum of the effective strain rates on the surface of the work piece [26]. Castro et al. adopted the direct differentiation method to obtain sensitivity information in preform optimization design of a two-step forging process [27].

Preform optimization based on sensitivity analysis is an efficient algorithm to find a optimal preform shape, but it requires gradient information of the objective function with respect to the design variables. Depending on the complexity of the problem, obtaining gradient information may be difficult and several non-gradient-based preform optimizations have been proposed to avoid using gradient information. Castro et al. adopted a genetic algorithm to eliminate the barreling in the hot-forging process [28]. Thiyagarajan and Grandhi proposed an optimization algorithm for a three-dimensional (3D) preform shape design based on the response surface method, in which the preform shape was treated as a linear combination of various billet shapes called basis shapes, where the weights for each basis shape were used as design variables [29]. Hong et al. suggested an iterative preform design method to reduce flash formation and forging load. The optimal preform shape was found by iteratively mapping the shape of the formed flash of reduced size to the initial billet shape [30].

Due to various combinations of the forging processes and complexity of the plastic deformation, most preform design methods are specifically limited to certain processes and the prediction of the preforming number and obtaining of the preform shape is still a difficult and time-consuming task during the forging process design, which needs further research efforts to advance the design methodology.

2.2 Preforming for tube hydroforming process

2.2.1 Tube hydroforming system

In recent years, the tube hydro-forming (THF) process has received increased attention in the automotive and aerospace industries owing to its numerous advantages over stamped and welded assemblies. The advantages of THF include part consolidation, weight reduction, higher part quality, fewer secondary operations, reduced dimensional variations, and improved structural strength and stiffness. However, this process has also some drawbacks, such as slow cycle time, expensive equipment and lack of extensive knowledge base for process and tool design, which leads to appearance of defects in the hydro-formed part [34].

A typical Hydroforming process is the T-shape joint forming processes as shown in Fig.2-2. Firstly, a straight tube is properly positioned in the die which has the same shape as the desired part (Fig.2-2.a). Then the die is closed by the ram of the press and the axial cylinder drives the punch to contact the tube end tightly without leakage (Fig.2-2.b). After die closing and complete sealing, the forming oil is pumped into the tube cavity and pressurized, while the axial punch compresses the tube axially and the counter punch retracts gradually to support the protrusion part (Fig.2-2.c). Finally, the formed T-shape is rejected after die opened and axial punch retracted (Fig.2-2.d).

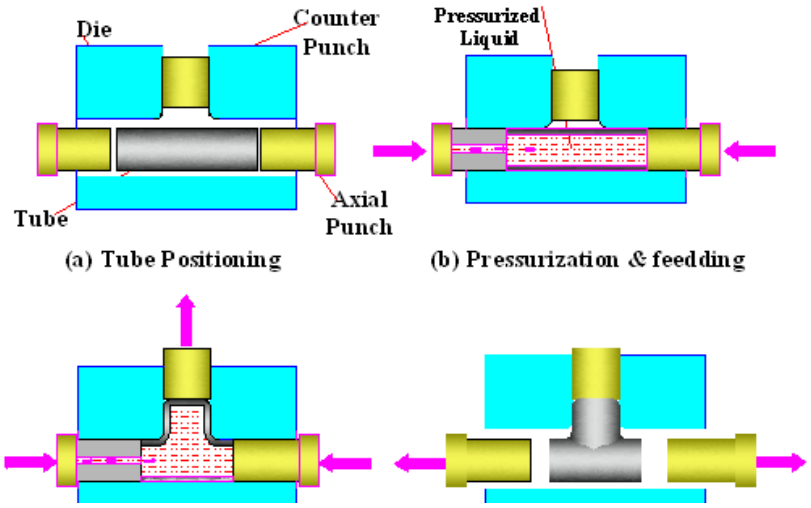

Fig.2- 2 Typical tube hydroforming process

Depending on the shape complexity of the tubular part and formability of the tubular material, the incoming straight tube may need to be preformed, such as pre-bending, crushing. The pre-bending process is mostly used to bend the straight tube to curved longitudinal configuration to fit the final THF die cavity, which significantly deviates from the straight tube. Tube crushing is used to deform the tube in advance to avoid collision with the die during die closing, or to accumulate materials in the forming zone, if the part has cross section of complex shape or big expansion rate. Besides the careful determination of the process sequence, process variables such as loading path, friction condition and material properties play a critical role in the process design of the THF process. The influence of these process variables will be briefly discussed next.

The most concerned process variable in THF is the proper matching of the hydro-forming pressure with axial feeding. Tube failure is evident when excessive axial feeding results in wrinkling, whereas too much internal pressure leads to tube bursting. In the last decade, a number of algorithms such as sensitivity analysis, response surface technology **[35-36]**, and adaptive methods **[37-39]** have been proposed for loading path

development to avoid the forming failure.

The quality and properties of the tubular material can highly affect the THF process. Fuchizawa **[40-41]** investigated the effect of the strain-hardening exponent and plastic anisotropy on the THF process. The study showed that more uniform thickness distribution, greater expansion, and less hydro-forming pressure can be achieved by increasing the strain-hardening exponent while the plastic anisotropy can affect internal pressure requirement or the maximum expansion of the tube. Thus the material properties (elasticity modulus, yield stress, ultimate tensile strength, ductility, and anisotropy) should be determined carefully for THF process to form the part with desired quality. Currently, the tubular bulge test has been widely used to determine the properties of tubular materials due to the similar stress conditions with the actual THF process and greater effective strain achieved **[42]**.

The friction control and lubrication play a key role in the THF process, because the friction can highly influence the thinning distribution, surface integrity, forming load, and tool wearing. In the THF process, the actual friction coefficient is a function of contact pressure, sliding velocity, sliding distance, material properties and surface roughness of the surfaces in contact. During the THF process, the friction condition changes due to variation of the actual tribological variables mentioned above. Thus, the friction coefficient is not constant with respect to the process time. Depending on the different deformation mechanism, three friction zones are identified in THF: guiding zone, transition zone and expansion zone. Accordingly, experimental tests **[43-44]** have been developed to mimic the friction characteristics in the respective zones to evaluate the lubricant performance in the THF process.

The influence of the process variables on the tube Hydroforming are briefly reviewed above and the major issues need to be considered in the tube Hydroforming process design is summarized as:

a) Tube Material properties and quality
b) Pre-forming design (bending, crushing) and post- forming (punching, trimming) operations
c) Loading path determination and optimization
d) Design of dies and tools
e) Friction condition evaluation and lubricant development

2.2.2 Preforming for tube hydroforming process

During the hydro-forming of a long tubular part of complex cross section, the axial feeding provides limited material flows and the pure expansion occurs at some middle part of the tube due to the geometrical constrain or friction conditions. In this case, the crushing operations are used to deform the tubes in advance and accumulate a certain amount of material in the large expansion zone of the final THF process to avoid excessive thinning. There are two types of crushing operations, one is crushing the larger-diameter tube in the radial direction to accumulate material, and another is crushing the tube in the axial direction to accumulate the material.

2.2.2.1 Preforming by crushing tube in the radial direction.

Normally, a radial crushing operation is needed to deform a big tube (Fig.2-3.b), having close circumferential length with the final part, to a preformed shape to fit the final THF die, if the tubular part has a complicated cross section shape with the aspect ratio significantly deviating from the round shape (Fig.2-3.c). Sometimes, a lower internal pressure is applied in the radial crushing operation to avoid folding or excessive hoop wrinkle. If the tubular part is directly hydro-formed with a small tube (Fig.2-3.a), the expansion rate is too high and tube will burst during the direct hydroforming. Actually, the radial crushing operation can reserve significant amount of material in the forming zone of the final THF process to avoid bursting. Sometimes, the radial crushing is just

used to deform a tube to a shape to fit the final THF die and avoid the pinching (Fig.2-4) of the tube during the die closing. In some cases, the radial crushing and final THF are fused into a single process to reduce the process stage and save production cost. Next, two cases of the radial crushing will be illustrated.

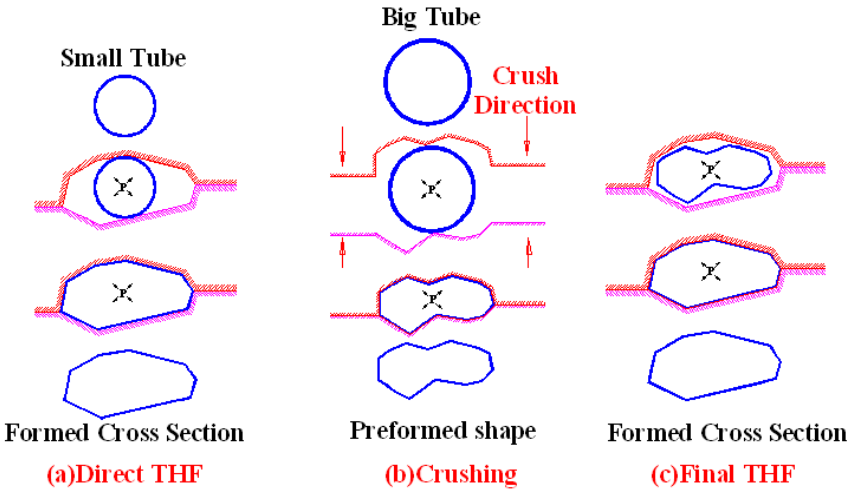

Fig.2- 3 Radial crushing operation for the cross section Hydroforming

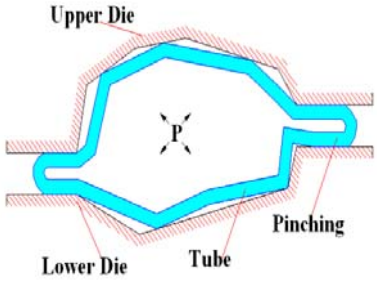

Fig.2- 4 Pinching of the tube during die closing

Hwang et al,. **[45]** hydroformed a large-size tube into square-cross section in a process fusion of the crushing and THF process (Fig.2-5). He found that thickness the distribution of the part formed by process fusion is much better than that of the direct

expansion, whereas the internal pressure and crushing force are significantly less than that of direct expansion.

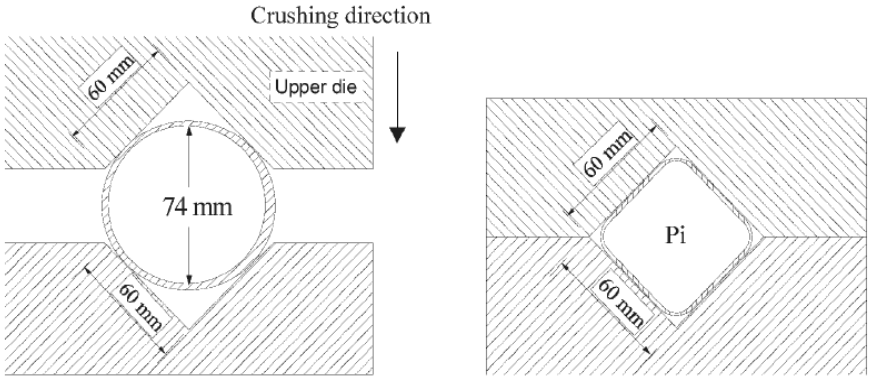

Fig.2- 5 Process fusion of the crushing and THF to form the square cross section.**[45]**

A lower arm of the suspension component is hydro-formed to substitute the traditional stamp-weld part by combined processes of the prebending, crushing and THF **[46].** Due to the limited material flow in the middle part of the lower arm, a larger-diameter tube ,which is bigger than the minimum cross section of the lower arm, is initially prebent to fit the die(Fig.2-6.a), then it is radially crushed to reduce the cross section size(Fig.2-6.b) and finally Hydro-formed by higher pressure and axial feeding (Fig.2-6.c).

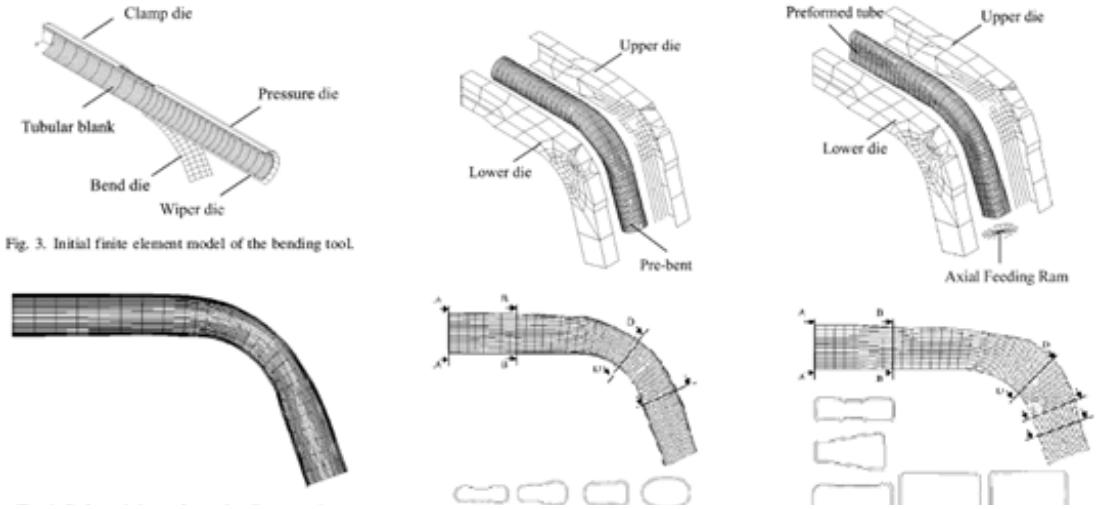

Fig.2- 6 Multip-stage tube hydroforming process **[46]**

2.2.2.2 Preforming by crushing tube in the axial direction.

Besides the radial crushing, the longitudinal crushing is also an effective measure to accumulate the material in the form of axisymmetric wrinkle formation (Fig.2-7) in the forming zone. Normally, the wrinkle formation due to the excessive axial feeding should be avoided during the hydro-forming process and the forming window without wrinkle is the zone ABCDE as shown in Fig.2-7.c. However, if the wrinkle formed during the process can be flattened by the higher pressure at the end of the process, the forming window ABCDE can be expanded to AB'CDE and the formability of the THF process can be improved.

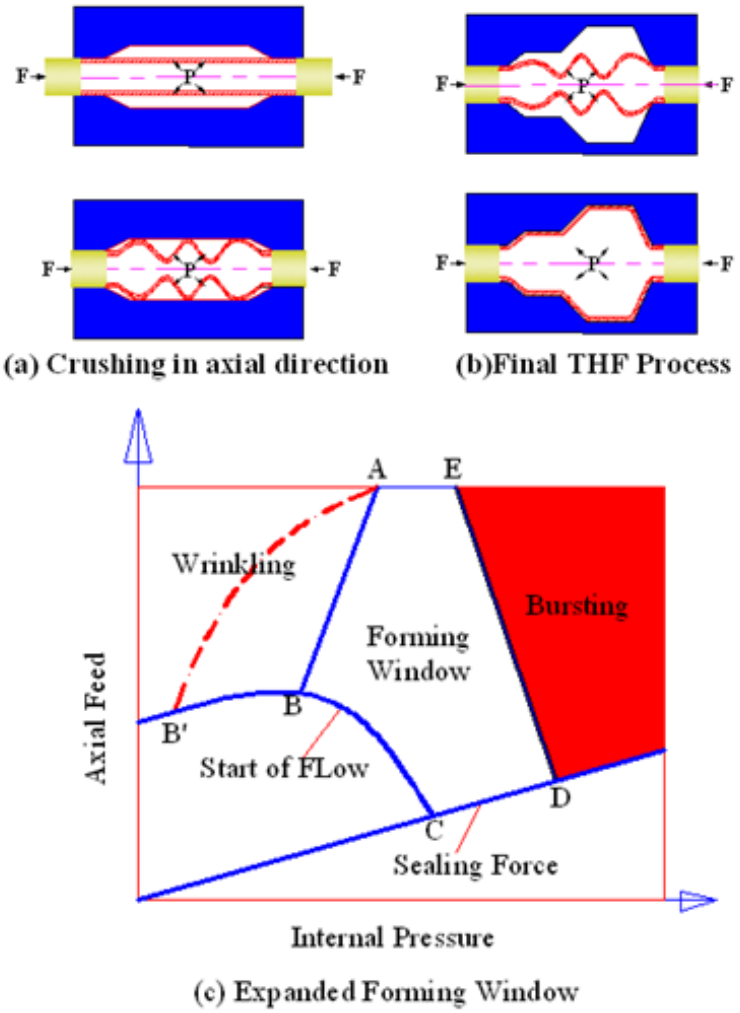

Fig.2- 7 Axial crushing and expanded forming window

In the conventional tube hydroforming process, the wrinkle is considered as failure and should be avoided. Therefore, most researches are working to develop accurate loading path to avoid wrinkle and bursting. But the research on how to use the wrinkle formation to expand the forming window is still limited. Yuan and his colleagues **[47-48]** initially investigated the effect of the wrinkle behavior in the tube bulging process and found that the wrinkle formed in the tube bulging process can be classified into three types, i.e. useful wrinkles, dead wrinkles and bursting wrinkles. The useful wrinkle can serve as material accumulation in the formation to increase the formability of the bulging process.

The expansion rate of the Aluminum-alloy A502 tube reached 34% (Fig.2-8) with useful wrinkles compared with 10% expansion rate of the bulging process without wrinkle. A method based on the geometrical condition **[48]** was developed to estimate the axial feeding amount and thinning rate for the bulging process with useful wrinkles. Lang et al., **[49]** investigated the influence of the die cavity shape of the preforming process on wrinkle development and found that the die of 25-degree taper angle is more favorable than the die of 45-degree tape angle to form useful wrinkles in the multiple stage bulging process. Wang et al.,**[50]**, hydro-formed an unsymmetric tubular part by using the useful wrinkles to accumulate material in the forming zone.

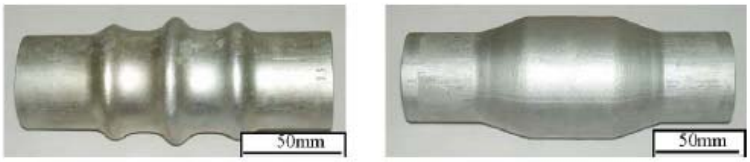

Fig.2- 8 The bulging process with useful wrinkle of Aluminum Alloy tube **[47]**

From the discussions above, the wrinkle formation can improve the formability of the THF process if the wrinkle is removable. The same observation is also found in the tube Hydroforming process with pressure pulsation. A loading path with pressure oscillation **[51]** was used to hydro-form a bugle-shape without bursting, while the one without pressure oscillation bursts (Fig.2-9). The mechanism of the formability improvement by the pressure pulsation is investigated by K. Mori and his colleagues,**[52]**. It was found that formability improvement due to oscillating pressure is associated with repeated small wrinkling (Fig.2-10) and the amplitude of the pressure oscillation has greater effects on the formability improvement than the frequency. Hama et al.,**[53],** simulated the hydro-forming process of the automotive component (Fig.2-11.a) with internal pressure oscillation (Fig.2-11.b). The simulation results agree well with the experiment

and shows that the lower friction coefficient roughly has the same effects as the pressure pulsation to improve the expansion on the automotive component. M.Loh-Mousavi et al.,**[54]**, simulated the Hydroforming process of the T-shape with pressure pulsation and the same result as that in **[20]** was found.

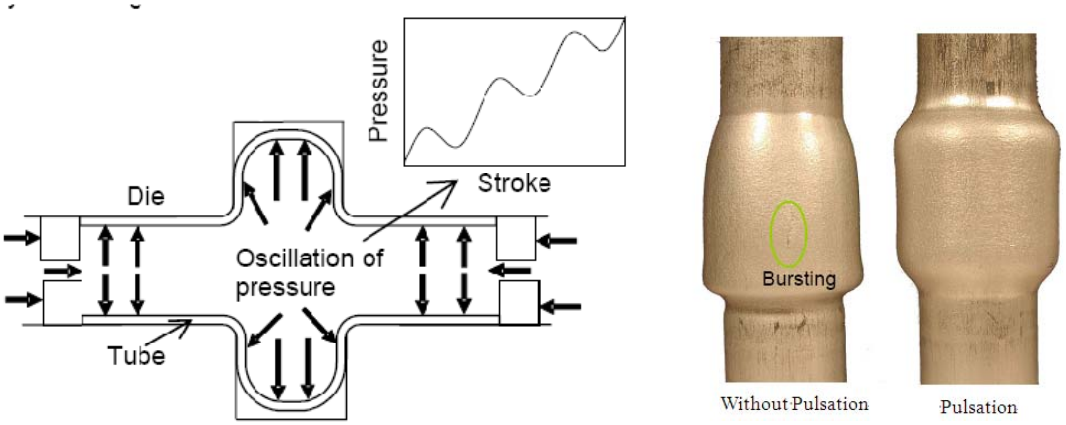

Fig.2- 9 Formability improvement of tubular part by pressure pulsating in THF**[51]**

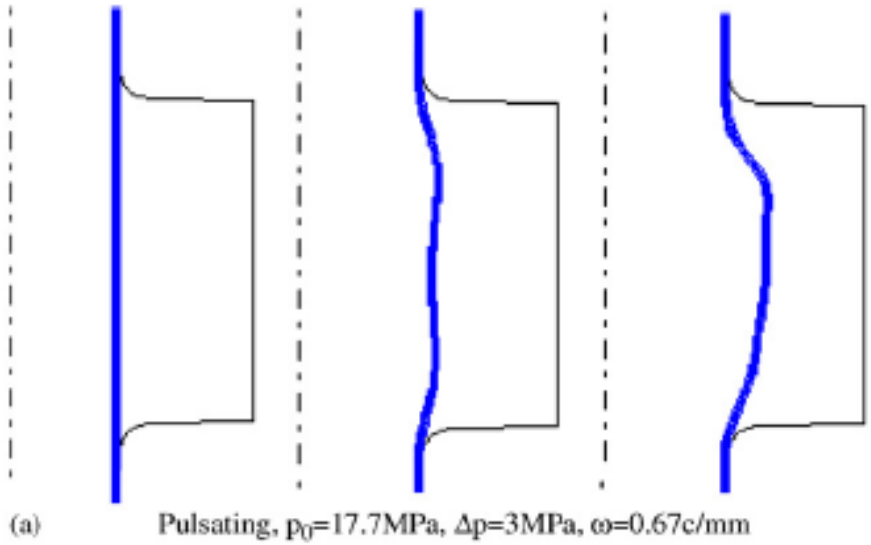

Fig.2- 10 Deformation process of the bulged tube with minor wrinkles **[52]**

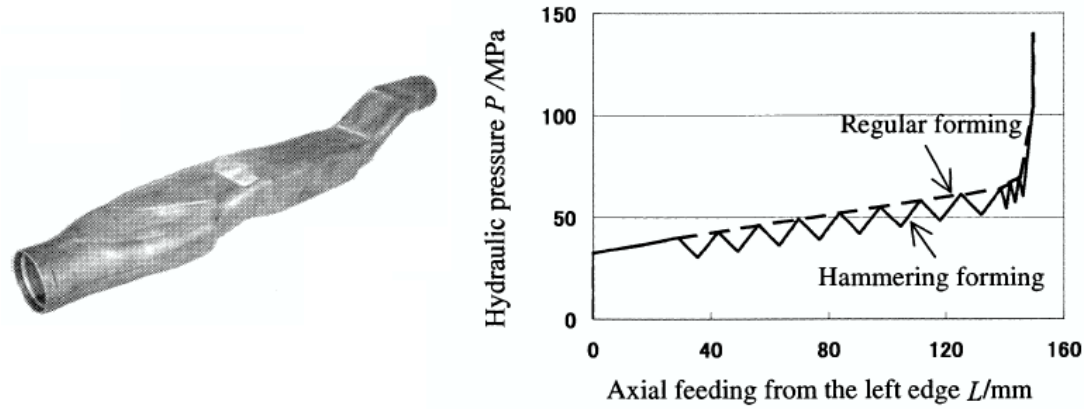

Fig.2- 11 (a) Automotive component (b) Loading path with pressure pulsation [53]

In summary, the removable wrinkle in the THF process can improve the formability of the tube. In general, two types of initial loading paths can be used to form wrinkles, one is the lower pressure with high axial feed, another is the pressure pulsation. Both types of loading paths end up with higher pressure to remove the wrinkle or calibrate the final shape. Yuan and his colleges initially used the wrinkle formation in the bulging process of Aluminum alloy tubes, and a method based on geometrical condition is developed to estimate the axial feed amount and average thinning rate of the bulged tube. However, how the wrinkle develops and how the process variables such as material properties, geometrical size and loading path affect the wrinkle characteristics are still not clear. These two issues are critical for the axial crushing operations and need further research efforts.

2.2.3 Wrinkle formation theory for tube under axial compression

As discussed previously, the formability improvement in the THF process can be achieved by the proper material accumulation in the forming zone by radial crushing or longitudinal crushing. The wrinkle formation characteristics in the longitudinal crushing of the tube can be affected by the loading path (internal pressure Vs axial feed), die geometrical shape, friction conditions and material properties. Thus it is important to

understand the plastic wrinkle evolution for the better design of the axial crushing process. In the last half century, a number of analytical models of plastic wrinkles have been developed to understand the wrinkle evolution characteristics in the structure design. Hills theory **[55]** of bifurcation analysis of elastic-plastic solids laid down the basis for the critical condition analysis of plastic wrinkle onset. The bifurcation analysis of the plastic wrinkle onset based on the "J2 deformation theory" **[56]** generally yields much better agreement with experiment than that of "J2 flow theory" **[57]**. Tvergaard **[58]** investigated the influence of various geometric and material parameters on the elastic-plastic wrinkle of cylindrical shells based on "J_2-flow", "J_2-deformation" and "J_2-corner" theories. He found that the general tendency is that "J_2 corner theory" predicts a buckling load higher than that of "J_2 deformation theory", but lower than that of "J_2 flow theory".

2.2.3.1 J2 deformation theory

It was commonly known that the relationship between the stress tensor (σ_{ij}) and deviatoric stress (S_{ij}) can be given by equation (2-1) **[62]**.

$$S_{ij} = \sigma_{ij} - \frac{1}{3}\sigma_{kk}\delta_{ij} \tag{2-1}$$

Three invariant J_1, J_2 and J_3 of the deviatoric stress S_{ij} can be expressed by the following equations.

$$\begin{aligned} J_1 &= S_{kk} = 0 \\ J_2 &= \frac{1}{2}S_{ij}S_{ij} = \frac{1}{2}(S_1^{\,2} + S_2^{\,2} + S_2^{\,2}) \\ J_3 &= \det|S| = \frac{1}{3}S_{ij}S_{jk}S_{ki} = S_1S_2S_3 \end{aligned} \tag{2-2}$$

Where S_1, S_2 and S_3 are principle stresses of deviatoric stress tensor S_{ij}. It was postulated by Von Mises that materials will yield once the second invariant J_2 reaches a critical value. The yielding criterion can be written in the form of equation (2-3). The criterion leads to a circular cylindrical surface in the (σ_1, σ_2, σ_3) space.

$$J_2 = \frac{1}{6}\left[(\sigma_1 - \sigma_2)^2 + (\sigma_2 - \sigma_3)^2 + (\sigma_3 - \sigma_1)^2\right] = k^2 \tag{2-3}$$

Assuming the yielding surface is Mises type represented by equation (2-3), the equivalent stress can be defined as follows,

$$\sigma_e = \sqrt{3J_2(s_{ij})} = (\frac{3}{2} S \bullet S)^{1/2} = \frac{\sqrt{2}}{2}\sqrt{(\sigma_1 - \sigma_2)^2 + (\sigma_2 - \sigma_3)^2 + (\sigma_3 - \sigma_1)^2} \tag{2-4}$$

Once the material yields, the plastic deformation occurs. There were two kinds of theories used to model the plastic deformation process. One is "J2 deformation theory" and another is "J2 flow theory". The "deformation theory" was developed by Henky and Nadai to analyze the plastic deformation problem with total stress-strain relationship. In deformation theory, the plastic strain components are proportional to the deviatoric stress components, with the scalar function of proportionality depending strictly on J_2 as follows:

$$\varepsilon_{ij}^{\ p} = g(J_2) S_{ij} \tag{2-5}$$

The function $g(J_2)$ can be determined through the uniaxial tensile test. Furthermore, the equation (2-5) can be transformed to equation (2-6) after the function g(J2) is calibrated by uniaxial test.

$$\varepsilon_{ij}^{\ p} = \frac{3}{2}[\frac{1}{E_s(\sigma_e)} - \frac{1}{E}] S_{ij} \tag{2-6}$$

For the purpose of measuring the plastic deformation, equivalent plastic strain is defined as equation (2-7).

$$\varepsilon^{p}{}_{e} = (\frac{2}{3}\varepsilon^{p} \bullet \varepsilon^{p})^{1/2} \tag{2-7}$$

By adding the elastic strain component from Hooks law, the relationship between the total strain and stress can be modeled as:

$$\varepsilon_{ij} = \frac{1+v}{E}\sigma_{ij} - \frac{v}{E}\sigma_{kk}\delta_{ij} + \frac{3}{2}[\frac{1}{E_s} - \frac{1}{E}]S_{ij}$$
$$\varepsilon_{ij} = \frac{1+v_s}{E}\sigma_{ij} - \frac{v_s}{E}\sigma_{kk}\delta_{ij}, v_s = \frac{1}{2} + \frac{E_s}{E}[v - \frac{1}{2}] \tag{2-8}$$

The rate form of the equation (2-8) is given as follows:

$$d\varepsilon_{ij} = \frac{1}{E}\Big[(1+v)d\sigma_{ij} - vd\sigma_{kk}\delta_{ij}\Big] + \frac{3}{2}(\frac{1}{E_s} - \frac{1}{E})ds_{ij} + \frac{9}{4}(\frac{1}{E_t} - \frac{1}{E_s})\frac{s \bullet d\sigma}{\sigma_e}S_{ij} \tag{2-9}$$

For the plane stress condition without in plane shearing deformation, the rate form of J2 deformation theory can be further reduced to equation (2-10).

$$\begin{Bmatrix} d\varepsilon_x \\ d\varepsilon_\theta \end{Bmatrix} = \frac{1}{E_s}\begin{vmatrix} 1+q(2\sigma_x - \sigma_\theta)^2 & -v_s + q(2\sigma_x - \sigma_\theta)(2\sigma_\theta - \sigma_x) \\ -v_s + q(2\sigma_x - \sigma_\theta)(2\sigma_\theta - \sigma_x) & 1+q(2\sigma_\theta - \sigma_x)^2 \end{vmatrix}\begin{Bmatrix} d\sigma_x \\ d\sigma_\theta \end{Bmatrix} \tag{2-10}$$

Where:

$$E_s = \frac{\sigma_e}{\varepsilon_e}$$
$$v_s = \frac{1}{2} + \frac{E_s}{E}(v - \frac{1}{2})$$
$$q = \frac{1}{4\sigma_e{}^2}(\frac{E_s}{E_t} - 1)$$

The total stress-strain relationship shown in equation (2-8) offers the convenience of

mathematic manipulation and the derivation of closed-form solutions for several practical problems.

2.2.3.2 J2 flow theory

The nature of the plastic deformation is path dependent, which could not be fully characterized by the total stress-strain relationship. Thus, the incremental relationship between the stress and strain is required in formulation of the plastic deformation problem. In the J2 flow theory, the components of plastic strain increment is normal to the yielding surface and are linearly proportional to the components of stress increment as shown in equation (2-11) **[62].**

$$d\varepsilon_{ij}{}^{p} = \frac{1}{H}\left(\frac{\partial f}{\partial \sigma_{mn}} d\sigma_{mn}\right)\frac{\partial f}{\partial \sigma_{ij}} \tag{2-11}$$

Where f is the current yielding surface (equation (2-3)), and H is a scalar function of stress and of the loading history. A scalar measurement of plastic strain increment is called equivalent plastic strain increment which is defined as follows,

$$d\varepsilon^{p}{}_{e} = \left(\frac{2}{3} d\varepsilon^{p} \bullet d\varepsilon^{p}\right)^{1/2} \tag{2-12}$$

The total equivalent plastic strain can be obtained by summing all increments of equivalent plastic strain as equation (2-13):

$$\varepsilon^{p}{}_{e} = \int d\varepsilon^{p}{}_{e} \tag{2-13}$$

Substituting yielding function 2-4 into equation 2-11, incremental stress-strain relationship can be reduced to equation (2-14)

$$d\varepsilon_{ij}{}^{p} = \frac{1}{H}\left(\frac{9}{4\sigma_e{}^{2}} S \bullet d\sigma\right) S_{ij}, H = \frac{d\sigma e}{d\varepsilon^{p}{}_{e}} \tag{2-14}$$

By adding the incremental elastic strain from Hooks law, the model can be completed as:

$$d\varepsilon_{ij} = \frac{1}{E}\left\{\left[(1+v)d\sigma_{ij} - v d\sigma_{kk}\delta_{ij}\right] + 9Q(s \bullet d\sigma) S_{ij}\right\} \tag{2-15}$$

For the plane stress condition without in-plane shearing deformation, equation 2-15 can be expressed as:

$$\begin{Bmatrix} d\varepsilon_x \\ d\varepsilon_\theta \end{Bmatrix} = \frac{1}{E}\begin{vmatrix} 1+Q(2\sigma_x - \sigma_\theta)^2 & -v + Q(2\sigma_x - \sigma_\theta)(2\sigma_\theta - \sigma_x) \\ -v + q(2\sigma_x - \sigma_\theta)(2\sigma_\theta - \sigma_x) & 1+Q(2\sigma_\theta - \sigma_x)^2 \end{vmatrix} \begin{Bmatrix} d\sigma_x \\ d\sigma_\theta \end{Bmatrix} \tag{2-16}$$

Where: $Q = \frac{1}{4\sigma_e{}^{2}}\left(\frac{E}{E_t} - 1\right)$

2.2.3.3 Wrinkle onset

Considering an axially loaded circular cylindrical shell shown in Fig.2-12, the nonlinear equilibrium equations for axisymmetric deformations of such a shell can be given as equation 2-17.**[62]**

$$\begin{cases} \dot{N}_{xx}{}' = 0 \\ \dot{M}_{xx}{}'' - \frac{\dot{N}_{\theta\theta}}{R} + \sigma_{xx} t \dot{w}'' = 0 \end{cases} \tag{2-17}$$

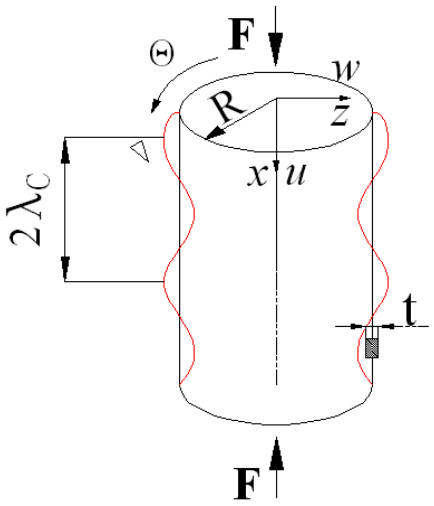

Fig.2- 12 Wrinkled tube and it's size

Where N_{xx} , M_{xx}, $N_{\theta\theta}$ and σ_{xx} are axial stress resultant, axial bending moment, hoop stress resultant and axial stress respectively. The kinematical equation **[62]** of the shell can be expressed as:

$$\begin{cases} \dot{\varepsilon}^{0}_{xx} = \dot{u}_{,x} \\ \dot{\varepsilon}^{0}_{\theta\theta} = \dfrac{\dot{w}}{R} \\ \dot{\kappa}_{xx} = -\dot{w}_{,xx} \end{cases} \tag{2-18}$$

The buckling mode satisfies the equilibrium equation (2-18) has the form as:

$$\begin{aligned} \bar{w} &= a\cos\left(\frac{\pi x}{\lambda}\right) \\ \bar{u} &= b\sin\left(\frac{\pi x}{\lambda}\right) \end{aligned} \tag{2-19}$$

By substituting (2-18), (2-19) into equilibrium equation (2-17) and using the constitutive equation (2-10) of J2 deformation theory, the critical axial stress σ_c and half

wave-length λ_c of the buckling mode can be obtained as: **[62]**

$$\sigma_c = \left(\frac{C_{11}C_{22} - C_{12}}{3} \right)^{1/2} \left(\frac{t}{R}\right) \qquad (a)$$

$$\lambda_c = \pi \left(\frac{C_{11}^{\ 2}}{12(C_{11}C_{22} - C_{12}^{\ 2})} \right)^{1/4} (Rt)^{1/2} \qquad (b) \qquad (2\text{-}20)$$

Where $C_{\alpha\beta}$ are the elements of the inverse of the constitutive matrix in equation (2-10).

2.2.3.4 Wrinkle evolution

After wrinkle onset, wrinkles start to grow with continual axial compression. In the series of papers **[59, 60],** Bardi, et al., investigated the wrinkle evolution characteristic of the circular tube under axial compression experimentally and analytically. Under the axial compression, the tube is deformed uniformly before the wrinkle onset point A (Fig.2-12). Then, the wrinkle grows stably with continued axial compression until the axial stress reached maximum on point B (Fig.2-12) where the wrinkle starts to collapse. With further compression, the wrinkle localizes or folds together after point C (Fig.2-12). Paquette et al., **[61]** investigated wrinkle evolution characteristic of the circular tubes under axial compression and internal pressure.

In the tube hydroforming process, the tube is subject to the internal pressure and axial compression simultaneously so that the wrinkle can be generated with the proper loading path. However, the research on how to control tube wrinkles and how the process variables influence tube wrinkle characteristics is still limited. By adopting the wrinkle onset theory and wrinkle evolution theory aforementioned to tube hydroforming process, the effect of the process variables such as loading path, die geometrical shape, friction conditions and material properties on the wrinkle characteristics can be investigated,

providing design guidance to the preforming process for material accumulation.

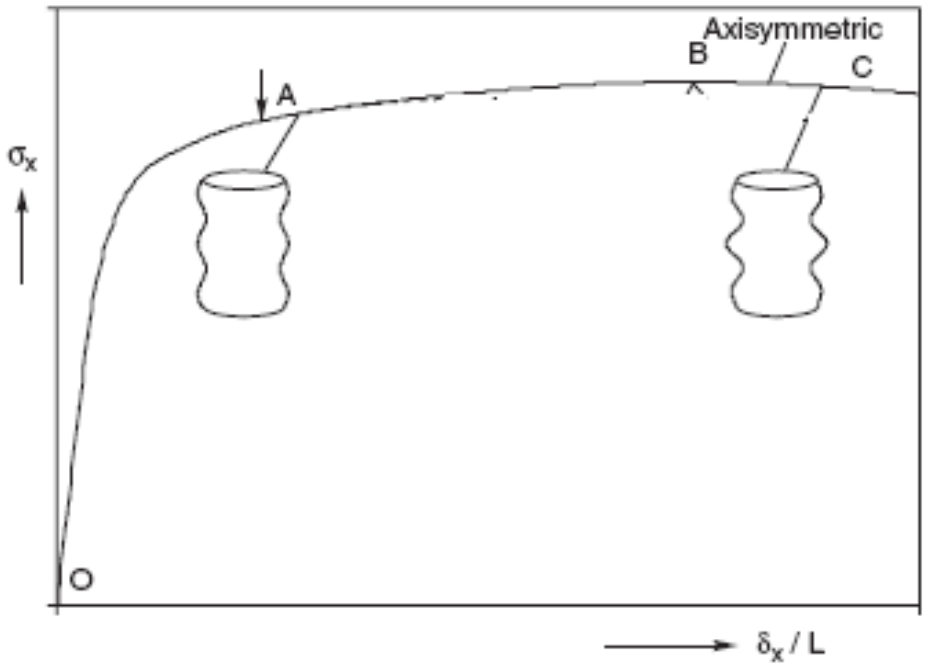

Fig.2- 13 Axial response of the circular tube during wrinkle onset and evolution **[59]**

2.3 Concluding remarks from literature review

2.3.1 Preform design for forging process

Preform design is critical for multi-stage forging processes to ensure the production of defects-free parts. Due to the geometry and material flow complexities in forging processes, finding the optimal preform shapes could be difficult and time consuming. In the last two decades, many numerical preform design methods have been developed to facilitate the forging process design, such as backward tracing method, sensitivity analysis method and some non-gradient methods. However, the applications of these methods are still time consuming and are limited to some specific cases, which needs

further research efforts to advance the design methodology.

2.3.2 Preform design for tube hydroforming process

Preforming wrinkles in the tube hydroforming process is an effective way to reserve material in the forming zone so that the excessive thinning can be avoided and formability can be improved. However, the research on the utilization of wrinkle formation in tube hydroforming process is still limited. Further research efforts are needed to understand the wrinkle evolution characteristic in the THF process. The analytical model on the wrinkle onset and wrinkle evolution recently developed for tubular structures could be extended to tube hydroforming process to investigate the effect of the process variables such as loading path, die geometrical shape, friction conditions and material properties on the wrinkle characteristics. Extension of this model to tube hydroforming has the potential for opening new avenues for perform design in THF.

PHASE I

PREFORM DESIGN FOR FORGING AND EXTRUSION PROCESSES

RESEARCH APPROACH AND TASKS IN PHASE I

Preform design is critical for multi-stage forging processes to ensure the production of defect-free parts. An efficient design methodology based on geometrical resemblance is proposed for the preform design in forging process. The premise of this methodology is such that the initial and subsequent simulations are carried out by constructing a slightly larger part which geometrically resembles the desired part. Initial FEA simulation of the larger part is performed with a reasonably guessed preform shape which may allow the occurrence of forming defects or flash formation. Then a series of intermediate resembling parts between the largest part and the desired part are constructed. The undeformed shape corresponding to the intermediate part could be obtained by backward tracing of material flow from the simulation results of the larger part. This undeformed shape is then taken as the preform shape of the intermediate part. The procedure is repeated until the intermediate part is geometrically close to the desired part, which leads to the preform shape. In order to realize and validate the proposed method, four tasks have been carried out in accordance to the sequence shown in Fig.I-1.

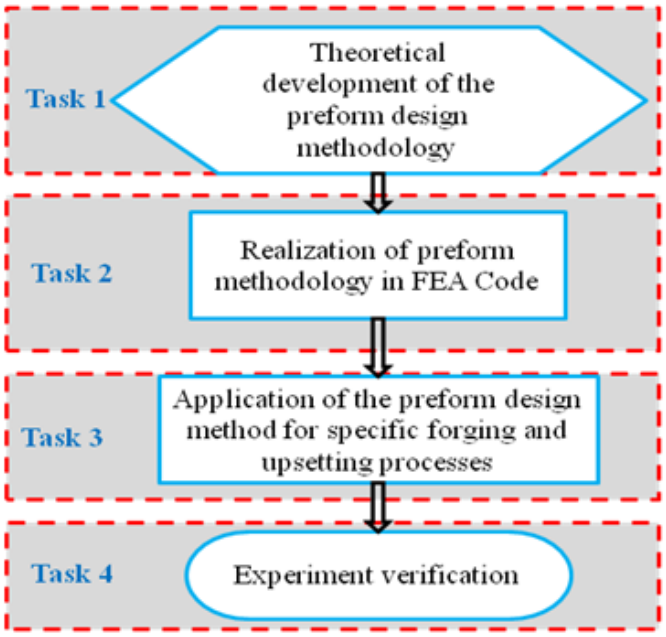

Fig.I- 1 Flow chart of the research in Phase I

Task 1: Theoretical development of preform design methodology

Based on the assumption that the preform shape of the desired part can be obtained by tracing back the material flowing in the forging process of the enlarged part, a preform design methodology based on the geometrical resemblance is developed to compute the preform shape which can avoid the forming defects in the finish forging process.

Task 2; Realization of the preform design methodology in the Deform 2D

In this task, incorporating the preform design method into commercial FEA code Deform 2D was discussed and realized

Task 3: Application of the preform design method in the specific forging and upsetting process

In this task, the preform design method was applied to the flashless forging of an axisymmetric web-rib part, extrusion process of a stud, and upsetting process of a shaft.

It was proven to be an efficient preform design methodology which required a few iterations to find the proper preform shape.

Task 4: Experimental verification of the preform design method

In this task, experiments were carried out on the flashless forging of the axisymmetric rib-web part to verify the proposed preform design method.

CHAPTER 3: PREFORM DESIGN FOR FORGING AND EXTRUSION PROCESSES

3.1 Preform design based on the geometrical resemblance

The primary criterion in preform design of a multi-stage forging process is that the forged part should be free of defects such as, die under-fill, folding, laps, fracture, etc. In other words a successfully forged part means that its preform shape should lead to good material flow patterns to avoid any forming defects. Figures 3-1 and 3-2 are used to illustrate the geometrical resemblance methodology in preform design. Assume that Part X_a shown in Fig.2b is the part whose preform shape needs to be found, and Fig. 3-2a shows the optimal die preform shape found. Figure 1 shows axisymmetric upsetting process of part X_b with preform shape P_b. A curve X_a is constructed inside the part X_b and its undeformed shape P_a can be obtained by backward tracing of the material flow via FE simulation. It can be seen from Figs. 3-1 and 3-2 that deformation process of P_a to X_a in upsetting process of X_b (Fig. 3-1) is close to upsetting of P_a to X_a directly (Fig. 3-2) if X_a is geometrically close to X_b. Thus it is reasonable to assume that the preform shape of X_a upsetting process can be referred to the undeformed shape P_a of X_a in upsetting X_b process if X_a is geometrically close to X_b and resembles X_b. When X_a and X_b are not geometrically close enough, a series of intermediate resembling shapes can be constructed to trace the preform shape of X_a.

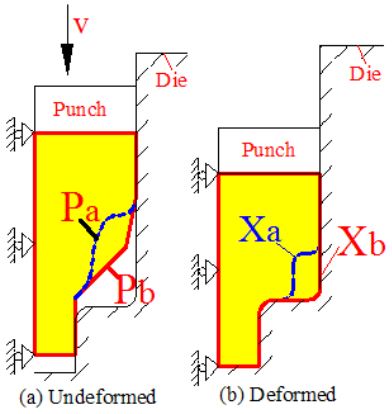

Fig.3- 1 Forging of part X_b

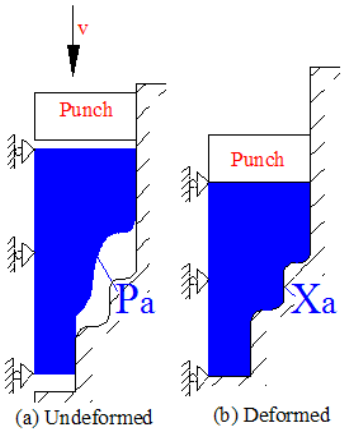

Fig.3- 2 Forging of part X_a

Based on the above assumptions, the preform design methodology is proposed as follows. The illustrations for the design of preform shape P_a for the part X_a is given in Figs. 3-3 and 3- 4.

1) Let the final shape X_a of part-a be known [Fig 3-3]: Construct a bigger part X_d which resembles X_a geometrically and contains the shape of X_a.
2) Design preform shape P_d of part X_d. In this step the preform shape P_d does not strictly need to form part X_d without defects. Under-fill and the flash forming are allowed since the necessary condition is such that the deformed shape X_d should at least contain the shape of X_a.
3) Construct an intermediate shape X_c between X_a and X_d by the offset method $X_c=X_a+f$, where f is the offset distance. Here the preform shape P_c of part X_c can be obtained by tracing backward the material flow using FE simulation results of forging process of X_d.
4) Construct another intermediate shape X_i (eg. X_b) between X_c and X_a by the offset method $X_i=X_a+\alpha f$, where $\alpha<1$. Now repeat step-3 by gradually reducing α and then finding the preform shape P_i of X_i that is close to X_a.

5) Iterate step-4 until X_i is very close to X_a. Then the preform shape P_a of X_a can now be found by tracing backward the material flow from the FE simulation results of the forging process of P_i.

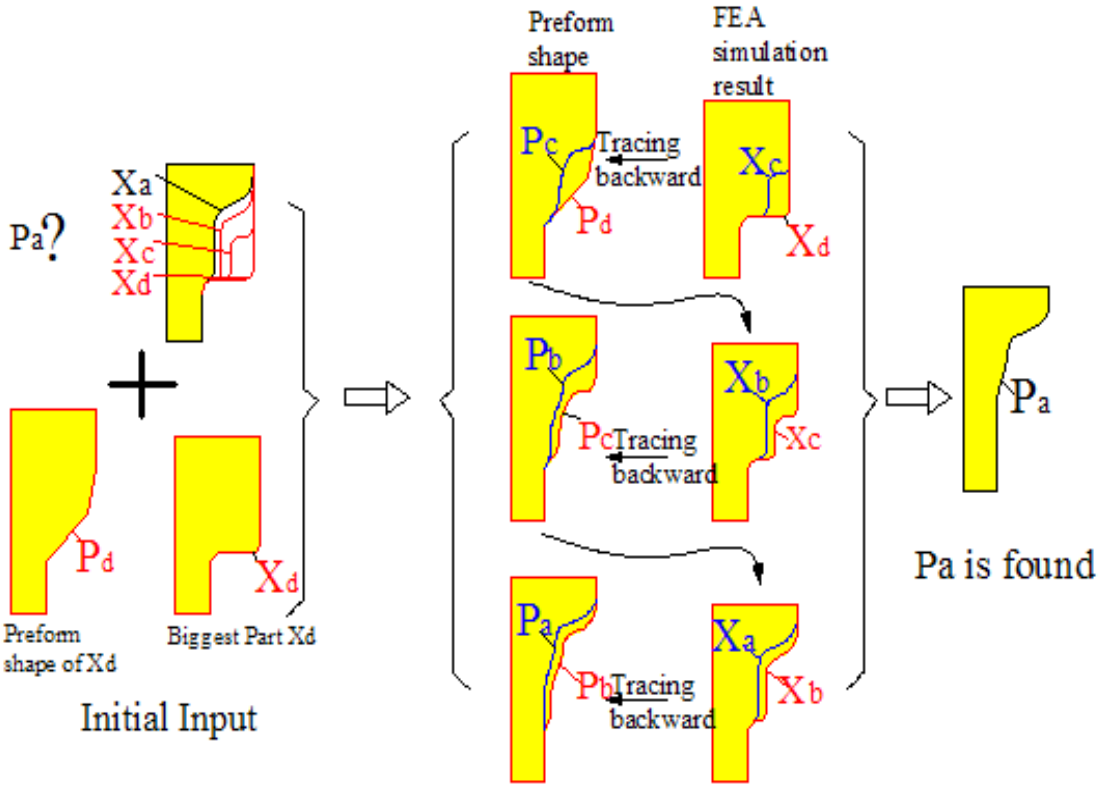

Fig.3- 3 Illustration of preform design of part-a

Using the proposed methodology, a reasonable good preform shape can be found by a few FE iterations when the initial constructed part X_d is close to X_a. This method is easy to apply and can be incorporated into the commercial FE packages for preform design.

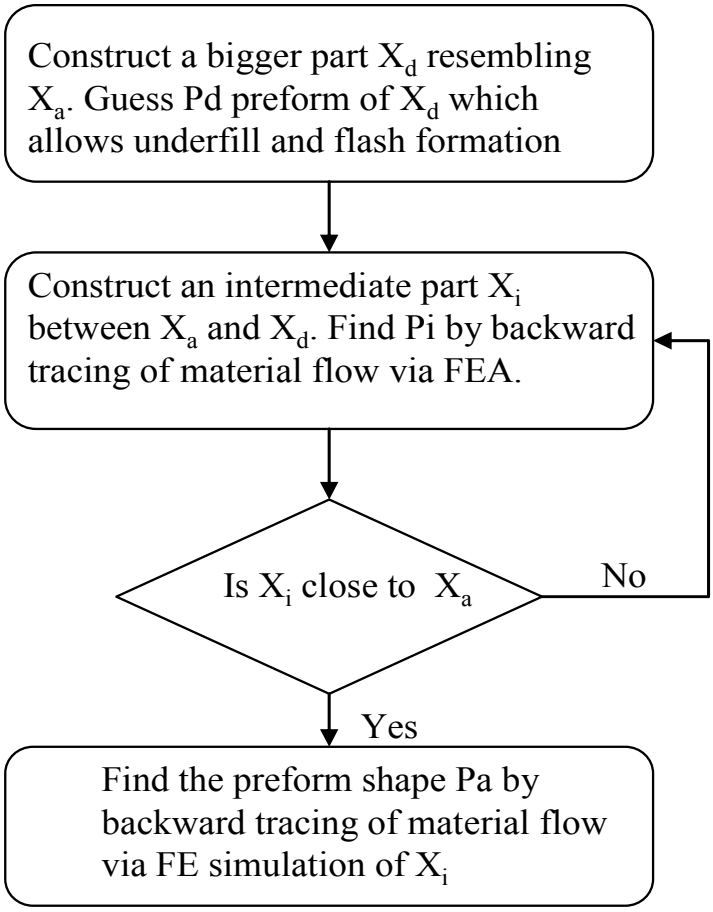

Fig.3- 4 Flow chart of preform design

3.2 Realization of the preform design methodology in 2D FEA code

Current, This methodology is developed in Deform 2D to design perform shape of axisymmetric forging part. In Deform 2D, the 'Track Point' function can track the deformation history of specific material points on the forging part. Based on this function, the undeformed shape corresponding to specific deformed shape can be obtained in three steps:

1) Discretize the profile shape X_a' of the deformed part into a series of points (Fig.3-5.b)

2) Trace back the undeformed location this series of points

3) Connect the locations before deformation of this series of points to approximate the undeformed shape Pa' (Fig.3-5.a). The shape approximation by connecting series of points leads to insignificant volume loss which can be compensated by adjusting the coordinates of some points on the undeformed shape.

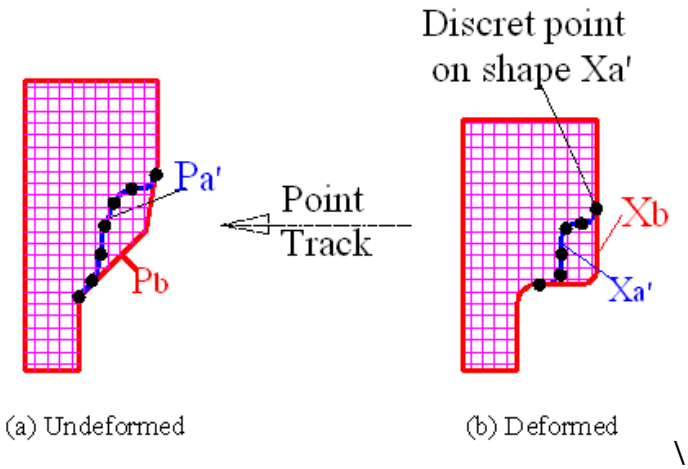

Fig.3- 5 Track point function in Deform 2D

3.3 Applications for 2D closed die forging processes

3.3.1 Preform design based on geometrical resemblance for 2D closed die forging

In the forging process of rib-web part, billet material is difficult to flow into rib cavity due to the high ratio of rib height to rib thickness. Preform of the rib-web part is designed to facilitate the material flowing, improve the die fill and achieve flashless forging. Fig.3-6 Show an axisymmetric rib-web part with height-to -thickness ratio of 2.0. Without the performing pass, under fill and flash formation were observed in the FEA simulation of the direct forging (Fig.3-7a). The billet material of this rib-web part is copper. The flow

stress of copper is expressed as $\bar{\sigma} = 560\bar{\varepsilon}^{0.46}$ which is obtained from the experiment conducted in Advanced Manufacturing Lab.

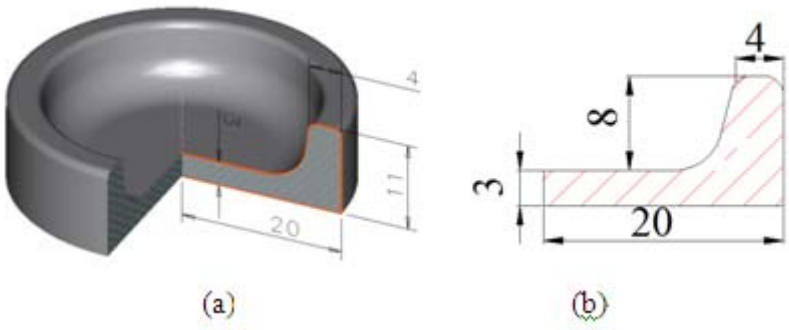

Fig.3- 6 Axisymmetric H-shape with H/B=2.0

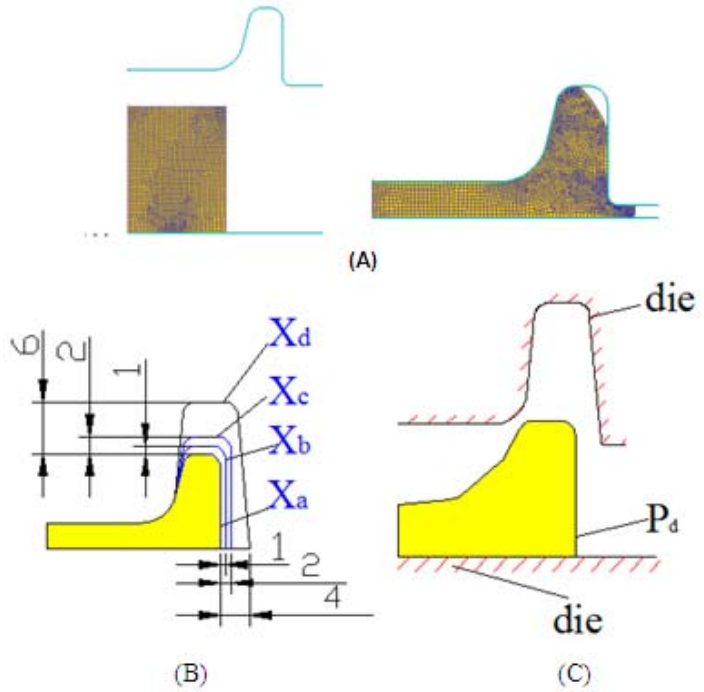

Fig.3- 7 X_d and guessed P_d

The proposed preform design method is applied to this part as discussed below. The

simulation were carried out using commercial FE package, DEFORM.

- For the preform design of this part, the first step is to construct a series of bigger parts X_b, X_c, X_d and design a reasonable preform shape P_d of X_d as shown in Fig.3-7. Fig.3-7b shows a series of constructed bigger parts X_b, X_c, X_d . These parts are constructed by offsetting the top and side edges of X_a by a distance. Figure Fig.3-7c shows the guessed preform shape P_d of part X_d. P_d has a bevel shape at the center in order to improve the material flow. It should be noted that P_d is not strictly required to form X_d. Underfill and flash are allowed, but at least the deformed shape of P_d should contain X_c to make the backward tracing method applicable.
- *Iteration 1*:After X_d and P_d are constructed, FEA simulations are carried out to simulate the forming process of X_d. Fig.3-8(a) and Fig.3-8(b) show the initial and the final steps of FE forging simulations of X_d respectively. From the results it can be seen that underfill occurs in the forming of X_d. It can be observed that the deformed shape of X_d surrounds X_c. A series of track points along X_c are made to find the preform shape P_c of X_c as shown in Fig.3-8(c) and Fig.3-8(d).
- *Iteration 2*: Use the P_c as the billet shape of X_c and simulate the forming process of part X_c (Fig.3-8e and Fig.3-8f). Then construct track points along X_b (Fig.3-8g) to trace backward the undeformed shape of part X_b as preform shape P_b of X_b (Fig.3-8h).
- *Iteration 3*: Use the P_b as the billet shape of X_b and simulate the forming process of part X_b (Fig.3-8i and Fig.3-8j). Then construct track points along X_a (Fig.3-8k) to trace backward the undeformed shape of X_a as preform shape P_a of X_a (Fig.3-8l).

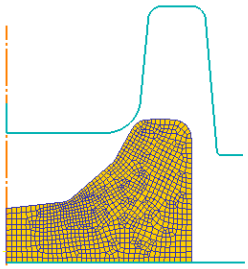

(a) Initial step of X_d simulation

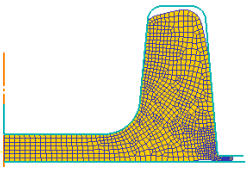

(b) Final step of X_d simulation

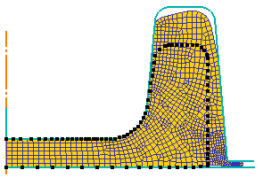

(c)Track points along the X_c

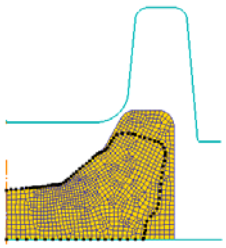

(d) P_c of X_c at initial step

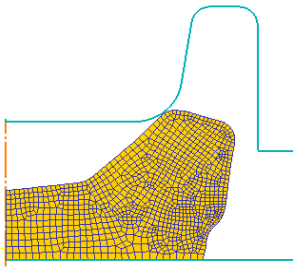

(e) Initial step of X_c simulation

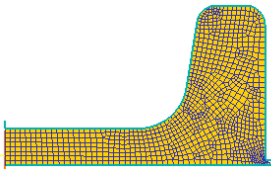

(f) Final step of X_c simulation

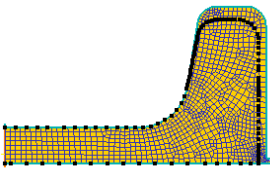

(g) Track points along the X_b

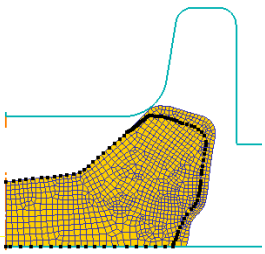

(h) P_b of X_b at initial step

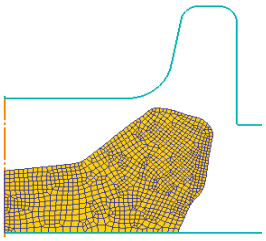

(i) Initial step of X_b simulation

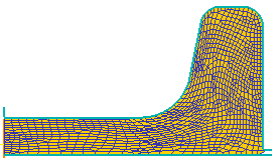

(j) Final step of X_b simulation

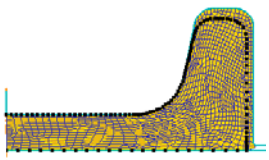

(k) Track points along the X_a

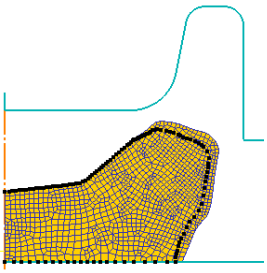

(l) P_a of X_a at initial step

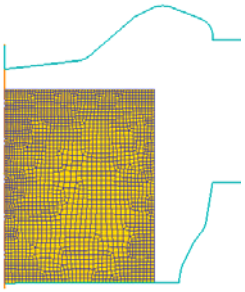

(n) Initial step of preforming

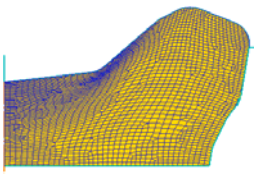

(o)Final step of preforming

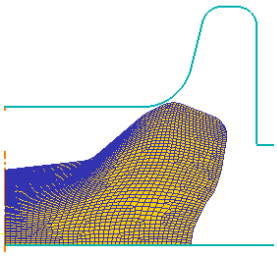

(p) Initial step of finish forging

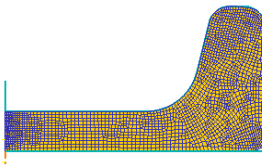

(q) Final step of finish forging

Fig.3- 8 Preform design of X_a by tracing backward method

Based on the preform shape of Pa, the initial billet shape can be found by the constant volume condition. The diameter and the height of the initial billet are assumed to be 25 mm and 16.34 mm respectively. Fig.3-8 (n) and Fig.3-8 (o) show the initial and the final steps of the preforming simulation. Fig.3-8 (p) and Fig.3-8 (q) show the initial and final steps of finish forging of Xa. Fig.3-9 shows the effective strain distribution of part Xa, where the maximum and minimum values are 3.08 and 0.268 respectively. Fig.3-10 shows the die loads in the both stages, where the load in preforming is about 750KN and the load in finish forging is about 973K N.

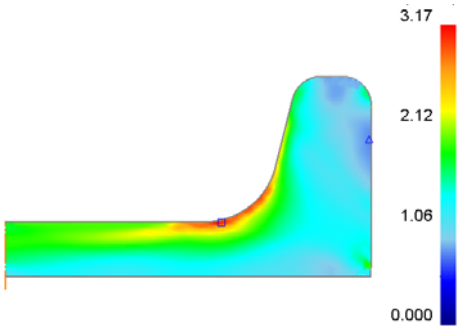

Fig.3- 9 Effective strain distribution of X_a

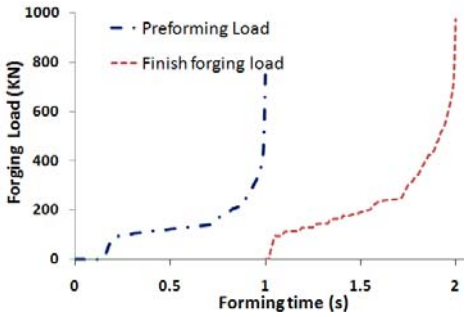

Fig.3- 10 Die load of preforming and finish forging

3.3.2 Preform design for flashless forging of axisymmetric part with multiple ribs

Fig.3-11(a) shows an axisymmetric part with three ribs. The span between rib-2 and rib-3 is two times of that between rib-1 and rib-2. The rib height-to-width ratios are 1, 2 and 3 for the three ribs respectively. Due to the high rib height-to-rib width ratio, preform stages are required to forge a flashless part. As shown in Fig.3-11(c), under fill occurs and flash forms in the forging process without preform stages. The preform shape of this part can be designed with the proposed method.

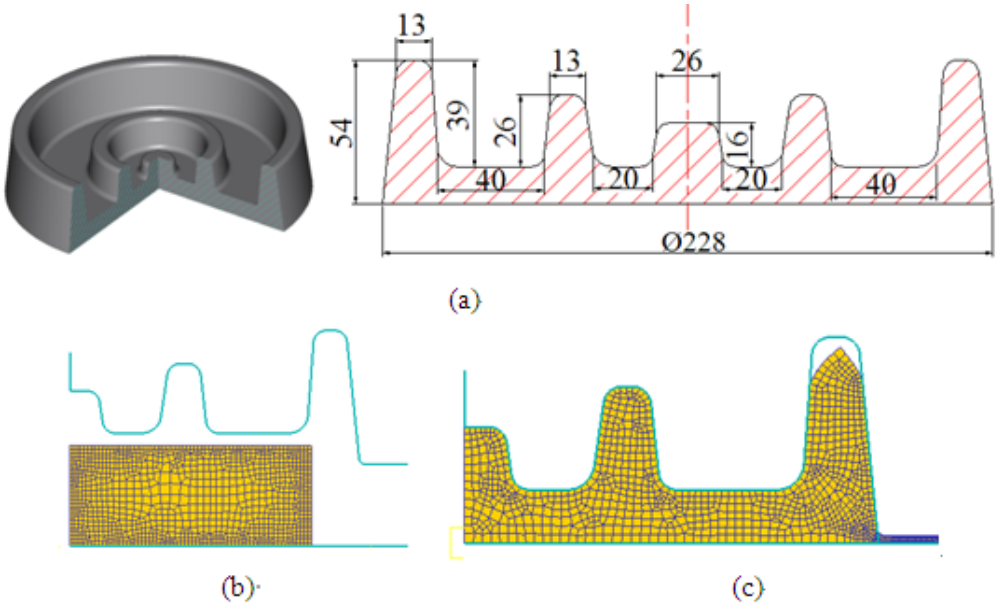

Fig.3-11 (a) Axisymmetric part with multiple ribs, (b) Forging process without preform, (c) Defect in forging process

This part is forged at elevated temperature to reduce the flow stress and ease the material flow in the forging process. Therefore the billet and the tool are heated to 1000^0C and 200^0C respectively. The geometrical size and the axisymmetric model of this part are shown in Fig.3-12. AISI-4034 is used in the FE simulation. The preform shape of this part can be obtained as follows:

The first step is to construct a bigger part X_c and design a reasonable preform shape P_c of X_c. Fig.3-11c shows that underfill and flash will be formed if the part is formed without a preform. This is due to high rib height-to- width ratio. Therefore X_c is constructed by offsetting the top edge of rib-2 and rib-3 by 10 mm each and side edge of rib-3 by 5 mm (Fig.3-12). The preform shape P_c of bigger part X_c is initially designed as shown in Fig.3-12. However preform P_c is not strictly required to form X_c , i.e., die under fill and flash formation are allowed, but at least the deformed shape of P_c should contain X_a to

make the backward tracing method applicable .

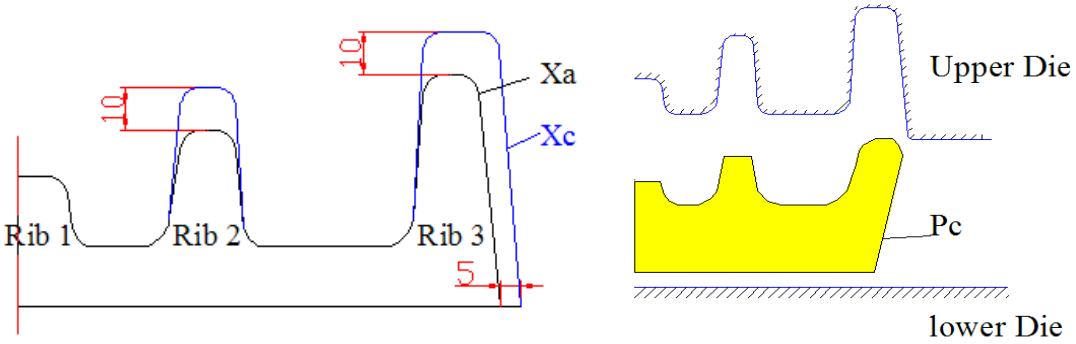

Fig.3- 12 Constructed X_c and guessed preform shape P_c

After the X_c and P_c are constructed, FE simulations are carried out to simulate the forming process of X_c. Fig.3- 13(a) and 3-13(b) show the initial and the final steps of FE forging simulations of X_c. It can be seen that X_c is forged completely with flash formation. Then a series of track points along X_a are made to find the preform shape P_a of X_a as shown in Fig.3-13(c) and 3-13(d). In this problem, the intermediate shapes are not used and the preform shape is found by only one iteration due to the fact that the shapes of X_a and X_c are simple and geometrically close. Fig.3-13(d) shows the undeformed shape of X_a which is taken as preform shape P_a of X_a after removing some noise point marked by circles in Fig.3-13(d). Fig.3-13(e) shows the preform shape P_a of X_a. Once the preform shape Pa is found, the initial billet shape can be obtained by the constant volume condition. The radius and height of the initial billet is assumed to be 90 mm and 43.6 mm respectively. Fig.3-13(f) and 12(g) show the initial and final steps of preforming simulation. Fig.3-13(h) and 3-13(i) show the initial and final steps of finish forging of Xa. Fig.3-14 shows the effective strain distribution of part Xa where the maximum and the minimum values are 3.34 and 0.276 respectively. Fig.3-14 shows the

die loads in the preform and finish forging stages, where the loads are 2.35×104 kN and 2.75×104 kN respectively

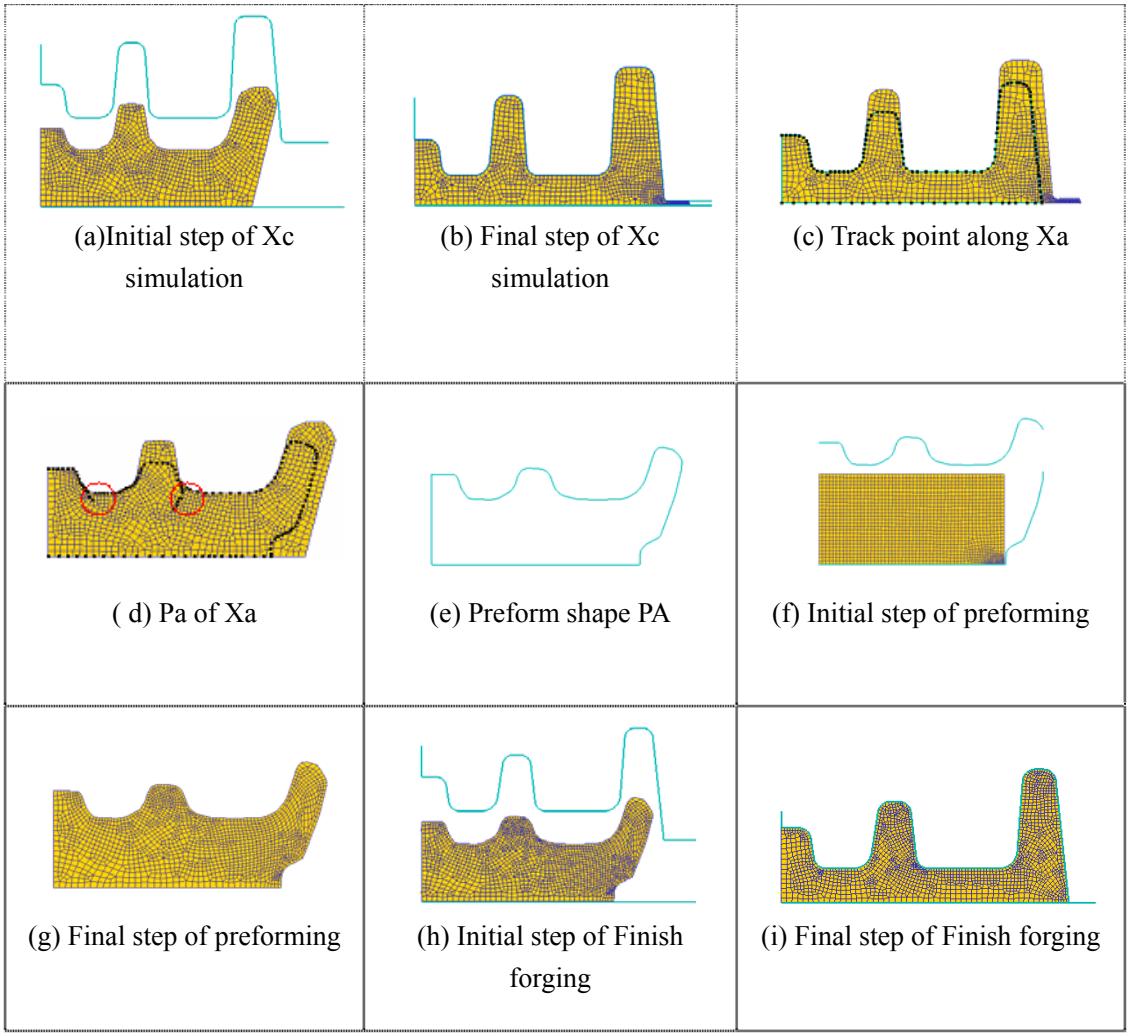

Fig.3- 13 Preform design of X_a by tracing backward method

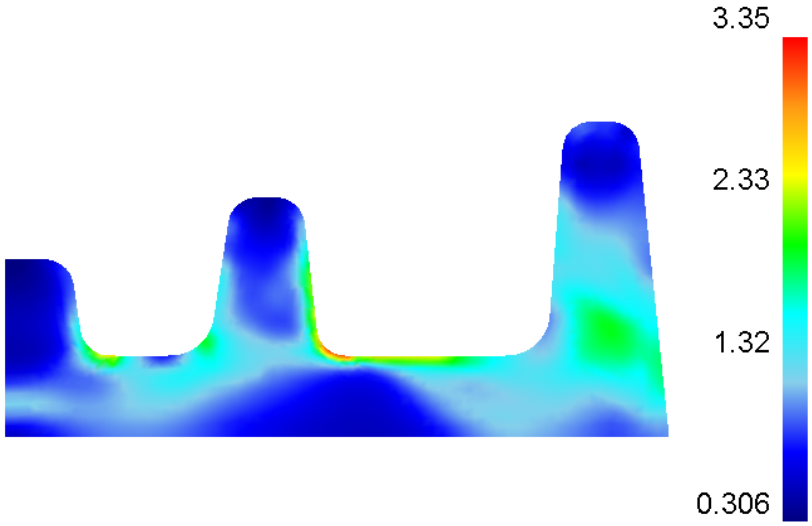

Fig.3- 14 Effective strain distribution

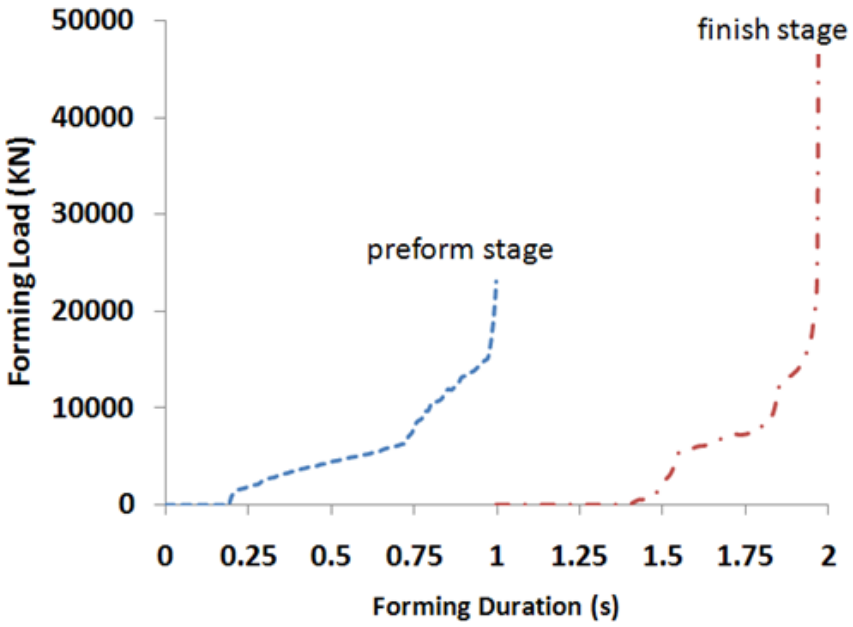

Fig.3- 15 Die load of perform and finish forging

3.4 Applications for 2D extrusion and upsetting processes

3.4.1 Preform design for cold heading of a stud

Generally the forming process of the stud requires several passes such as extrusion process, heading process, etc. In the heading process of the stud, the preform design is a critical step to avoid forming defects like folding or under fill of the die corner. Fig.3-16 shows the typical forming sequences of the stud consisting of extrusion, preforming and heading process. The preformed shapes play an important role for a successful heading operation. Usually a barrel shape is used in heading process to enhance the die fill of the corner and to avoid flash formation. However improper barrel shape may results in folding, under fill and flash formation as shown in Fig.3-16.

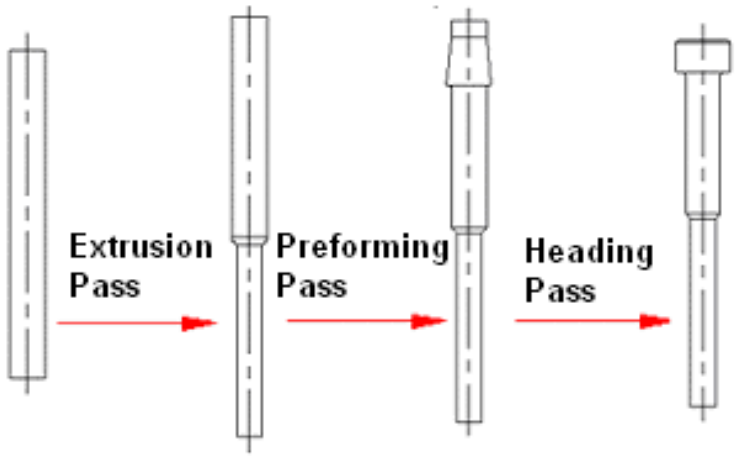

Fig.3- 16 Forming sequences of the stud

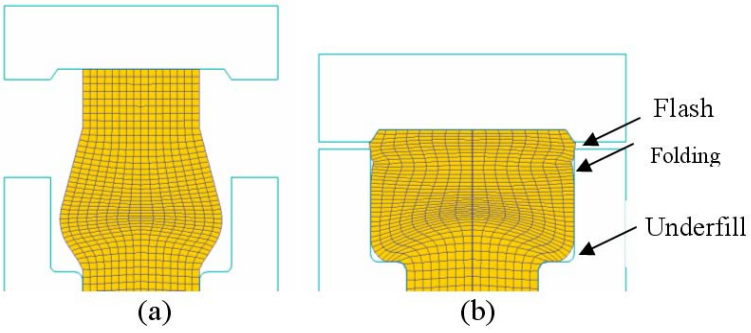

Fig.3- 17 (a) Preform shape (b) Forming defect of the stud in the heading pass

Using the proposed method, the preform design of the stud can be carried out as described below. Material AISI 4140 is used.

- First step is to construct a series of bigger parts for X_c and X_b resembling the stud X_a as shown in Fig.3-18 by offsetting the side edge by 2 and 4 mm respectively.
- Then give a reasonable guess for the preform shape P_c of bigger part X_c (Fig.3-19a) and simulate the forming process of X_c (Figs.3-19b and 3-19c).
- Construct track points along X_b from the simulation results of forming of X_c (Fig.20d) and trace backward to obtain preform shape P_b of X_b (Fig.3-19e).
- Simulate the forming process of X_b (Fig.3-19f and 3-19g) and construct track points along X_a (Fig.3-19h) , then trace backward the undeformed shape P_a of X_a which is assumed to be preform shape of X_a (Fig.3-19i and 3-19j).
- Simulate all three passes to verify the preform shape of X_a. (Fig.3-20).

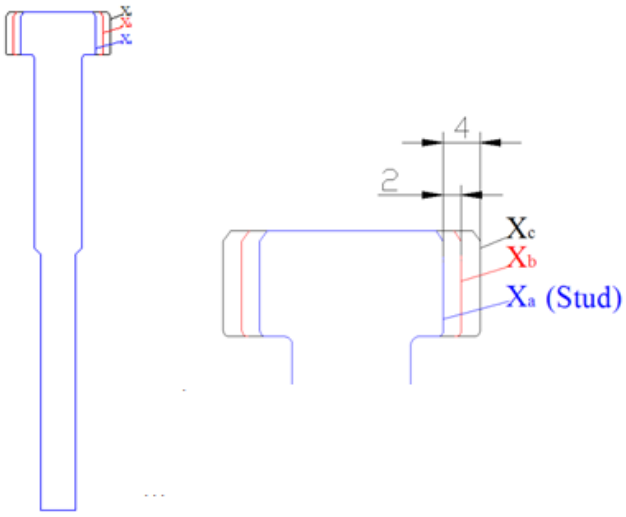

Fig.3- 18 Construction of a series of parts resembling the stud

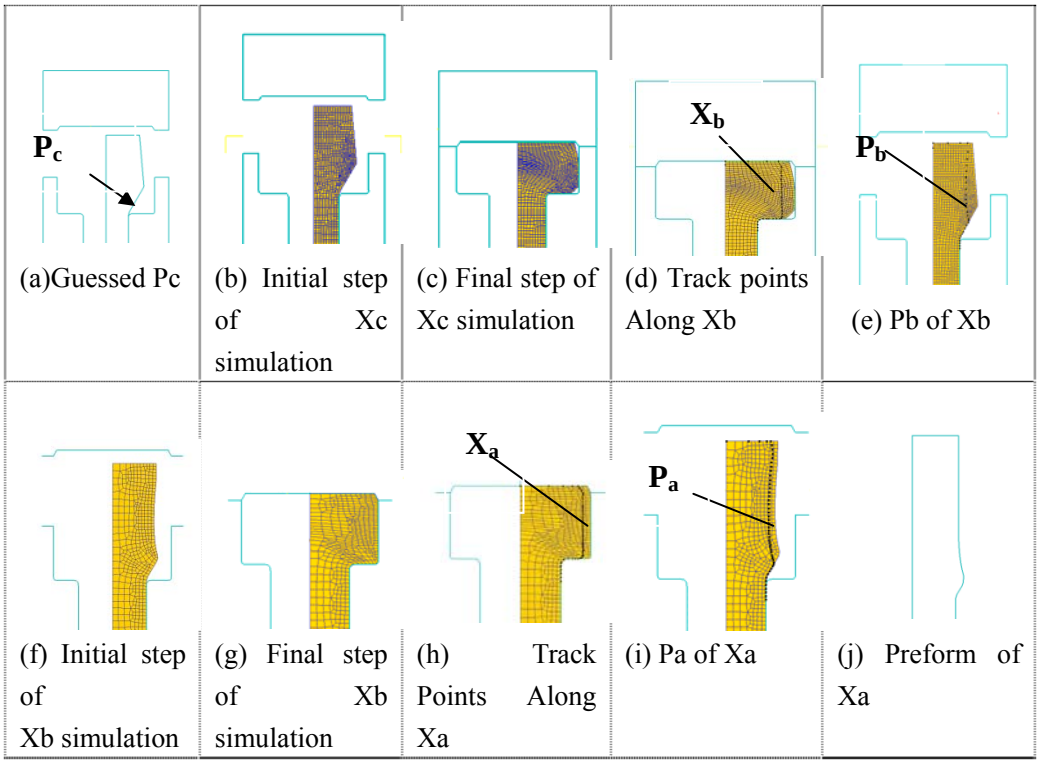

(a)Guessed Pc | (b) Initial step of Xc simulation | (c) Final step of Xc simulation | (d) Track points Along Xb | (e) Pb of Xb

(f) Initial step of Xb simulation | (g) Final step of Xb simulation | (h) Track Points Along Xa | (i) Pa of Xa | (j) Preform of Xa

Fig.3- 19 Preform shape design of stud X_a

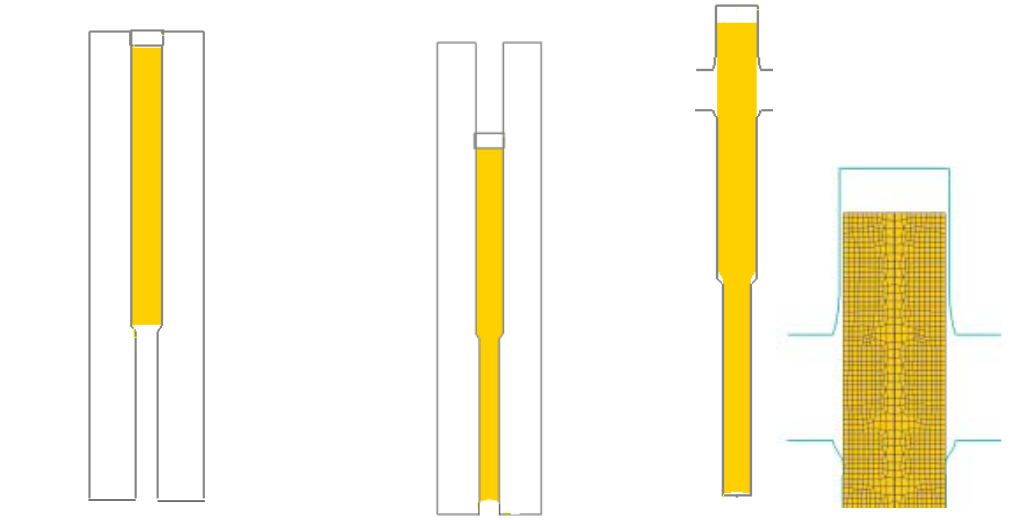

(a)Extrusion-Initial step (b)Extrusion Final step (c)Preforming- Initial step

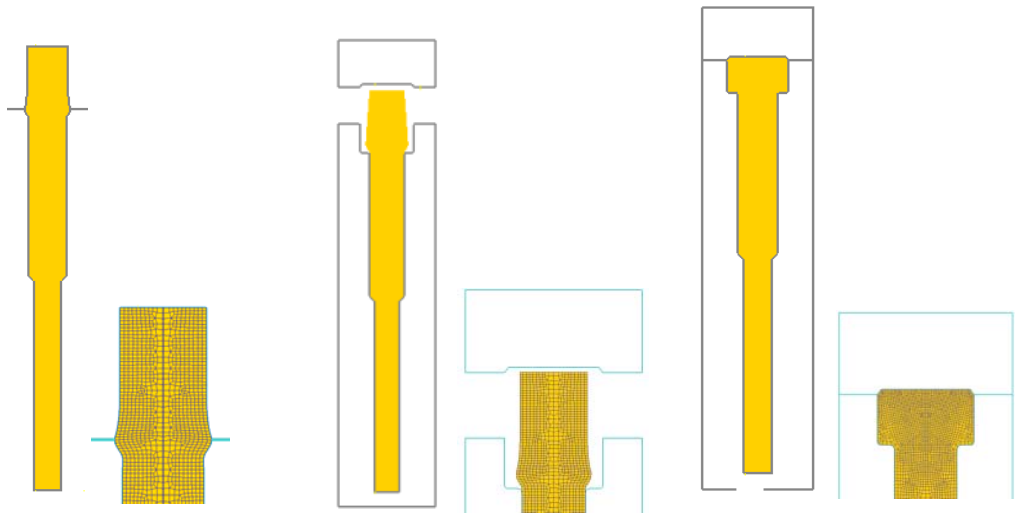

(d) Preforming- Final step (e)Heading- Initial step (f) Heading- Final step

Fig.3- 20 FE simulation of three passes of stud forming

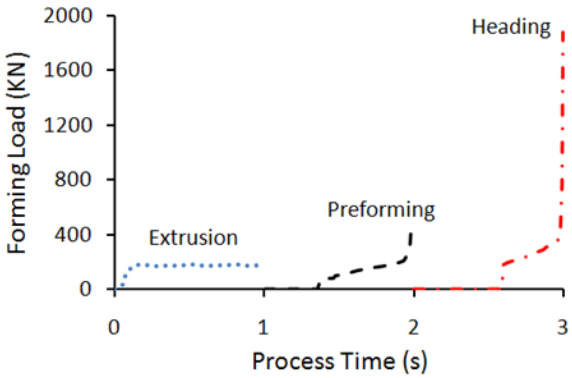

Fig.3- 21 Forming loads and effective strain distribution for three passes of stud forming

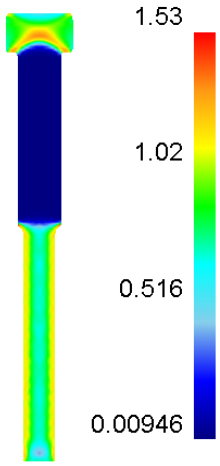

Fig.3- 22 Effective strain distribution

Fig.3-20 shows FE simulations of three passes which verifies the designed preform shapes of the stud. Fig.3-22 also shows the effective strain distribution of three passes where the maximum strain is about 1.5. The forming loads for the three passes are 177 kN, 503 kN and 1879 kN respectively as shown in Fig.3-21.

3.4.2 Preform design for 2D upsetting process

In shaft upsetting process, improper preform shape (Fig.3-23a) may result in folding and under-fill problems near the shaft shoulder as shown in Fig.3-23 (b). The proposed preform design method based on the geometrical resemblance is used to find a proper preform shape for this shaft upsetting process.

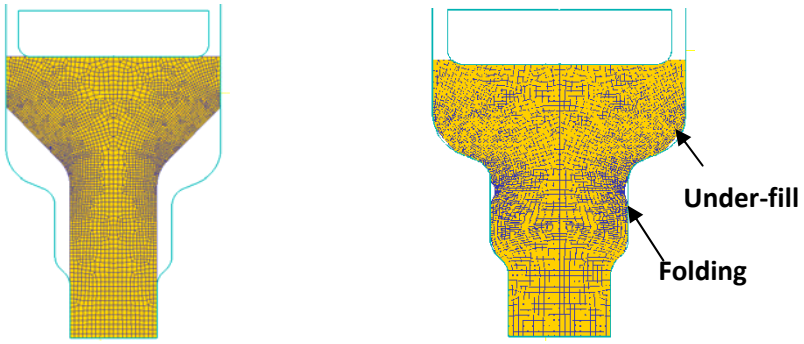

Fig.3- 23 (a) Improper preform shape (b) Forming defects

Due to the symmetry of the shaft geometry, only half model (Fig.3-24a) is used in the preform shape design. The billet material is AISI-4140. In order to improve the formability the upsetting process is done at elevated temperature, where the billet and die are heated to 1000^0C and 200^0C respectively. Fig.3-24(a) shows the detailed geometrical shape and size of the shaft represented by X_a. As discussed earlier, the forming defects occur around the shaft shoulders, thus the preform shape corresponding to the shoulder feature forming is critical for the successful upsetting process. Accordingly, a series of parts having similar shoulder features with that of the shaft are constructed to find the proper preform shape P_a of shaft X_a.

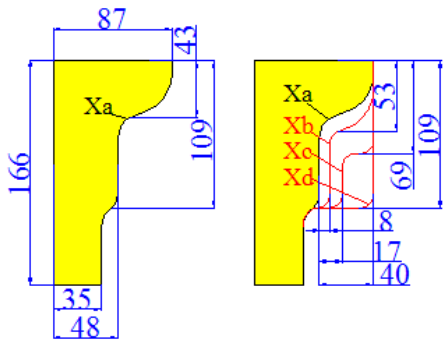

(a) (b)

Fig.3- 24 (a) Half geometrical model of shaft, (b) A series of parts constructed to resemble the shaft

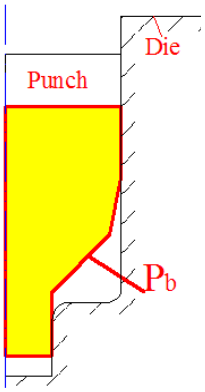

Fig.3- 25 Guessed preform shape P_d of shape X_d

Using the proposed preform design method, the preform can be obtained as follows:

- Construct a series of bigger parts X_b, X_c and X_d by offsetting the shaft shoulder feature as shown in Fig.3-24(b).
- *Iteration 1*: Guess a reasonable preform shape P_d (Fig.3-25) for bigger part X_d (Fig.3-26b). Then construct track points along X_c (Fig.3-26c) for backward tracing to obtain undeformed shape of part X_c as preform shape P_c of X_c (Fig.3-26d).
- *Iteration 2*: Use the P_c as the billet shape of X_c and simulate the forming process of part X_c (Fig.3-26e and Fig.3-26f). Then construct track points along X_b (Fig.3-26g) to trace backward the undeformed shape of part X_b as preform shape P_b of X_b (Fig.3-26h).
- *Iteration 3*: Use the P_b as the billet shape of X_b and simulate the forming process of part X_b (Fig.3-26i and Fig.3-26j). Then construct track points along X_a (Fig.3-26k) to trace backward the undeformed shape of X_a as preform shape P_a of X_a (Fig.3-26l).

The basic preform shape P_a of shaft is found. However P_a has an undesired barreling feature (Fig.3-26l) which gives ejection problem in the upsetting process. This bulge

feature should be replaced by flat feature with the same volume. Fig.3-27 shows the preform shape of shaft upsetting and FEA verification results where no forming defect is found. The maximum effective strain is 3.56 as observed in Fig.3-28. The effective strain and forming load for the preform and finish stages are shown in Fig.3-28and Fig.3-29.

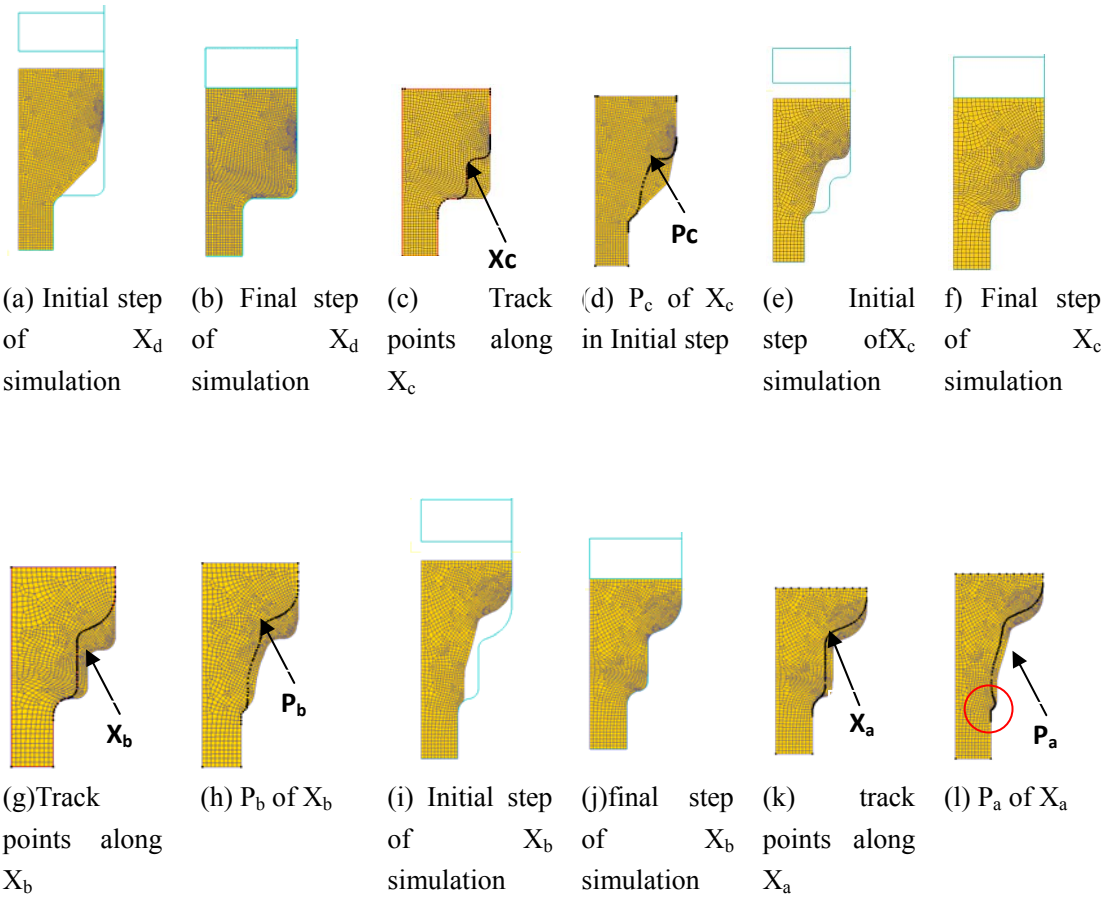

(a) Initial step of X_d simulation (b) Final step of X_d simulation (c) Track points along X_c (d) P_c of X_c in Initial step (e) Initial step ofX_c simulation f) Final step of X_c simulation

(g)Track points along X_b (h) P_b of X_b (i) Initial step of X_b simulation (j)final step of X_b simulation (k) track points along X_a (l) P_a of X_a

Fig.3- 26 Preform design of shaft upsetting process

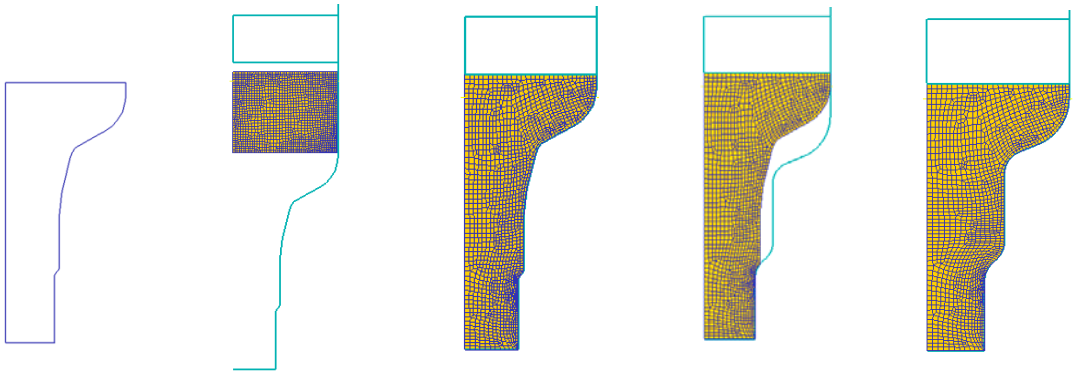

(a)Preform shape of shaft (b)Extrusion-initial step (c)Extrusion-final step (d)Upsetting-initial step (e)Upsetting-final step

Fig.3- 27 FE simulation of two-stage forming of shaft

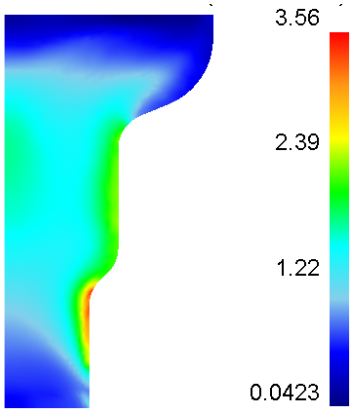

Fig.3- 28 Effective strain distribution of shaft

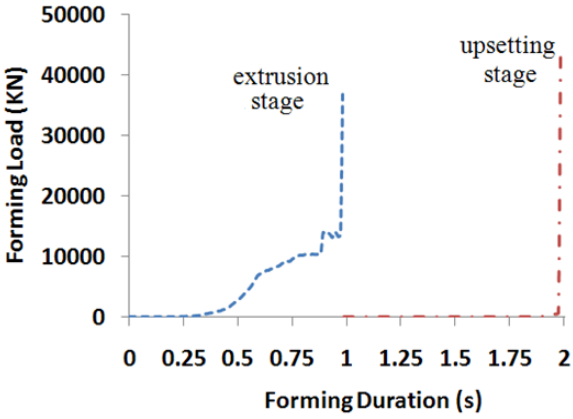

Fig.3- 29 Forming load of shaft upsetting process

3.5 Experiment verification of the preform shape from geometrical resemblance method

Experimental validation for the preform design methodology presented in section3.1.1 was carried out for flashless forming of the axisymmetric rib-web part shown in Fig.3-6. The preform dies were fabricated based on the preform shape obtained by FE simulations, as shown in Fig.3-9. Figure 3-30 shows the drawings of the upper and lower preform dies, and Fig. 3-31 shows the actual die sets used in the experiments. The material used for validation was annealed copper alloy 101. The annealing procedures were such that the samples were heated in a furnace to a maximum temperature of 1100 ˚F under nitrogen. The furnace was then switched off. When the temperature dropped to 150 ˚F, the samples were taken out of the furnace. Annealed copper billet samples 16mm long were cut from a rod of diameter 25.4 mm. Before the experiment, a liquid lubricant was applied to the surfaces of the upper and lower dies. In order to observe under-fill and flash formation, the first set of experiments was carried out using final dies without the preform die set. Figure 3-32 shows under-fill and flash formation as predicted using FE simulation.

Figure 3-33 shows that using preform and final die sets, the part is fully formed. The maximum preform load and the maximum load for the final die obtained in the experiments were 800 kN and 1200 kN, respectively (Fig.3-34). These values are in agreement with the forming loads obtained in the FEA simulations shown in Fig.3-10, indicating that this methodology is suitable for designing preform dies. Validation of the developed preform method was not carried out for steel samples because the maximum tonnage for the hydraulic press used was 150 tons, whereas the FE simulations of the rib-web part using AISI 1015 material indicated that a maximum forging load of 170 tons is needed for final stage forging.

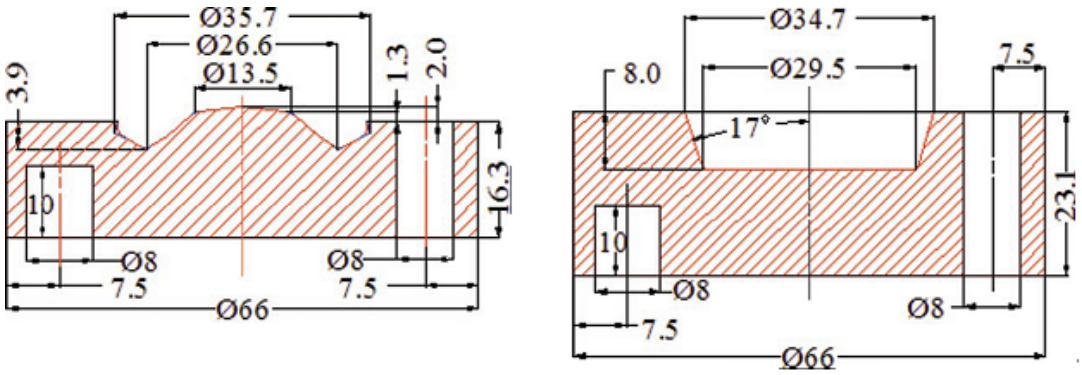

Fig.3- 30 Drawing of upper and lower preform dies

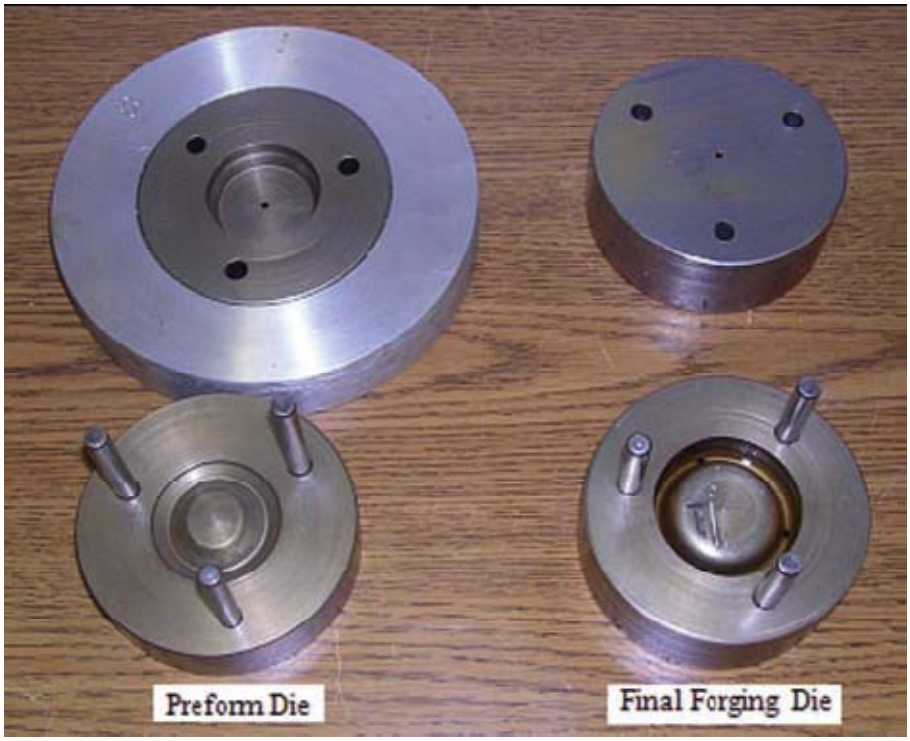

Fig.3- 31 Fabricated preforming dies and final forging dies

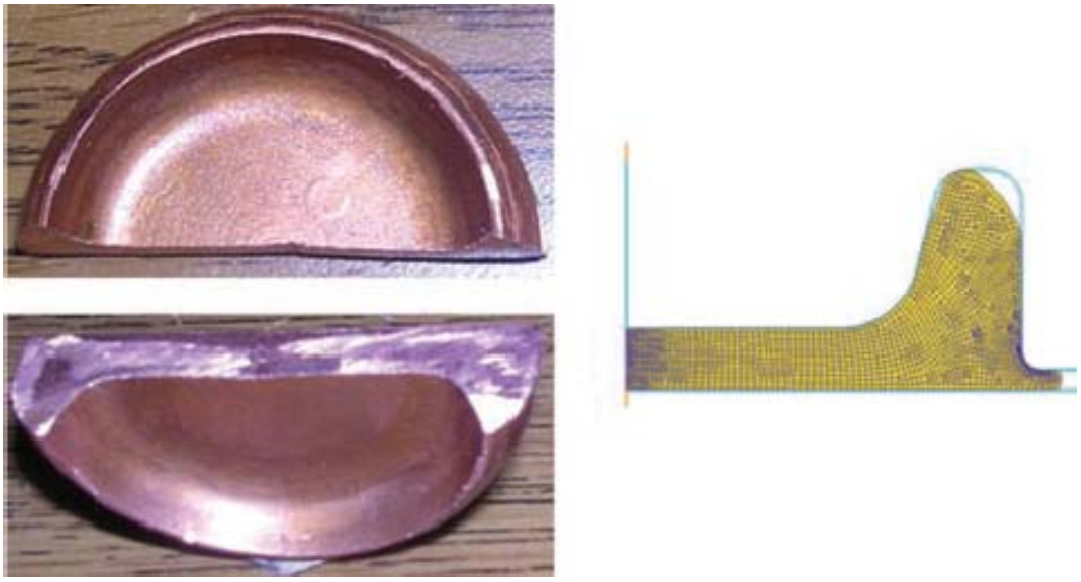

Fig.3- 32 Underfill and flash formation

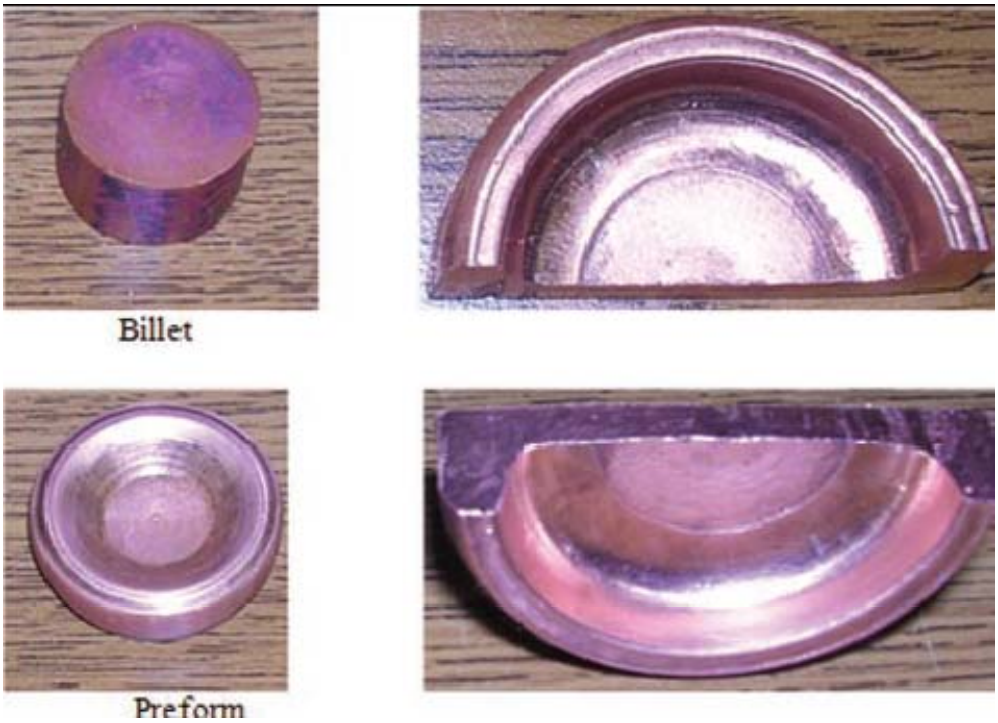

Fig.3- 33 Preform and final geometry

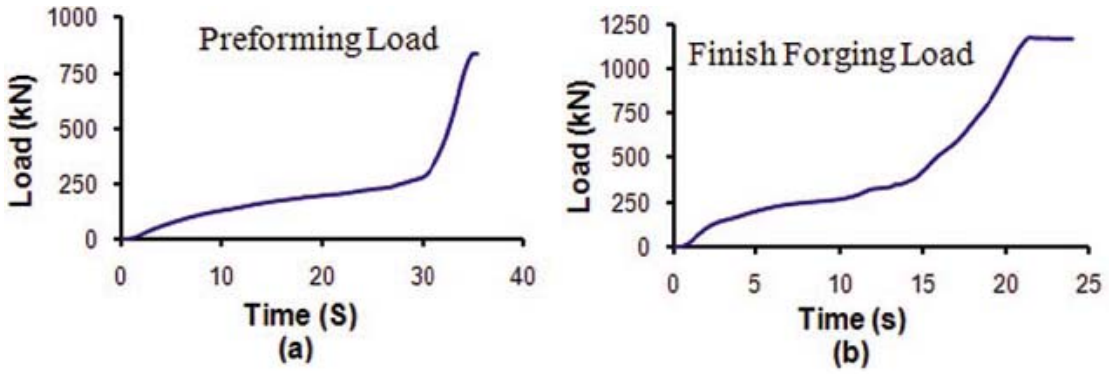

Fig.3- 34 (a) Preform load and (b) Final forming load

3.6 Conclusions

An efficient design methodology based on geometrical resemblance is proposed for the preform design in forging and extrusion processes. In order to verify this preform design methodology, several case studies on forging and extrusion processes have been carried out. The methodology has been proven to be computationally efficient since it requires fewer numbers of iterations. Experimental verification was also carried out for the Axisymmetric Rib-web part, which showed results similar to those obtained via the finite element method.

PHASE II

PREFORM DESIGN FOR TUBE HYDROFORMING PROCESS

RESEARCH APPROACH AND TASKS IN PHASE II

In order to develop a preforming process for THF, the tubular parts applicable to axisymmetric wrinkle formation are first classified and identified. Then, the material model suitable for full strain range is developed which will be used in the analysis of the wrinkle evolution in the THF process. Then an analytical model of plastic wrinkle is used to study the wrinkle formation characteristics in the THF process. In this model, the tube deformation process before wrinkle onset is modeled based on J2 plastic flow theory, while the critical condition check for wrinkle onset is computed on J2 deformation theory. After wrinkle onset, the wrinkle evolution is modeled through post buckling analysis. With the guidance from analysis results of the analytical model, a preforming scheme is proposed to accumulate the material in the forming zone based on the wrinkle formation, which can be flattened by the higher pressure in the final THF process. The preforming scheme based on the wrinkle formation is used in the tube bulging process to investigate the effect of the process variables such as material hardening coefficient, tube thickness and tube length on the formability of THF through parameter studies. Finally, an experiment is designed to verify the developed preforming scheme. To accomplish the objectives for this phase II, six tasks are carried out as outlined in Fig.II-1.

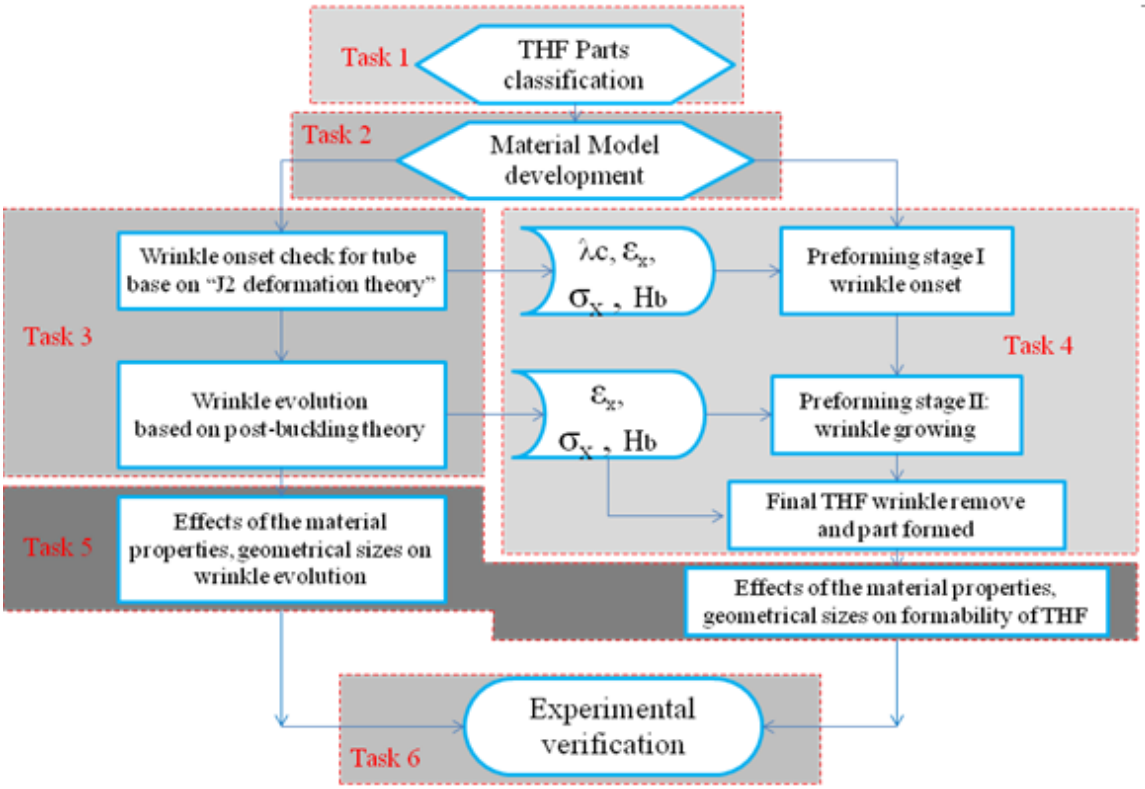

Fig.II- 1 Research approach in Phase II

Task 1: THF part classification

The parts formed by the THF process most have an oblong shape on which the two dimesion sizes of the cross section are significantly less than the longitudinal size of the part. According to the subsidiary feature, the tubular parts can be classified into three major groups:

1) Oblong shape with unilateral feature, such as T shape and Y-shape.
2) Oblong shape with axisymmetric feature, such free bulge shape.
3) Oblong shape with varying cross sections.

During the preforming stage, wrinkles are formed to accumulate material in the forming zone to improve the formability of the final THF process as shown in Fig.II-2 and

Fig.II-3. Fig.II-2, shows a tubular part with length L ,die span L_s ,initial radial R and profile radius R_i. If the wrinkle formation is used in the preform stage, the part profile should contain the space as shown in Fig.II-2 to accomodate the axiymmetric wrinkle growth. The wrinkle growing space has a maximum radius R_L, which can determine the maximum wrinkle growth.

Tab.II- 1 Tubular part classification

Tube with Unilateral Feature	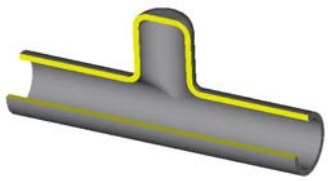	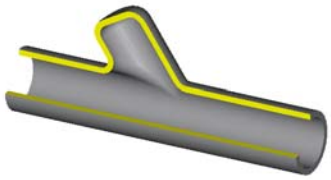
Tube with Rotationary Sysmmeric Feature,	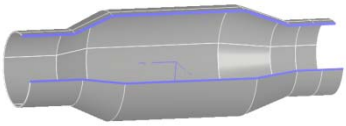	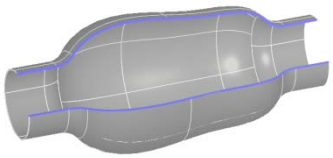
Tube with Varying Cross Sections	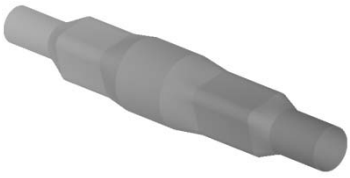	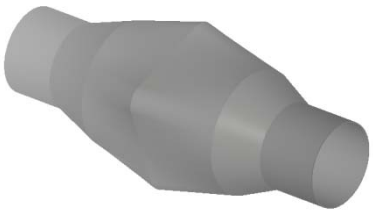

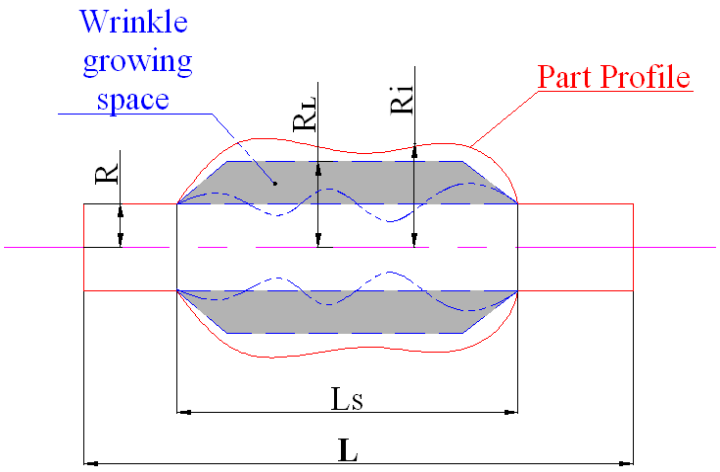

Fig.II- 2 Part profile allowing wrinkle growing fully in the forming zone

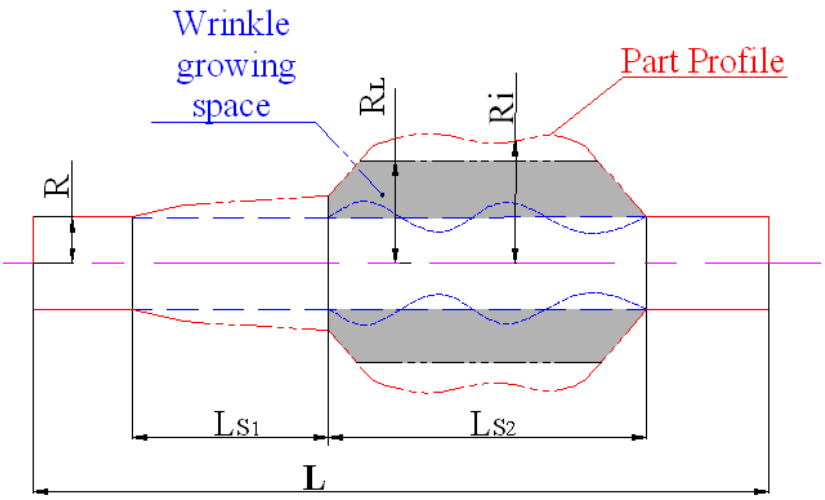

Fig.II- 3 Part profile allowing wrinkle growing in the local forming zone.

Fig.II-2 and Fig.II-3 show two kinds of part profiles. The profile of the part in Fig.II-2 varies gradually and allows wrinkle growing fully along all the die spans. However, the part profile in Fig.II-3 changed rapidly and zone L_{s2} needs more material to be accumulated to form bigger bulge compared to zone L_{s1}. Both of these two figures show that the part profile should contain a rotationary axisymmetric space which allows the

axisymmetric wrinkle be to formed in the preform stage. According to the tubular part classificaton, the tubular part with rotationary feature or with varying cross section can contain a rotationary wrinkle growing space. Thus the wrinkle-formation preforming stage can be applied to the tubular part group 2 or 3. Group 1 has a unilateral feature and the part profile does not contain rotationary axiymmetric space, thus no wrinkle can be formed in the preforming stage to accumulate material.

Task 2: Material model development

Currently, both Ramberg–Osgood equation and power law material model do not fit the stress-strain curve in the full range. Thus a piecewise function was developed to fit the stress-strain curve in full range. The detailed material model can be found in chapter 4.

Task 3: Analytical model development for wrinkle onset and evolution

In this task, an analytical model of plastic wrinkle is used to study the wrinkle formation characteristics in the THF process. In this model, the tube deformation process before wrinkle onset is modeled based on J2 plastic flow theory, while the critical condition check for wrinkle onset is computed on J2 deformation theory. After wrinkle onset, the wrinkle evolution is modeled through post buckling analysis. The detailed analytical model can be found in Chapter 5.

Task 4: Preform design based on the wrinkle formation for tube hydroforming process

With the guidance from analysis results of the analytical model, a two-stage preforming process based on wrinkle formation is developed for the tube hydroforming process to accumulate material in the forming zone, thus reducing the thinning rate and improving the formability. In preforming stage one, the wrinkle onset is triggered with limited axial

compression. In preforming stage two, the wrinkle grows stably and uniformly to a certain height. Then the preformed wrinkles are flattened to conform to the die shape in the final tube hydroforming process. The detailed preforming scheme can be found in Chapter 5.

Task 5: Investigation of the effect of process variables on the formability of THF

The preforming scheme based on the wrinkle formation is used in the tube bulging process to investigate the effect of the process variables such as material hardening coefficient, tube thickness and tube length on the formability of THF through parameter studies. The detailed investigation can be found in Chapter 6

Task 6: Experimental verification

In this task, the two-stage preforming scheme was verified by three bulging experiments with preforming wrinkles, where SS 304 tubing and Al 6061 tubing were used. The experimental detail can be found in Chapter 7.

CHAPTER 4: MATERIAL MODEL

4.1 Material model and their limitations

The common material model used in the buckling analysis in the steel structure design is the modified Ramberg–Osgood equation as shown equation (4.1), which is suitable for the small strain range. However, in the metal forming process, deformation of the material can reach high strain level such as 0.2 ~1.0, where the Ramberg-Osgood equation does not fit the stress-strain curve. Usually the power law (Eq.4.2) can fit the stress-strain curve better in the high strain range.

$$\varepsilon = \frac{\sigma}{E}\left(1 + \frac{3}{7}\left(\frac{\sigma}{\sigma_y}\right)^{n^*-1}\right) \tag{4.1}$$

The variables E, σ_y, and n* in equation 4.1 represent Young's Modulus, yield stress and plastic hardening related parameter respectively.

$$\sigma = K\varepsilon^n \tag{4.2}$$

The constants K and n in equation 4.2 represent material strength coefficient and strain hardening exponent respectively.

4.2 Triple piecewise material model

In order to accurately predict initiation of tube wrinkles as well as wrinkle growth, a material model that can handle both low and high strain range is necessary.

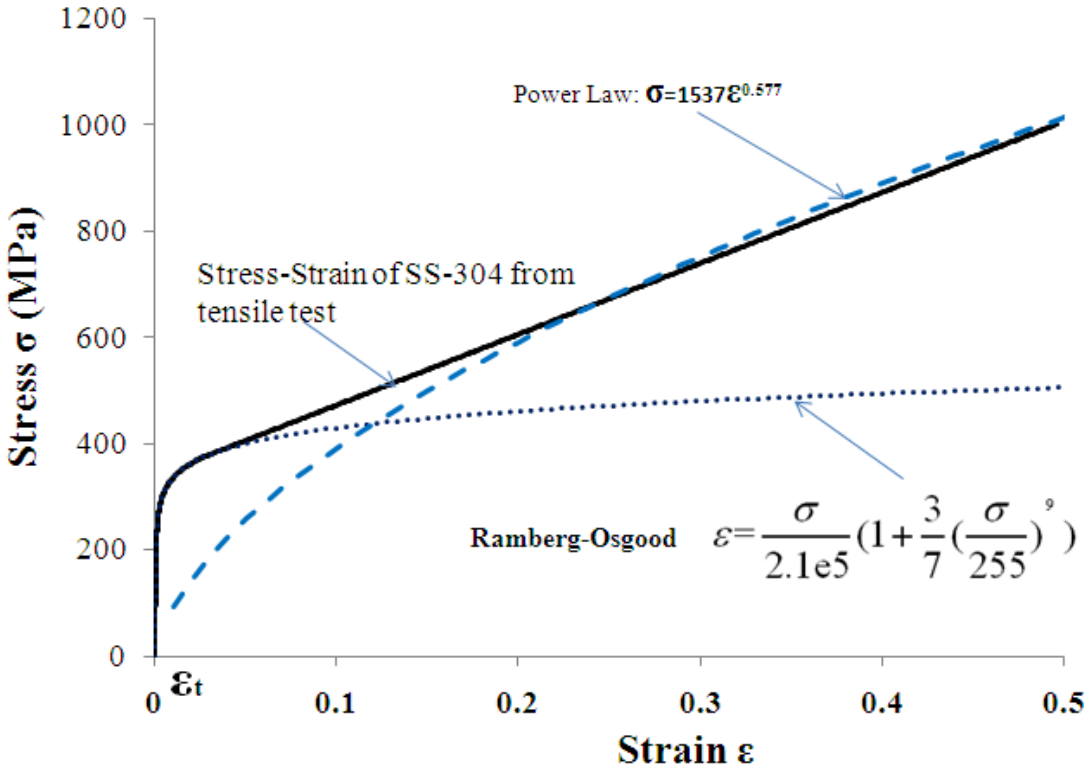

Fig.4- 1 Stress-strain curve of SS 304

Fig.4-1 shows the stress-strain curve of a SS 304 tube. As shown in the Fig.4-1, the RO model fits the stress-strain curve very well in the range of 0.0 ~ 0.1, while the power law model fits the high strain range from 0.2~0.5 well. Thus, a material model for full strain range is required. Here, a triple piecewise material model is proposed as shown in equation 4.3. In the small strain range of 0 ~ ε_t, the RO model is used to fit the stress-strain curve, while the power law is used in the high strain range of 0.2 and above. A linear model is used to connect the RO model and power law model in such a way that the line is tangential to the RO curve and pass through a strain of 0.2 on the power law curve.

$$\begin{cases} \varepsilon = \dfrac{\sigma}{E}(1+\dfrac{3}{7}(\dfrac{\sigma}{\sigma_y})^{n^*-1}) & \varepsilon \le \varepsilon_t \quad RO \quad Model \\ \varepsilon = \varepsilon_t + \dfrac{\sigma - \sigma(\varepsilon_t)}{Slp(\varepsilon_t)} & \varepsilon_t < \varepsilon < 0.2 \quad Linear \quad Model \\ \sigma = K\varepsilon^n & \varepsilon \ge 0.2 \quad Power \quad Law \quad Model \end{cases} \tag{4.3}$$

Where (ε_t ,σ_t) is the transition point between the linear model and the RO model. Slp, is the slop of transition point at RO model curve. And it can be computed as:

$$p(\varepsilon_t) = \frac{E}{(1+\dfrac{3}{7}n^*(\dfrac{\sigma_t}{\sigma_y})^{n^*-1})} \quad or \quad Slp(\varepsilon_t) = \frac{\sigma_{0.2} - \sigma_t}{\varepsilon_{0.2} - \varepsilon_t} \tag{4.4}$$

Tab.4- 1 Fitted material parameters of SS 304 and Al 6061

Material Properties	SS 304	Al 6061
Young's Modulus *E* (GPa)	205	69
Yield Stress σ_y (MPa)	255	55
n^*	10	9
strength coefficient *K* (MPa)	1527	152
Strain hardening exponent *n*	0.577	0.162
ε_t	0.029	0.20
Poisson Ratio *v*	0.30	0.33

In order to study the influence of the material hardening exponent n on the tube formability, a family of curves based on this material model are generated by changing the strain hardening exponent n and n*. As a case study to show how this model is utilized, SS 304 material with strain hardening exponent n=0.57 is used together with assumed material with lower strain hardening exponents. The following assumptions are used:

1) Family curves have the same young's modulus E as SS 304,
2) Family curves coincide at the same point where the strain level is 1%.
3) The upper bound curve has n=0.577, and n*=10 , while the lower bound curve has n=0.043, and n*=34

An algorithm to determine the hardening exponent n assuming n* is known was developed. The algorithm procedures are given below.

1) According to the assumption (a), (b), the yield stress σ_y can be computed based on the RO model equation (4.1).
2) The upper-bound curve has transition point (ε_{t1}, σ_{t1}) , while the lower bound curve has a transition point (ε_{t2}, σ_{t2}). Assuming the transition point of the family curves are linearly changing from (ε_{t1}, σ_{t1}) to (ε_{t2}, σ_{t2}) (Tangential points line shown in Fig.4-2), when the parameter n* is changed from 10 to 34, then the transition point (ε_t, σ_t) can be obtained once the n* is defined.
3) Once the transition point (ε_t, σ_t) is determined, all the parameters of the linear model can be computed. The linear section spans from transition point to the point of strain level 0.2.
4) Above the strain level of 0.2, the material model is described by the power law model. The parameters of the power law model is found by fitting power law curve through three sampling points which are extrapolated from linear model at three strain level

0.2, 0.4 and 0.6 respectively

By this algorithm, family curves with changing n* from 10 to 34 are obtained and the corresponding strain hardening exponent n can found by the fitting algorithm. Fig. 4-2 show several curves with different strain hardening exponent n. One characteristic of the family curve is that the parameter n* decreases with the increase of the strain hardening exponent n. This characteristic can be found on the SS 304 and Al 6061.

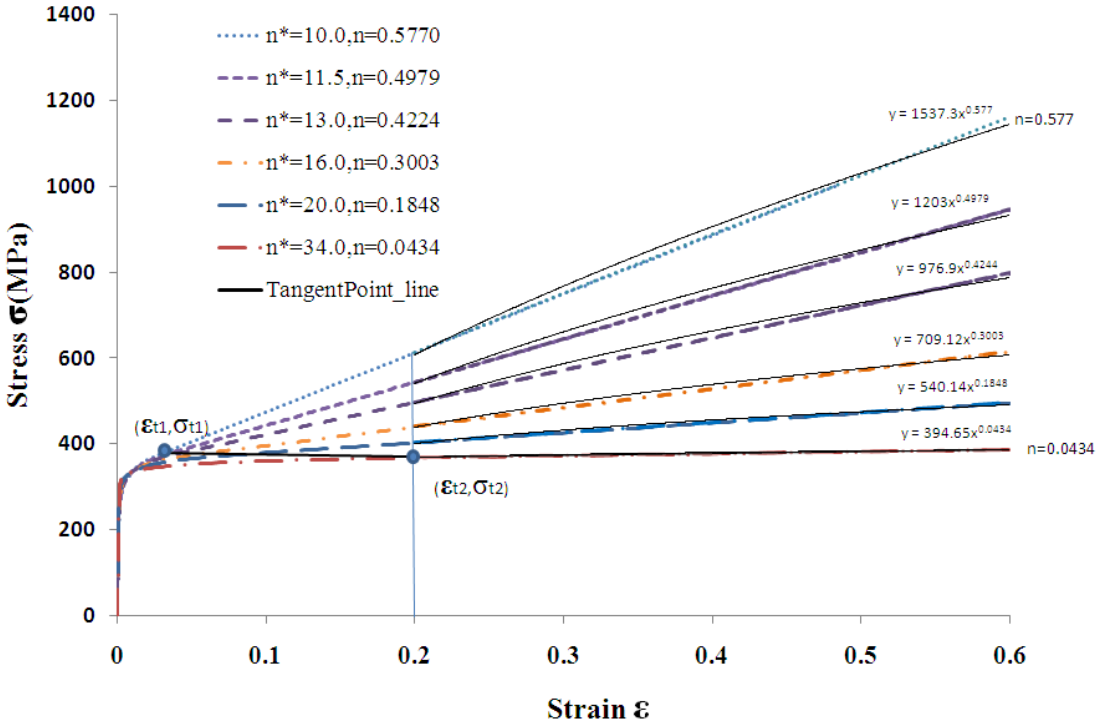

Fig.4- 2 Family curves

4.3 Conclusions

A triple piecewise material model for full range was developed which can be used in the analysis of wrinkle onset and wrinkle growth. A family of curves based on this model was generated by changing the strain hardening exponent n, which can be used to study the effect of the strain hardening exponent on the tube formability.

CHAPTER 5: PREFORM DESIGN BASED ON WRINKLE FORMATION FOR THF PROCESS

5.1 Analytical modeling of the wrinkle evolution

In order to study the wrinkle characteristics in the tube hydroforming process, an analytical model based on the post buckling analysis of the circular tube under internal pressure and axial compression is used to model the wrinkle evolution process. The model used in this study is based on the work of Bardi, et al.**[59-63]**. The tube (Fig.5-1) subject to internal pressure and axial compression (Equation 5.1) expands in the radial direction and contracts in the axial direction uniformly before wrinkle onset. The uniform deformation process can be modeled by J2 flow theory (see section 2.2.3). During the uniform deformation process, the wrinkle will be triggered once the wrinkle onset condition (equation 5.2) is satisfied

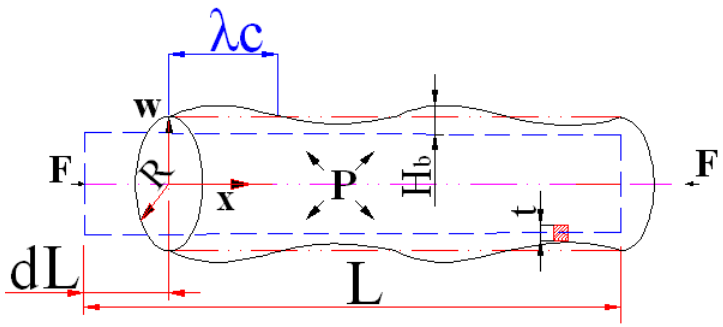

Fig.5- 1 Wrinkled tube

$$\Delta = \frac{dL}{L} \times 100\% \tag{5.1}$$

$$\sigma_c = \left(\frac{C_{11}C_{22} - C_{12}}{3} \right)^{1/2} \left(\frac{t}{R} \right) \tag{5.2}$$

$$\lambda_c = \pi \left(\frac{C_{11}^{\ 2}}{12(C_{11}C_{22} - C_{12}^{\ 2})} \right)^{1/4} (Rt)^{1/2} \tag{5.3}$$

Where: σ_c is critical stress, λc is half wave length and C_{ij} is constitutive matrix elements of "J2 deformation theory". After wrinkle onset, the wrinkle grows with continual axial compression. The half wave length of the triggered wrinkle can be computed through equation (5.3). Wrinkle growth can be modeled by the post buckling analysis by assuming initial tube geometrical imperfection (equation5. 4) and sinusoidal wrinkle pattern (equation 5.5).

$$\overline{w} = -tw_o \cos\left(\frac{\pi x}{\lambda_c}\right) \tag{5.4}$$

$$w = a_0 + \sum_{i=1}^{Nw} a_i \sin\left(\frac{i\pi x}{\lambda_c}\right) \tag{5.5}$$

Where: $\overline{w}$ is geometrical imperfection, w_0 is the imperfection factor and, w, is the radial displacement. According to the wrinkle pattern (equation5.5), the wrinkle growth height can be calculated as equation (5. 6).

$$H_b = |a_0| + \sum_{i=1}^{Nw} |a_i| \tag{5.6}$$

Where: a_i is the amplitude of the sinusoidal function in the wrinkle pattern equation.

Detail information of the analytical model can be found in appendix. Based on the analytical model for the plastic wrinkle evolution in the appendix, the state variable, such as critical axial stress σ_c , critical strain ε_c and half wave length λ_c, axial stress σ_x, hoop stress σ_θ, axial stress resultant N_x, hoop stress resultant N_θ, and the wrinkle height H_b can be obtained by the computation procedure given in Fig.5-2 and briefly discussed below.

1) Before the wrinkle onset, the tube is deformed uniformly under imposed axial strain ε_x and internal pressure P. This deformation process can be modeled incrementally by J_2 flow theory equation (A6)
2) During the iterative solution of the uniform deformation process, the critical condition of plastic wrinkle onset is checked in every iteration step based on the critical stress σ_c condition in equation (A7). The critical stress σ_c is computed and is compared to the axial stress σ_x of the uniform deformation process.
3) If the critical stress σ_c is equal to the axial stress σ_x of the uniform deformation process, then the wrinkle starts and output critical axial stress σ_c , critical strain ε_c and half wave length λ_c Otherwise, go back to step 1 where computation of uniform deformation process takes place.
4) Once the wrinkle starts, the computation of the wrinkle growth begins. The first step is to set the imperfection level based on the equation (A9) and the maximum axial strain ε_{xmax}
5) Continuously imposing the increment of average strain db_0, compute the displacement coefficient vector increment $\boldsymbol{dq}$ based on the equilibrium equation (A13). Then the displacement coefficient $\boldsymbol{q}$ can be obtained from equation (A16). After the displacement coefficient $\boldsymbol{q}$ is known, the wrinkle height H_b can be computed from equation 6.6

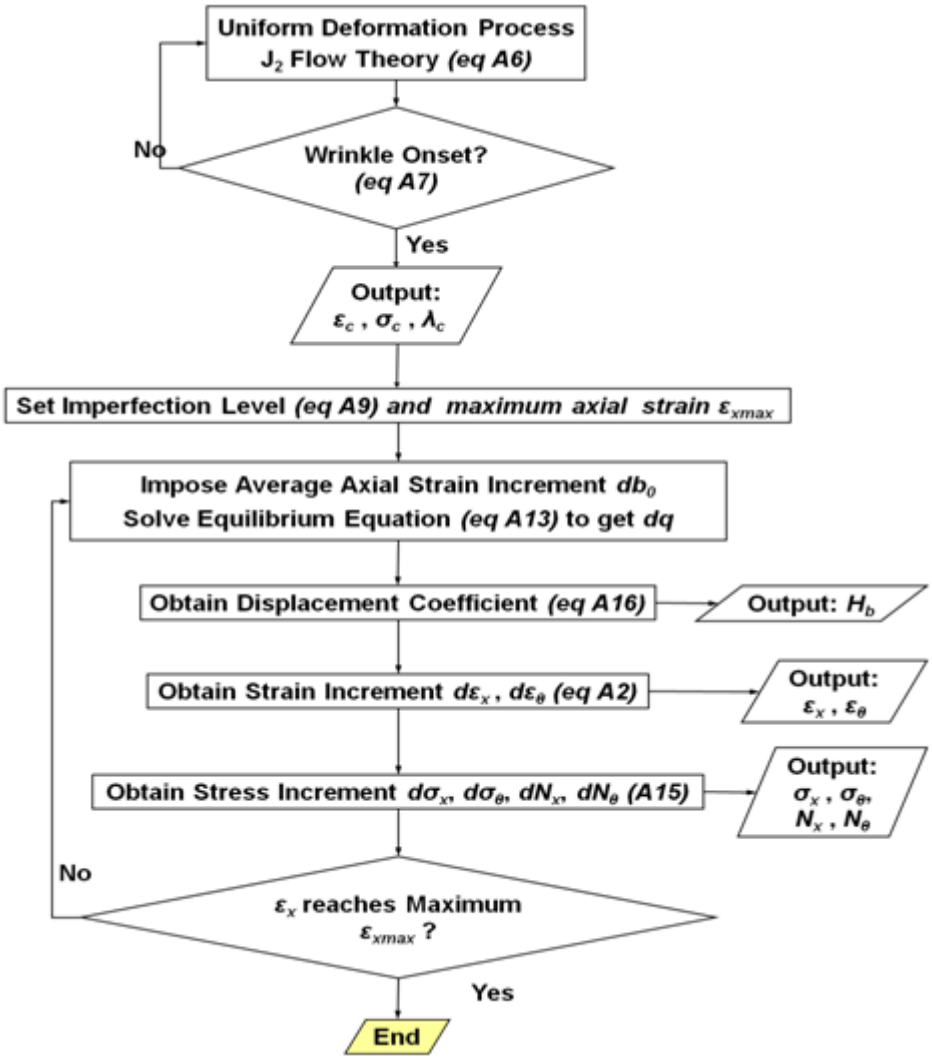

Fig.5- 2 Flow chart for computing state variables for the wrinkle evolution process

6) After dq is known, the strain increment $d\varepsilon_x$, and $d\varepsilon_\theta$ can be computed based on equation (A2). The total strain ε_x and ε_θ can be obtained by summing all the strain increment.

7) Then the stress increment $d\sigma_x$, $d\sigma_\theta$, and stress resultant increment dN_x, dN_θ can also be computed based on equation (A15). The total stress and stress resultant can be obtained by summing all the stress increment, and stress resultant increment respectively.

8) If the axial strain ε_x reaches the maximum ε_{xmax}, go to end. Otherwise, go back to step 4 for wrinkle growth computation of next iteration step.

Based on the analytical model discussed above, a program module was developed to compute the wrinkle evolution process, which is illustrated in Appendix B. Fig.5-3 shows a typical axial stress response of a wrinkled tube. According to the axial stress response curve, the wrinkle evolution process can be divided into three stages

1) Wrinkle onset at the critical axial strain ε_c:

   From the start of the compression to the wrinkle onset, the tube is deformed uniformly in the longitudinal direction and the radial direction. Once the wrinkle starts, the rigidity of the tube in the longitudinal direction will start to decrease.

2) Wrinkle growing:

   With further compression, the wrinkle will grow and the axial rigidity continue to reduce and finally the axial load will reach maximum at the limit strain ε_L

3) Wrinkle collapse at the limit strain ε_L:

   Once the axial load reaches maximum at the limit strain ε_L, the axial load will start to drop and the wrinkle will start to collapse.

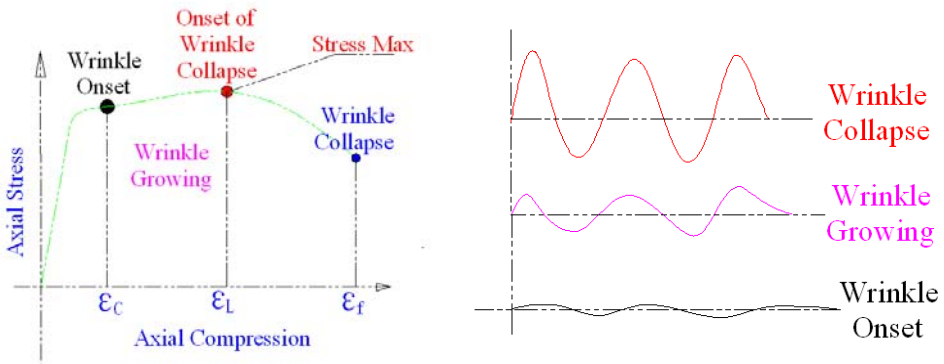

Fig.5- 3 Wrinkle evolution stage

This analytical model is capable of providing conditions for the initiation of wrinkles on a tubular structure that is subjected to axial compression and internal pressure. The variables of interest for the design of THF preform include half wave length λ_c, wrinkle growth height H_b, and critical strain ε_c. Critical strain refers to the minimum axial strain that will initiate a wrinkle as a function of tube internal pressure. Once the wrinkle has been initiated, other strategies are needed to control uniform growth of wrinkles since any further compression will collapse the wrinkles. Thus, control of wrinkles is carried out by constraining the boundary, as discussed in the next section.

5.2 The effect of the pressure on the wrinkle evolution characteristics

To design a THF preforming operation using wrinkle formation requires establishing (a) number of wrinkles that can be generated, (b) size of wrinkles, and (c) strategies for the control of wrinkle growth during hydroforming. All these aspects are related to internal pressure, axial compression, tube size, and material properties. The effect of pressure on wrinkle formation was investigated for SS 304 tubing by using the analytical model and finite element analysis (FEA). The material properties of the SS 304 are listed in the Tab.4-1 and the geometrical size of the tube is listed in the Tab.5-1. The imperfection factor used is 0.5%. Three different pressure levels P=0.0, P=10MPa and P=20 MPa were used.

Tab.5- 1 Geometrical sizes of the SS 304 tube

Outer Diameter D (mm)	34.95
Thickness t (mm)	1.65
Tube Length L(mm)	120

Fig. 5-4 and Fig. 5-5 show the influence of internal pressure on the half wave length obtained from the analytical model and FEA, respectively. Figure 5-4 shows that the half wave length λ_c increased from 8.4 mm to 12.3 mm when the internal pressure increased from 0 to 20 MPa. Fig. 5-5 shows that the half wave length under the three pressure conditions obtained from FEA simulation in Abaqus agree very well with the half wave length computed from the analytical model. The effect of pressure on wrinkle length is significant and determines the number of wrinkles that can be obtained. This is an important parameter in preform design. Under the tested conditions, wrinkle lengths of 18 mm, 23 mm, and 27 mm were obtained at pressures of 0 MPa, 10 MPa, and 20 MPa, respectively. Very small wrinkle heights were obtained of the order of 0.2 mm~0.35 mm (Fig. 5-5). Both the analytical model and FEA analyses showed that a wrinkle can be triggered at small axial compression. FEA showed that any further compression results in localization of some wrinkles and ultimate collapse. Fig.5-6 shows the effects of pressure on critical strain, which is the strain at which wrinkles can form. Critical axial strain increased from 1.6% to 2.3% when internal pressure increased from 0 to 20 MPa.

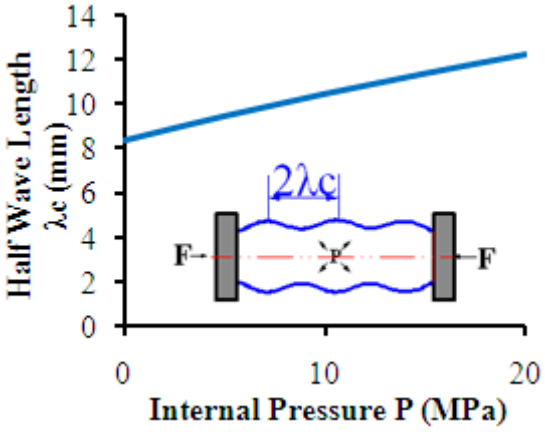

Fig.5- 4 Half wave length from analytical model

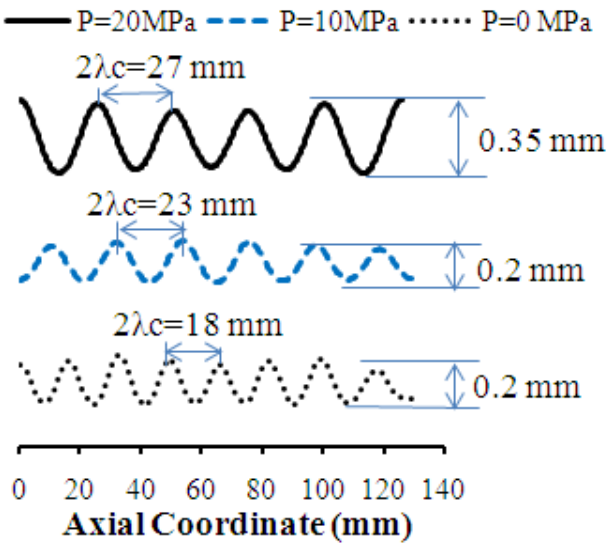

Fig.5- 5 Half wave length from FEA

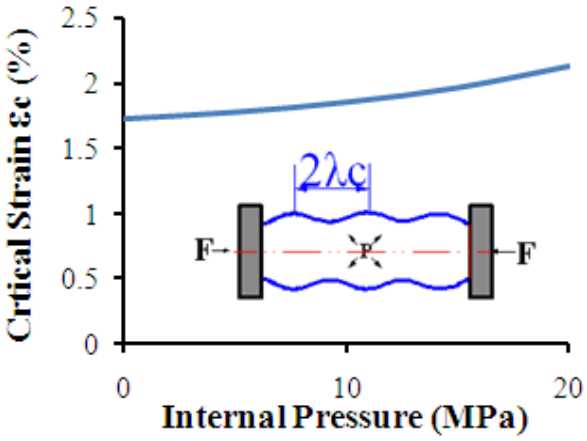

Fig.5- 6 Critical strain Vs internal pressure (constant pressure profile)

As discussed above, the analytical model can provide useful information for initiating wrinkles. On the other hand, it will be extremely difficult to determine wrinkle initiation by trial-and-error FEA iteration. In other words, after the initial wrinkle conditions are known from the analytical model, FEA can be employed in the preform design process. The strategy adopted in this study to control wrinkle growth is to constrain the outer tube

boundary by a die to allow wrinkles to grow to a much greater height, as shown in Fig. 8. Fig. 5-7 shows FEA simulation of axisymmetrical wrinkle growth inside the die with three internal pressure levels. The die cavity radius is 1.5 mm greater than the tube radius 17.5 mm, and the die cavity length L is 136 mm. The tube material is same as that used in the analytical model (Fig.5-5). Wrinkle amplitudes under pressures of 0 MPa, 10 MPa, and 20 MPa are 1.5mm, 1.2 mm, and 1.0 mm, respectively, which are significantly greater than one without control shown in Fig. 5-8. Thus wrinkle growth under die constraint is critical in determining the preform stages, as discussed in section 5.3.1.

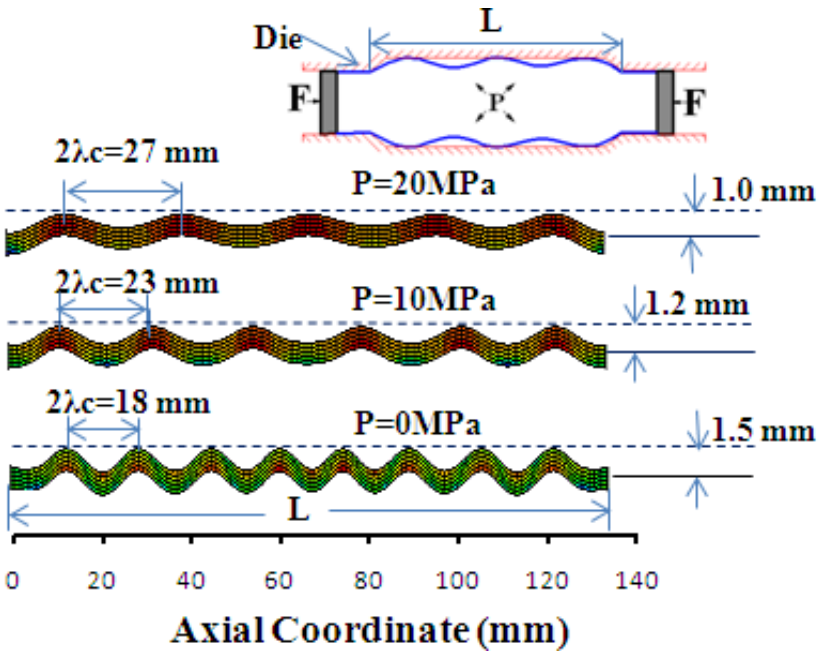

Fig.5- 7 Wrinkle development with die constrains

Due to the different wrinkle wave lengths triggered under different internal pressures, wrinkle evolution characteristics such as axial response and wrinkle growth height H_b vary. Fig. 5-8 shows the effect of pressure on wrinkle growth height. Wrinkle heights obtained from FEA are also shown in Fig.5-9. These wrinkle heights were obtained by

constraining the tube with a die for three pressure levels: P=0 MPa, P=10 MPa, and P=20 MPa. After wrinkle onset, the wrinkle starts to grow at the half wave length λ_c. Due to different half wave length λ_c, wrinkle growth height H_b develops differently for different pressures. Fig 5-10 shows the wrinkle growth height development with four different pressure profiles. Profiles with name of "P=0 Mpa" and "P=20Mpa" mean pressures are constant, while those with name of "P=0-20Mpa" and "P=20-30Mpa" mean that wrinkle onset pressures are at the level of first value (0 Mpa for "P=0-20Mpa" , 20 MPa for "P=20-30Mpa" respectively), then, pressures increase to the level of second value after wrinkles onset (20 Mpa for "P=0-20Mpa" , 30 MPa for "P=20-30Mpa" respectively). It can be seen that wrinkle-growth-height differences between constant pressure profiles and increasing pressure profiles after wrinkle onset are insignificant. Therefore pressure used after wrinkle onset has minor effect on wrinkle growth. Thus, wrinkle growth height H_b under constant pressure can be used to guide the preforming die shape design, even if the pressure used after wrinkle onset differs from the pressure used during wrinkle onset.

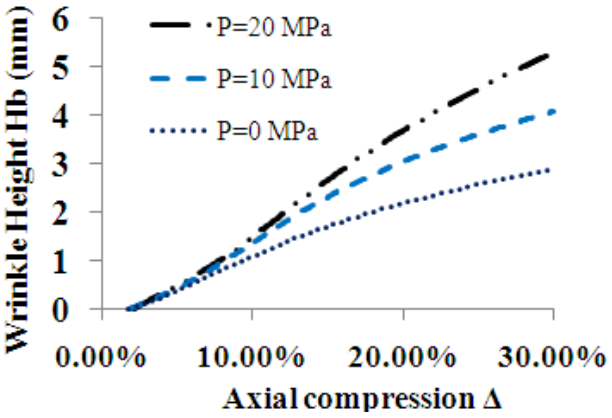

Fig.5- 8 Wrinkle height from analytical model

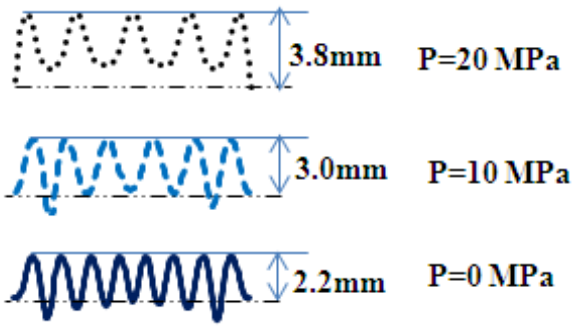

Fig.5- 9 Wrinkle height at 20% compression from FEA

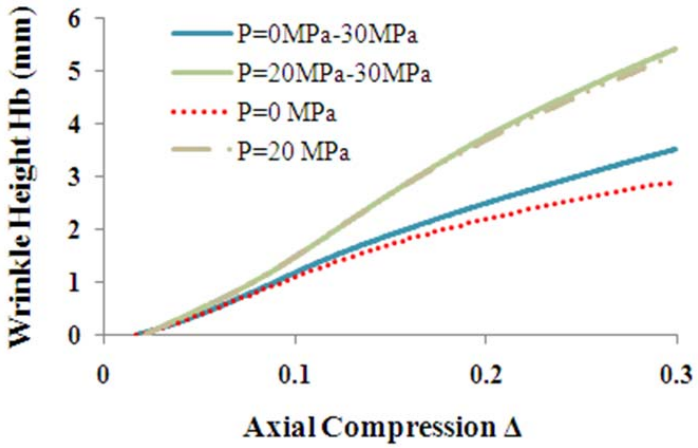

Fig.5- 10 Wrinkle growth height Vs axial strain at different pressure profile

Fig. 5-11 shows axial stress development during axial compression with different internal pressure levels. The higher the internal pressure, the lower the axial stress on the wrinkled tube in the initial compression range. With the increase in axial compression, the difference between the axial stresses under different pressures vanishes, as shown in Fig. 5-11. This suggests that internal pressure is critical for the determination of half wave length and the corresponding axial rigidity during wrinkle onset. The analytical results (Fig.5-12) also show that tube initial imperfection w_0 has negligible influence on wrinkle growth height H_b.

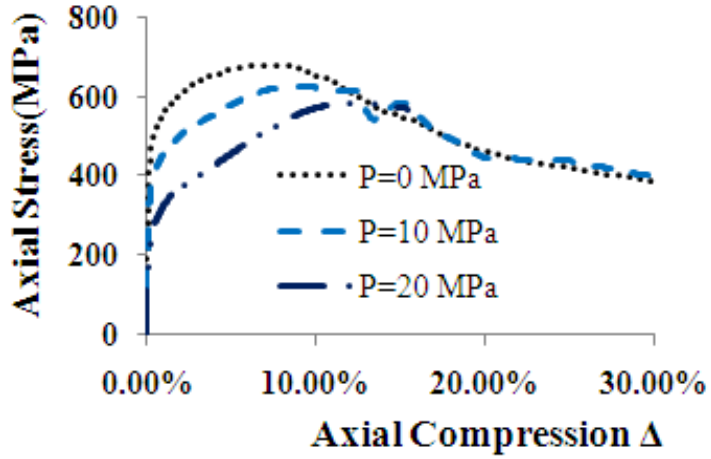

Fig.5- 11 Axial stress Vs axial compression under different pressure

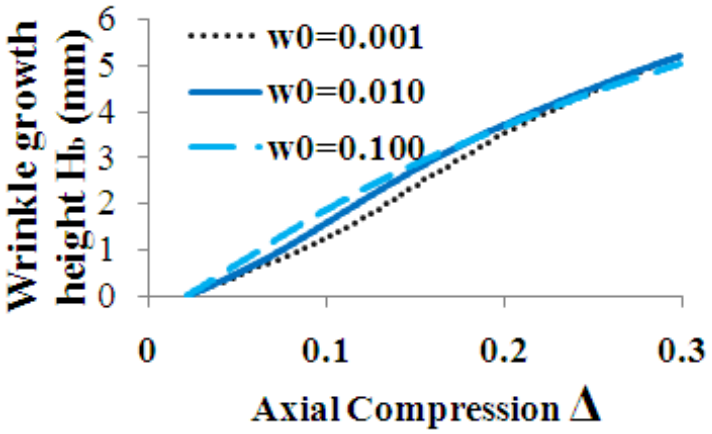

Fig.5- 12 Axial stress Vs axial compression under different pressure

5.3 Preforming based on the wrinkle formation in THF process

Wrinkle evolution in the tubular structure has three stages: wrinkle onset, wrinkle growth, and wrinkle collapse **[59].** When the tube is subject to axial load and internal pressure,

wrinkle onset is triggered at low axial strain. Then the wrinkle uniformly grows to its limiting state, where maximum axial load is reached. After reaching its limiting state, the wrinkle starts to collapse or localize. Thus, the limiting state is considered the failure of the tubular structure. However, in the THF process, wrinkle evolution is allowed to exceed the limiting state as long as the wrinkle is removable at the end of the process, because the axial compression is displacement-controlled, the capacity of the load-carrying just starts to decrease after the limiting state, and the tube still has some capacity to carry load.

Fig.5- 13 (a) Non-axisymmetric wrinkle (b) Localized wrinkle [16]

In this work, two kinds of wrinkles are considered as failure: non-axisymmetric wrinkle and wrinkle localization (Fig. 5-13). During wrinkle evolution, insufficient internal pressure can result in an un-axisymmetric wrinkle **[59]**, whose evolution is difficult to control. Thus, the un-axisymmetric (Fig. 5-13a) wrinkle should be avoided, which can be ensured by properly increasing the internal pressure. During the free growth of the wrinkle, wrinkle 2 localizes (Fig. 5-14a) due to initial tube imperfection. With continued compression, localized wrinkle 2 forms a folding (Fig. 5-14b) soon after wrinkle localization. The folding is difficult to remove by high pressure and should be avoided in the THF process. But if wrinkle growth height is constrained, the growth height of localized wrinkle 2 (Fig. 5-15c) will not lose its axial rigidity. Then, the constrained wrinkle 2 still has enough axial rigidity to deliver the axial compression force to wrinkle

1 or wrinkle 3, which leads to uniform wrinkle growth in all three wrinkles (Fig. 5-14d). In order to achieve balanced growth among wrinkles and to prevent the wrinkle from localization, a two-stage wrinkle preforming (Fig.5-15) is proposed to cause the material to be accumulated in the die cavity. The first stage of the preforming is to trigger wrinkle onset, and the second stage is to let wrinkle grow stably and evenly without folding. Then, the material accumulated in the die cavity will be expanded to conform to the die shape in the final THF process.

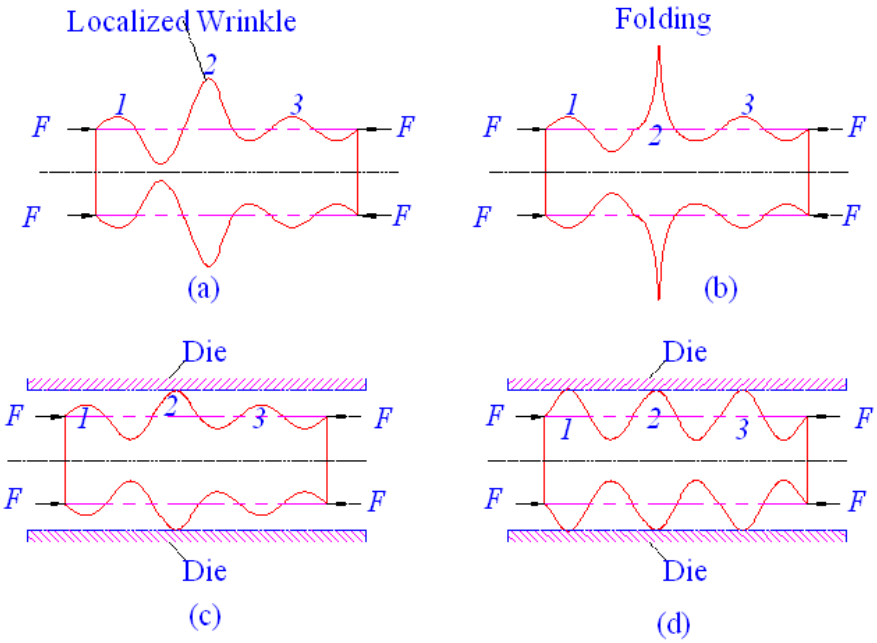

Fig.5- 14 Free wrinkle growth and constrained wrinkle growth in the die

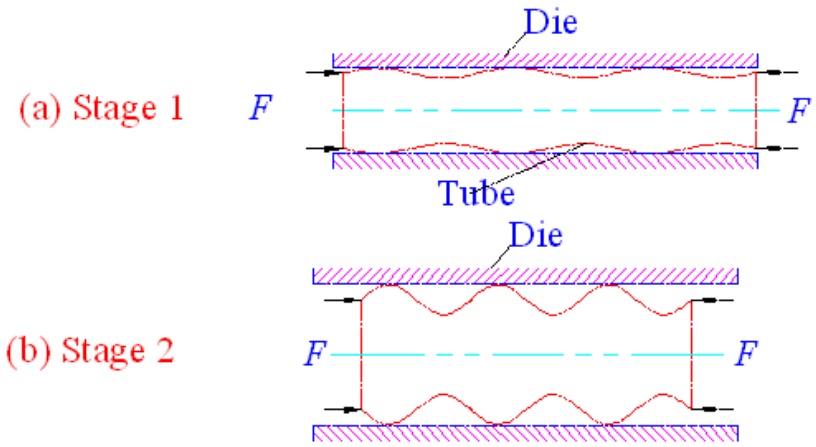

Fig.5- 15 Two-stage preforming to generate uniform wrinkle

5.3.1 Process design for the preforming stage I

The process design of the preforming stage includes die shape design, internal pressure determination, and axial feeding determination. During tube compression in the axial direction, the end wrinkle (Fig. 5-16a) occurs prior to the middle wrinkle's formation, due to the geometric constraint at the end of the guiding zone. Then the end wrinkle grows faster than the middle wrinkle and localizes to form un-removable folding with further axial compression. Therefore, the growth of the end wrinkle is expected to be limited during the preforming stage and leave enough axial rigidity for the axial feeding during the final THF process. Thus the preforming die (Fig.5-16b) is designed such that the growth of the end bulge is constrained and the middle wrinkle can grow higher than the end bulge, which will lead to a balance between the middle wrinkle's growth and end wrinkle's growth in the final THF process. The preforming process has two stages: wrinkle onset and wrinkle growth. During the initial axial compression, the internal pressure is kept lower to facilitate wrinkle occurrence while growth of the end wrinkle is constrained to R_1. During the wrinkle growth stage, the middle wrinkle grows to a height

of R_2, whereas the end bulge is still limited to R_1. The axial feeding, internal pressure, and die size in the preforming stage will be discussed next.

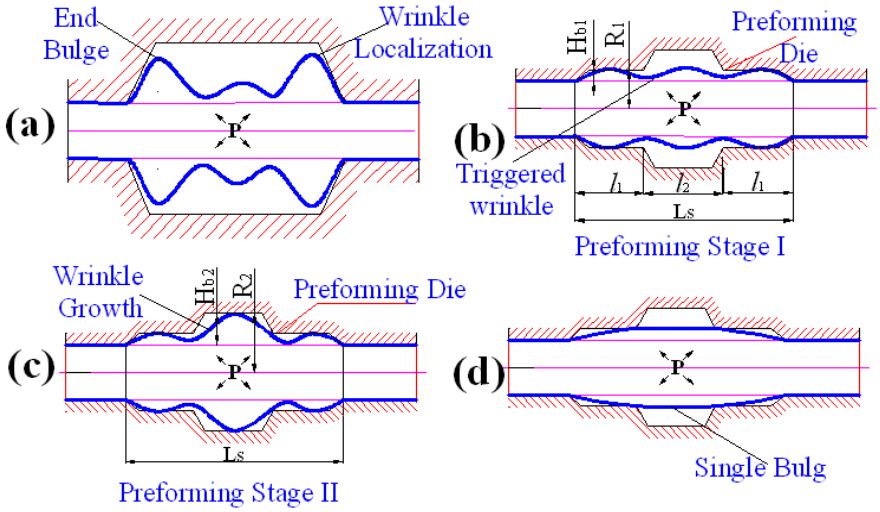

Fig.5- 16 The end bulge and preforming stage 1

According to the previous discussion, the plastic wrinkle on a tube can be triggered at small axial compression. Thus, the space on the die used to accommodate the initial wrinkle can be relatively small. Here, the dimension R_1 for wrinkle growth space (Fig. 5-16b) in preforming stage I can be just 1~4 mm greater than the blank tube radius. During wrinkle onset, axial compressive stress should play the major role to yield the tube and form the wrinkle, while the internal pressure should not exceed the pressure yielding the tube. Excessive pressure can cause a single bulge (Fig. 5-16d) and suppress the axisymmetric wrinkle. Normally, the pressure P_1 in preforming stage I for wrinkle onset can be estimated by using the equation below.

$$P_1 = f\sigma_y \frac{t}{R} \tag{5.7}$$

Where; σ_y is the yielding stress and f is a factor from 0 ~1.0 which can be determined through FEA simulations in such a way that the un-axisymmetric wrinkle does not occur.

Once the internal pressure in preforming stage I is selected, the axial feeding amount f_1 in preforming stage I can be determined based on the family of curves (Fig. 5-8) of wrinkle growth height H_b Vs. axial compression. From the curve of H_b Vs. Δ, the axial compression Δ_1 corresponding to the preforming die dimension H_{b1} can be located. Then the axial feeding amount can be computed by equation (5.8)

$$f_1 = \Delta_1 \times Ls \tag{5.8}$$

where Ls is die cavity span length (Fig.5-16.b)

After the internal pressure is selected, the half wave length λ_c can also be determined according to Fig. 5-4. Once the half wave length is known, the size of the preforming die section l_1 used to accommodate the end bulge can be determined to be the same as wave length $2\lambda_c$, as well as the size of the preforming die section l_2 used to accommodate the middle wrinkles can be designed to equal $2m\lambda_c$ (m is number of middle wrinkles). The total wrinkle number during preforming stage I can be computed by equation (5.9):

$$N = \frac{Ls}{2\lambda c} \tag{5.9}$$

5.3.2 Process design for the preforming stage II

In preforming stage II (Fig. 5-16c), the main goal is to accumulate the material in the forming zone through the stable growth of middle wrinkles. The process design of preforming stage II includes die shape design, internal pressure determination, and axial feeding determination. Die cavity height H_{b2} (Fig. 5-16c) should be determined such that the wrinkle with that height still has enough axial rigidity to transfer the compression force to other wrinkles and folding will not occur. Based on the relationship curve of axial stress with axial compression (Fig. 5-11) and the relationship curve of wrinkle growth height H_b with axial compression (Fig. 5-4), the axial rigidity of the desired wrinkle growth height H_{b2} can be evaluated through the following procedure:

1) Select the die cavity height H_{b2} and find the axial compression Δ_2 corresponding to H_{b2} according to Fig. 5-4.

2) Find the axial stress σ_x corresponding to axial compression Δ_2 on Fig. 5-11 to check whether the stress is great enough. If axial stress σ_x is very low or close to zero, axial rigidity must also be very low at the selected die cavity height H_{b2}, which should be reduced to increase axial rigidity.

Once the die cavity height H_{b2} is selected, the axial compression Δ_2 corresponding to H_{b2} can be determined based on Fig.5-4. Accordingly, axial feeding f_2 in preforming stage II can be computed as

$$f_2 = l_2 \times \left(\Delta_2 - \Delta_1 \right) \tag{5.10}$$

The pressure used for preforming stage II needs to be higher than yielding pressure to expand the material and inhibit the hoop wrinkle. The detailed pressure profile in stage II,

which can avoid the un-axisymmetric wrinkle, can be obtained by an iterative FEA procedure.

5.3.3 Process design of the final THF process.

The process design in the final THF process also includes die design and loading path design. The objective of the final THF process is to expand the accumulated material in the forming zone to conform to the die shape. Thus, the die cavity should have the same shape as the desired tubular part. The internal pressure should be high enough to flatten the wrinkled tube and deform the material to conform to the die shape. If the axial rigidity still has a margin for axial feeding, some axial feeding can be applied. The loading path can be obtained by iterating through FEA simulations.

5.3.4 Conclusions

An analytical model was used to study wrinkle onset and wrinkle evolution process in tube hydroforming process. With guidance from the analytical model, a scheme for THF preform design is developed and summarized in Fig. 5-17. The procedure starts with the determination of axisymmetric wrinkle formation and evolution using an analytical model. The analytical model provides information on wrinkle pitch (half wave length), axial compression, and wrinkle growth height to guide the design of the preform die. After the desired wrinkle evolution pattern is initiated, loading path (pressure Vs. axial feed) is then established via iterative finite element simulation. A good loading path for the preform is the path that will not allow formation of hoop wrinkles or folding. The loading path for the final stage is determined such that all wrinkles are removed during the calibration stage.

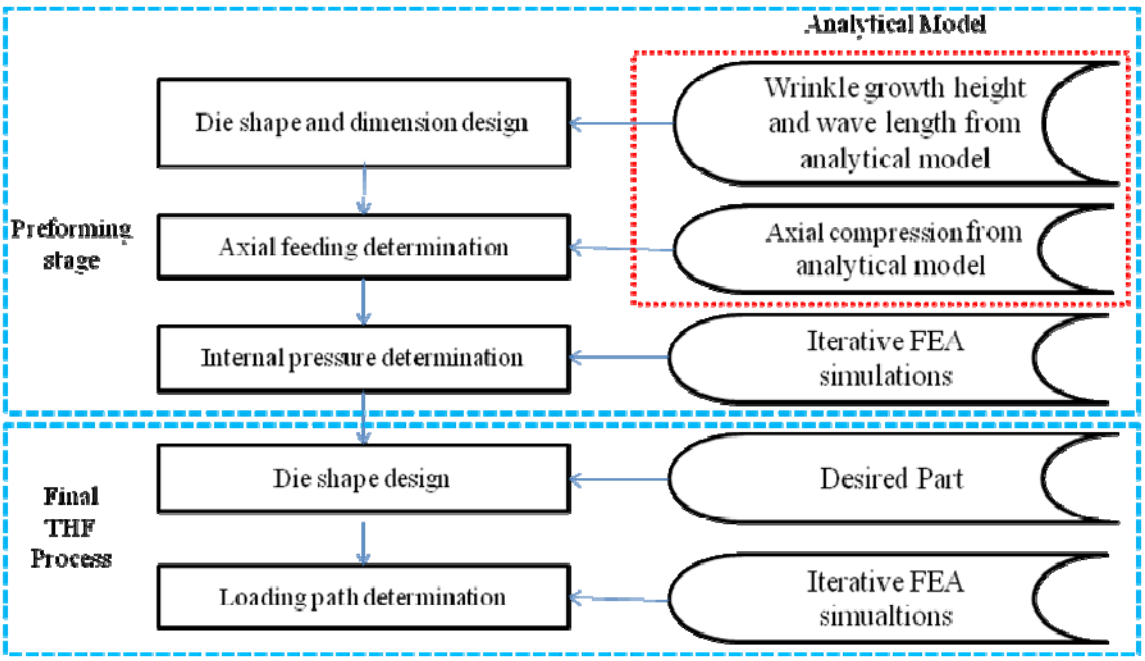

Fig.5- 17 Scheme of the process design in the preforming stage and final THF process

CHAPTER 6: EFFECTS OF THE MATERIAL PROPERTIES AND GEOMETRICAL SIZES ON FORMABILITY DURING THF PREFORMING

In order to investigate the effect of material properties and geometrical sizes on formability during preforming, the analytical model is firstly used to the study the influence of the strain hardening exponent n and tube thickness t on the wrinkle evolution characteristics such as critical strain ε_c , half wave length λ_c, axial stress σ_x, and wrinkle height H_b. Then the proposed two-stage preforming is applied to the tube bulging processes (Fig.6-1) .The parameters used in the study are shown in Tab.6-1, 6-2 and 6-3 respectively. The maximum expansion rates ER achieved in the bulging processes are compared to study the influence of the strain hardening exponent n on the formability. During the studies, the maximum thinning rate of different material are required as a criterion in preforming and bulging process design. Through a series of tube bulging experiments, it was found that the maximum thinning rates of SS 304 tube and Al 6061 tube are 22% and 18% respectively. Thus maximum thinning rate of 20% and 17% which are a little bit less than that obtained from experiments are used as a criterion in preforming and bulging process design. The expansion rate and thinning rate are defined in equation (6.1) and (6.2).

$$ER = \frac{D - D_0}{D_0} \times 100\% \tag{6.1}$$

$$TR = \frac{t_0 - t}{t_0} \times 100\% \tag{6.2}$$

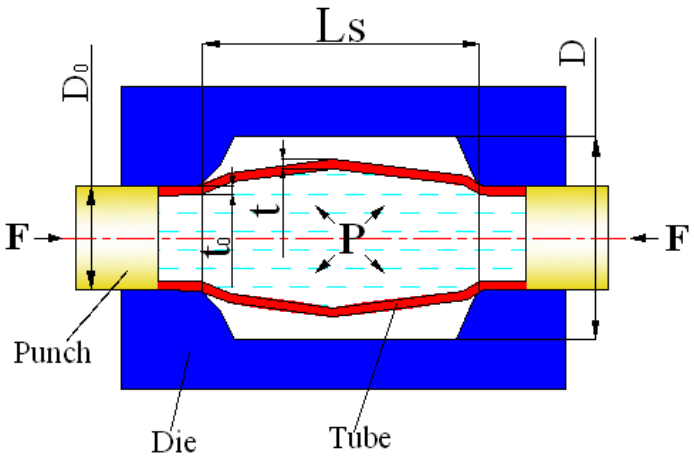

Fig.6- 1 Tube bulging process

Tab.6- 1 Matrix to study the effect of the strain hardening exponent n

Number	Strain hardening exponent n	Tube thickness t (mm)	Die span length Ls (mm)
1	SS 304 , n=0.577	1.65	100
3	Al 6061, n=0.162	1.65	100

Tab.6- 2 Matrix to study the effect of the tube thickness t

Number	Strain hardening exponent n	Tube thickness t (mm)	Die span length Ls (mm)
1	SS 304 , n=0.577	1.65	100
2	SS 304 , n=0.577	0.85	100

Tab.6- 3 Matrix to study the effect of the die span length Ls

Number	Strain hardening exponent n	Tube thickness t (mm)	Die span length Ls (mm)
1	Al 6061, n=0.162	1.65	100
2	Al 6061, n=0.162	1.65	150

6.1 Investigation of the effect of material hardening exponent on the formability during THF preforming

6.1.1 The effect of strain hardening exponent n on the wrinkle characteristics

The effects of the strain hardening exponent n on the wrinkle characteristics are investigated through wrinkle evolution analysis at three strain hardening exponent levels, n=0.04 ,n=0.30 and n=0.577 with the same tube size listed in Tab.5-1. The imperfection is set to be 0.5% and the internal pressure is zero. Fig.6-2 ~ Fig.6-5 show the effects of the strain hardening exponent n on the half wave length λ_c, critical strain ε_c, wrinkle growth height H_b and axial stress response σ_x. It can be seen that half wave length λ_c and axial stress response increase with strain hardening exponent n, while critical strain ε_c and wrinkle growth height H_b increase with the strain hardening exponent n. Fig.6-5 shows the axial stress response Vs axial compression with different n. The axial stress on the tube with lower strain hardening exponent n drop faster than that of the high strain coefficient n after the limited state, which indicates that the axial rigidity of tube with higher strain hardening exponent n is better and more material can be fed into the

forming zone. Thus the tube with higher n has better formability in the THF process with preforming.

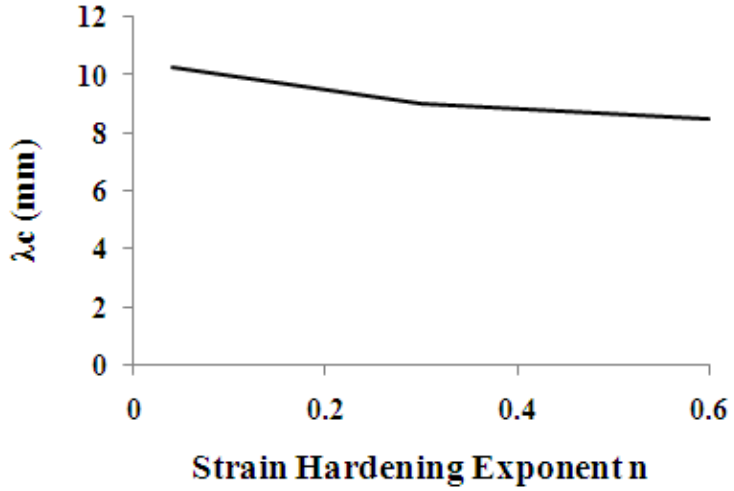

Fig.6- 2 Half wave length λ_c Vs strain hardening exponent n

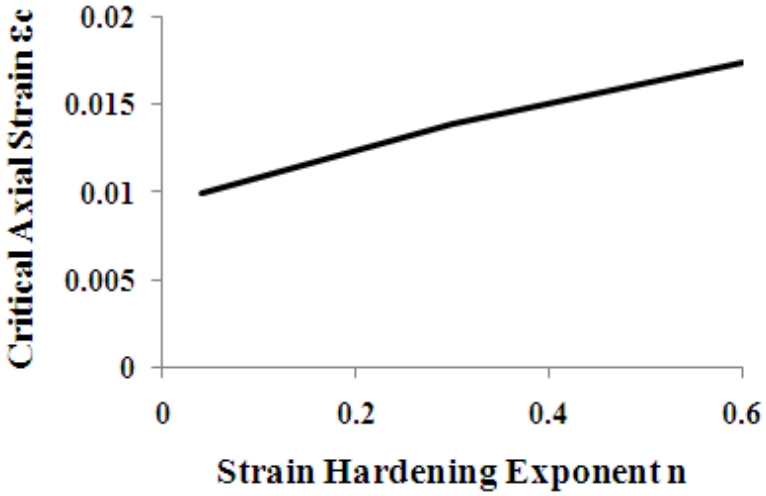

Fig.6- 3 Critical axial strain Vs strain hardening exponent n

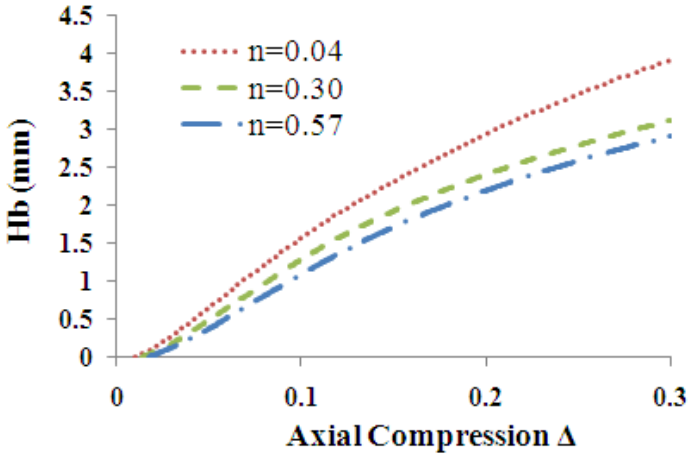

Fig.6- 4 Wrinkle growth height Vs axial compression with different strain hardening exponent n

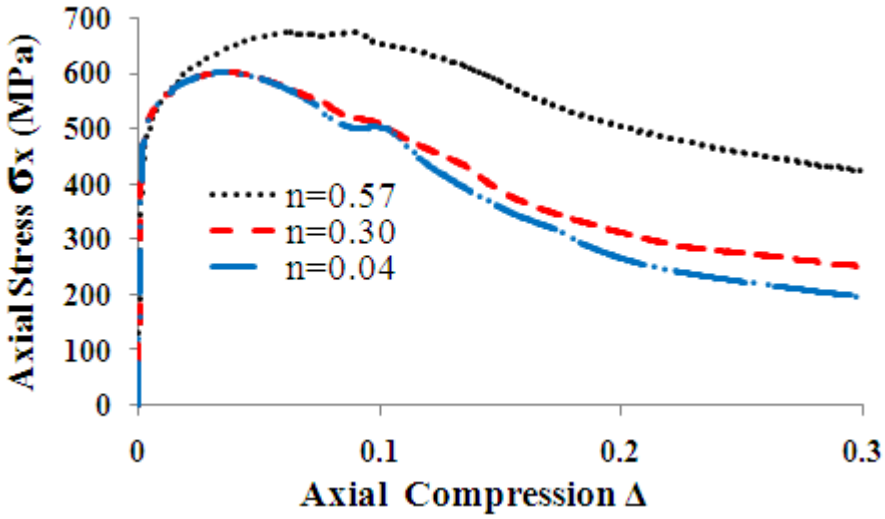

Fig.6- 5 Axial response Vs axial compression

6.1.2 The effect of the strain hardening exponent n on the formability during THF preforming

6.1.2.1 Preforming and bulging process of the SS 304 tube

The wrinkle formation characteristic of SS 304 tube will be used to guide the preform design of the bulging THF process. Fig.6-6 shows the bulging shape and the geometrical size. The diameter of the initial tube is 34.95 mm and the final bulged diameter is 60 mm. Thus the radial expansion rate is about 71.67% which is unachievable by direct THF without preforming. The typical expansion rate at room temperature is about 50% for the THF process.

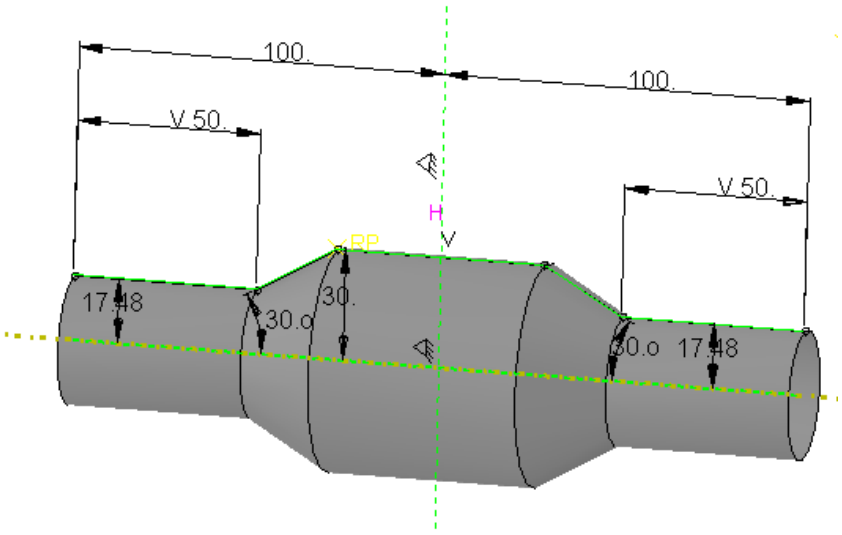

Fig.6- 6 Bulged shape

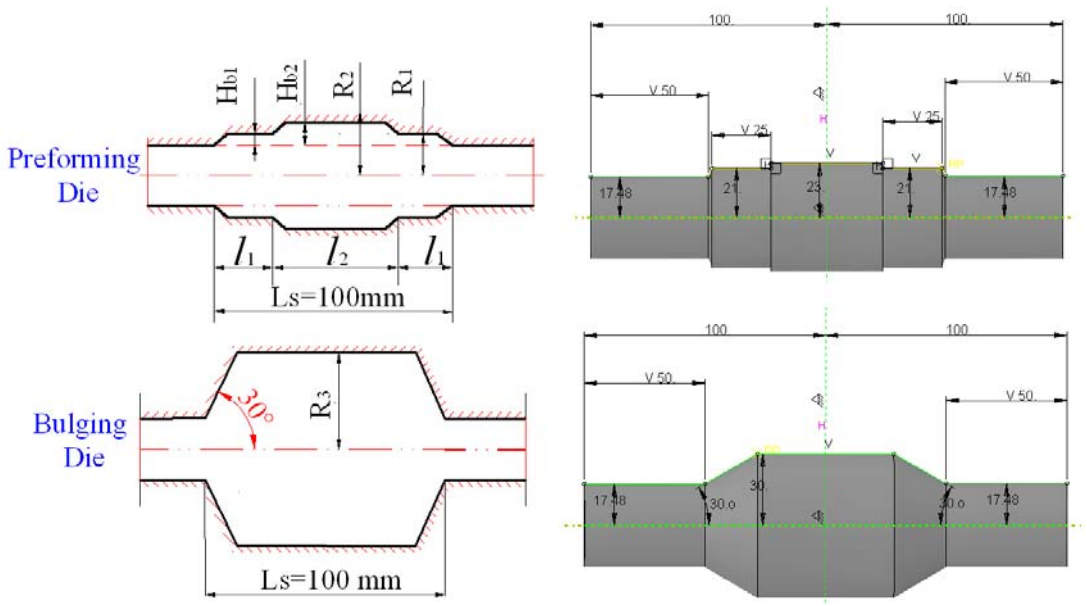

Fig.6- 7 Prefoming die and bulging die

The first step of preforming design is to design the die shape of the preforming stage 1 which is used trigger the wrinkle. In order to develop a uniformly distributed wrinkle pattern and to leave the axial rigidity for the wrinkle growth in the preforming stage 2, the height of wrinkle growth in the preforming stage 1 is designed to be 3.5 mm. Thus radius of the preforming die is designed to be 21 mm (Fig.6-7.a).

The second step is to select the internal pressure and axial feeding for the preforming stage 1. As discussed before, the lower pressure can lead to occurrence of the hoop wrinkle which is difficult to be removed by high pressure. Thus the pressure selection should start from upper end close to the yielding pressure. Here we will start with higher pressure which is about 75% of the yielding pressure. The yielding pressure can be computed as follows:

$$P_y = \sigma_y \frac{t}{R} = 255 \times \frac{1.65}{17.475} = 24Mpa$$
$$P = 0.75P_y = 18MPa \tag{6.3}$$

The internal pressure is about 18 MPa and the corresponding half wave length λ_c is about 12 mm according to Fig.5-6. The total die span Ls of the forming zone is 100 mm, thus the total wrinkle number N developed in the preforming stage can be computed as:

$$N = \frac{Ls}{2\lambda_c} = \frac{100}{2*12} \approx 4 \tag{6.4}$$

The axial feeding amount f_1 during the preforming stage 1 can be estimated based on Fig.5-11. According to the Fig.5-11, the axial compression Δ_1 corresponding to 3.5 mm wrinkle height under pressure 18 MPa is about 0.20. Thus the feeding is about 20 mm which is computed through equation (6.5). The displacement of the punch is 10 mm.

$$f_1 = Ls \times \Delta_1 = 100 \times 0.20 = 20mm \tag{6.5}$$

Thus, the internal pressure and the axial feeding for the preforming stage 1 is selected and applied to the FEA simulation in Abaqus. Fig.6-8 shows the formed wrinkle during the preforming stage 1. In total, 4 wrinkles are observed in the preforming stage 1. The loading path and the preform die shape have triggered the wrinkle formation successfully in the preforming stage 1.

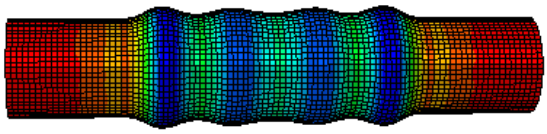

Fig.6- 8 The formed wrinkle during the preforming stage 1

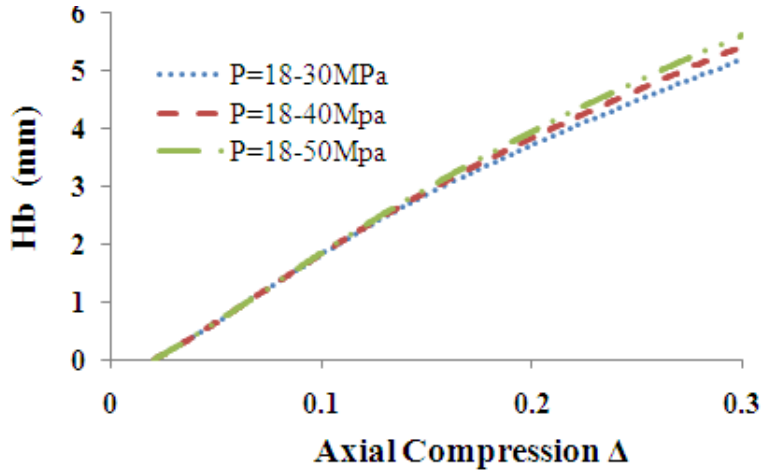

Fig.6- 9 Wrinkle growth Vs axial compression at different pressure profile

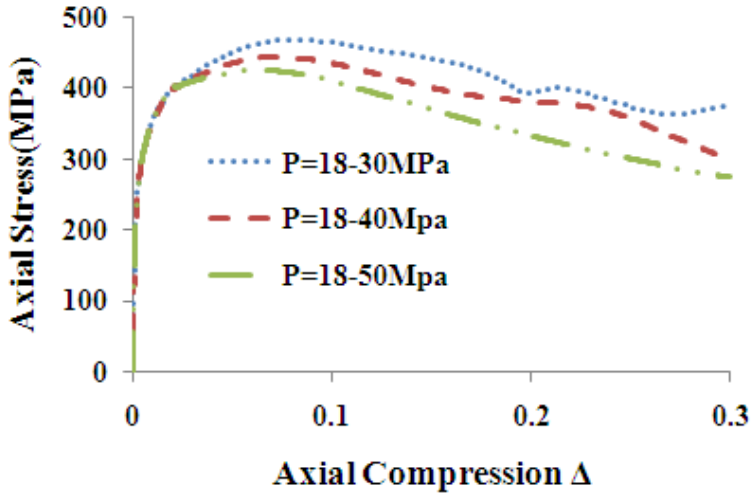

Fig.6- 10 Axial stress response at different linear pressure profile

The third step is to design the die shape of preforming stage 2 and find appropriate loading path to grow the wrinkle uniformly and stably. A parameter studies on the effect of the pressure profile on the wrinkle height H_b and axial response are carried out based on the analytical model. Fig.6-9 and Fig.6-10 show the effects of three pressure profile on the wrinkle height H_b and axial response. If the wrinkle height H_b is 5.5 mm, the corresponding axial compression $\Delta 2$ is about 0.34 and the axial stress is above 300

MPa, which means that the axial rigidity at compression of 0.34 is still good enough to transfer compression force. Thus wrinkle height H_b is selected to be 5.5 mm and accordingly, the ie shape of the preforming stage 2 is designed to be 23.0 mm, Then the axial feeding f_2 is about 7 mm which is computed through equation (6.6). The punch displacement is 3.5 mm. Through iterative FEA simulations, it is found that the linear pressure profile, where the pressure linearly increases from 45 MPa to 55 MPa, can let wrinkles grow stably without hoop wrinkle occurrence (Fig.6-11.)

$$f_2 = l_2 \times (\Delta_2 - \Delta_1) = 50 \times (0.34 - 0.20) = 7mm \tag{6.6}$$

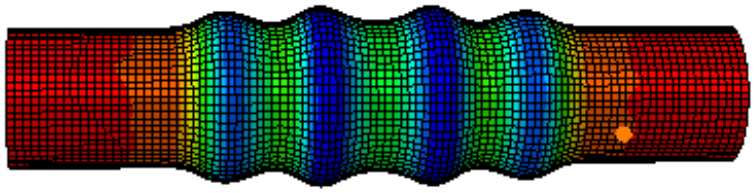

Fig.6- 11 Wrinkle growing in the preforming stage 2

The last step is to finally remove the wrinkle and expand the accumulated material to conform to the final die shape (Fig.6-7.c). It can be seen from Fig.6-9 that the axial rigidity of the tube having axial strain above 0.34 is still good enough to transfer the axial compression. Thus, 20-mm axial feeding is used in the final THF process and the punch displacement is 10 mm. The pressure is increasing from 55 MPa to 70 MPa when the axial feeding is increasing from 0 to 10 mm. After the feeding of 10 mm, the feeding is stopped and the pressure is increasing from 70 Mpa to 100 Mpa to remove the wrinkle and finally let the material conform to the die shape. Fig.6-12 shows the thickness distribution on the formed part where the wrinkle is finally flattened. Fig.6-13 shows the thinning distribution of the bulged part. The thinning rate at the bulge top is fluctuating around 20%, which is fairly uniform. In total, 47 mm axial feeding is achieved during the

forming of this bulged part which has an expansion rate of 71%. The process variables used in the preforming stage and final THF process are summarized in Tab.6-4.

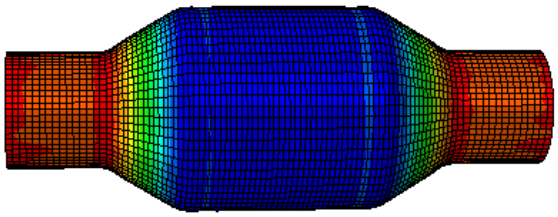

Fig.6- 12 Wrinkle removal and formed part

Tab.6- 4 Process variables in the preforming stages and final THF process for material SS 304

Process Variables	Preforming I	Preforming II	Final THF
H_b (mm)	H_{b1}=3.5	H_{b2}=5.5	
Die Radius (mm)	R_1=21	R_2=23	R_3=30
Die length (mm)	l_1=25	l_2=50	
Axial Compression	Δ_1=0.2	Δ_2=0.34	
Axial feeding (mm)	f_1=20	f_2=7	20
Pressure (MPa)	18	45 to 55	55 to 70 during Feeding 70 to 100 to remove wrinkle
λ_c (mm)	12		
Wrinkle number N	$N = 4$		

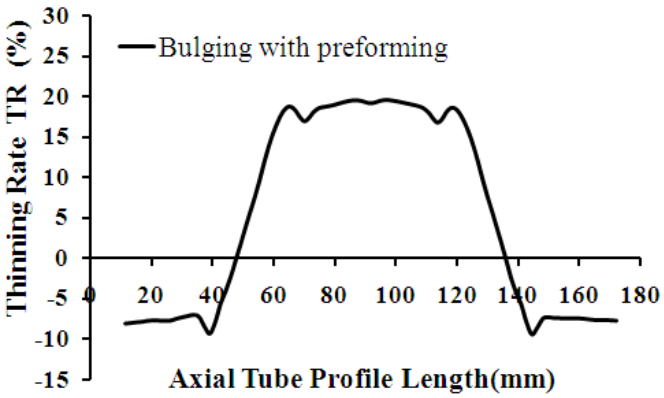

Fig.6- 13 Thinning distribution of the bulged part

In order to compare the formability improvement with conventional THF process without wrinkle formation, a conventional THF without wrinkle formation is simulated. The tube was bulged to 52-mm diameter.(Fig.6-14) in the direct bulging process where 20-mm axial compression and 70-MPa internal pressure were linearly applied. Fig.6-16 shows the thinning rate distribution and expansion rate of the bulged part formed with and without preforming. It can be seen that the thinning rate of the formed part are all about 20%, but the expansion rate of the part with preforming is 71% which is much higher than the 50% expansion rate of the part without preforming. Thus, the preforming of the wrinkle formation can significantly increase the formability of the THF process.

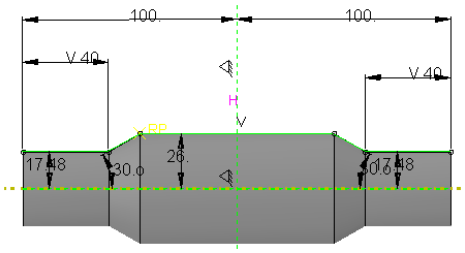

Fig.6- 14 Die for direct THF forming

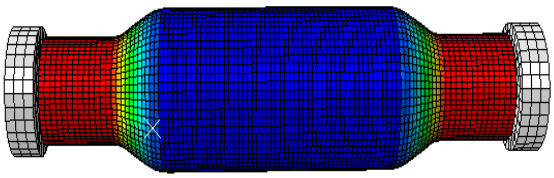

Fig.6- 15 Directly hydroformed part

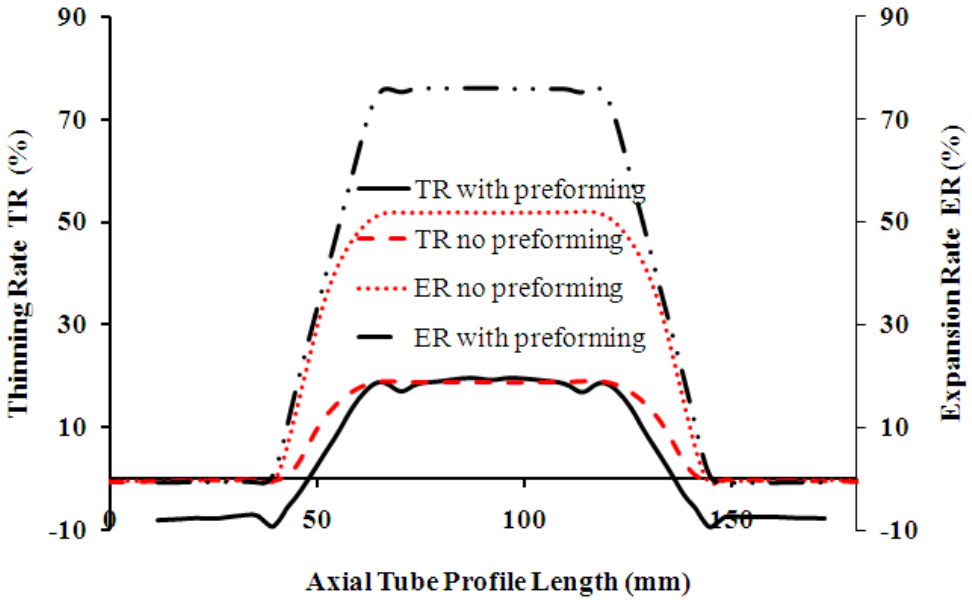

Fig.6- 16 Thinning rate and expansion rate comparison

6.1.2.2 Preforming and bulging process of the Al 6061 tube

Through the same procedure used in section 6.1.2.1, the analytical model is used to generate the half wave length curve (Fig.6-17), wrinkle growth curve (Fig.6-17) and axial stress response curve (Fig.6-19) to help the designer determine the die size and axial feeding amount of the preforming stage I and II. The internal pressure profile used in the preforming stage are determined through iterative FEA simulations in Abaqus to make sure that no hoop wrinkle will occur under such pressure profile. Tab.6-5 shows all the process variables determined in the preforming stage 1,2 and final bulging process. Fig.6-20 shows the wrinkle onset in preforming stage 1, wrinkle growth in preforming stage 2 and bulged shape in the final THF process. Fig.6-21 shows the thinning rate distribution and expansion rate distribution on the bulged part. The thinning rate at the bulge is fluctuating around 17.5%, In total, 35.4 mm axial feeding is achieved during the forming of this bulged part which has an expansion rate of 54%.

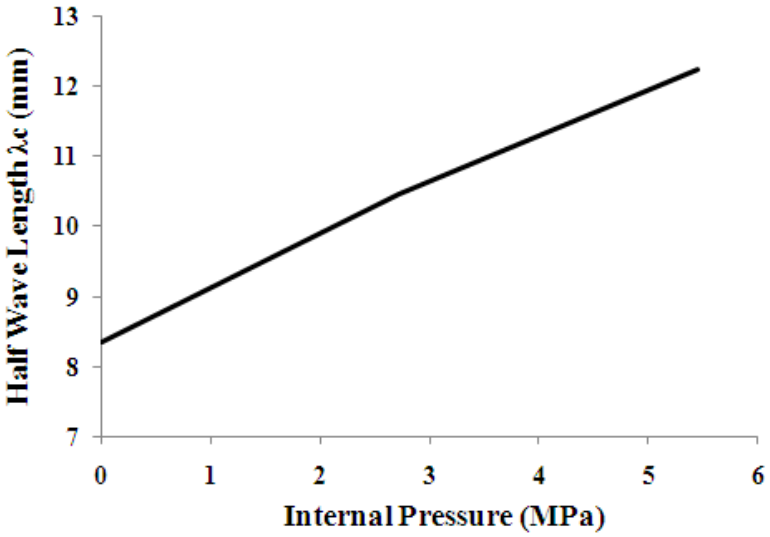

Fig.6- 17 Half wave length Vs internal pressure of Al 6061 tube.

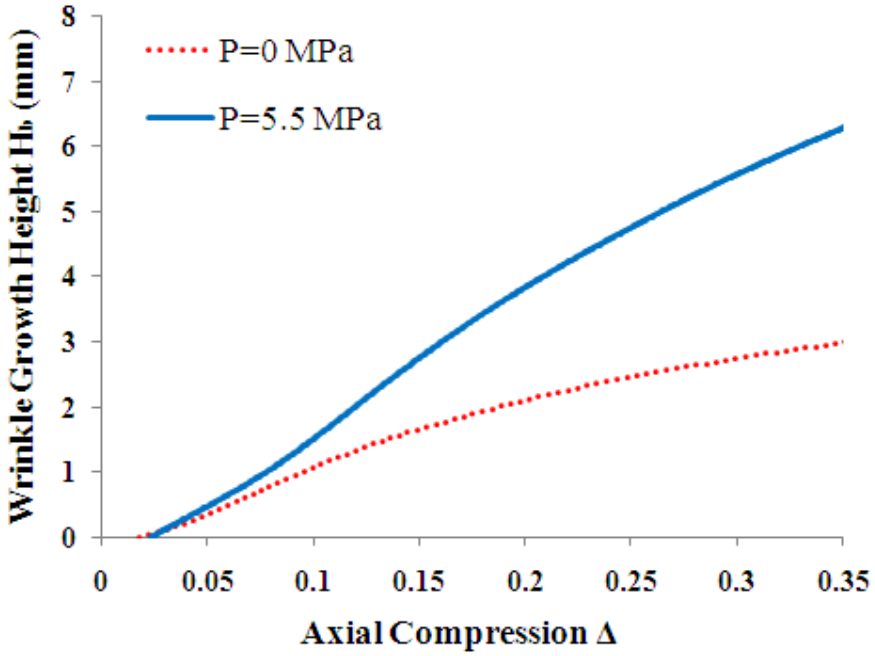

Fig.6- 18 Wrinkle height H_b Vs axial compression at different pressure .

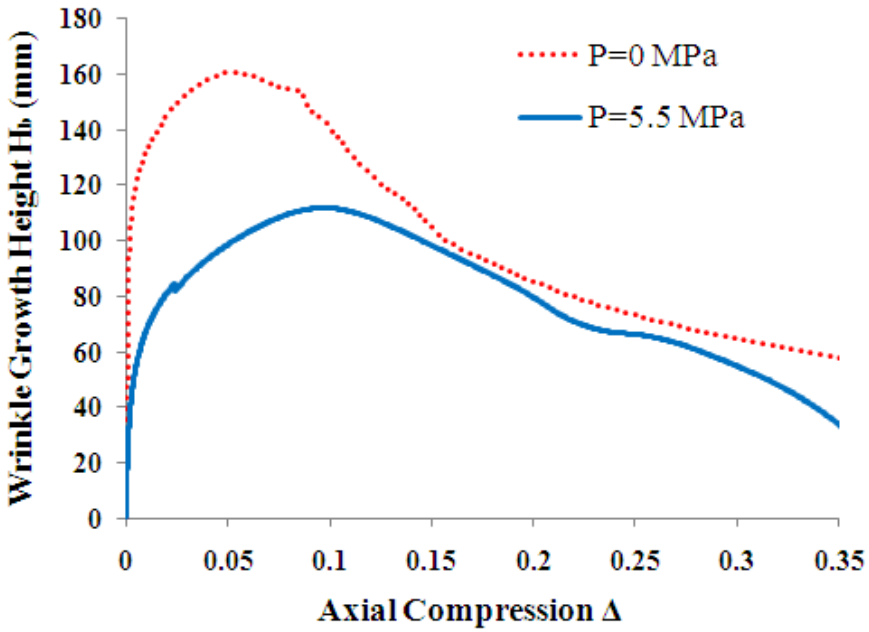

Fig.6- 19 Axial stress Vs axial compression at different pressure

Tab.6- 5 Process variables of preforming and final THF process of Al 6061 tube

Process Variables	Preforming I	Preforming II	Final THF
H_b (mm)	H_{b1}=1.5	H_{b2}=5.5	
Die Radius (mm)	R_1=19	R_2=23	R_3=27
Die length (mm)	l_1=25	l_2=50	
Axial Compression	Δ_1=0.10	Δ_2=0.326	
Axial feeding (mm)	f_1=10	f_2=11.4	14
Pressure (MPa)	4.5	8 to 9	10 to 13 during feeding 13-30 to remove wrinkles
λ_c (mm)	12		
Wrinkle number N	$N = 4$		

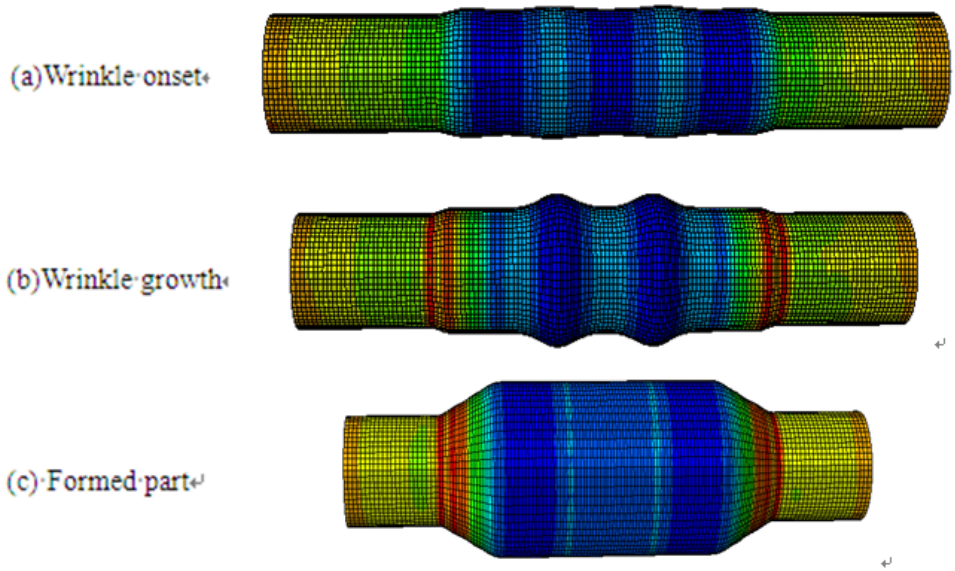

Fig.6- 20 Wrinkle evolution and formed part

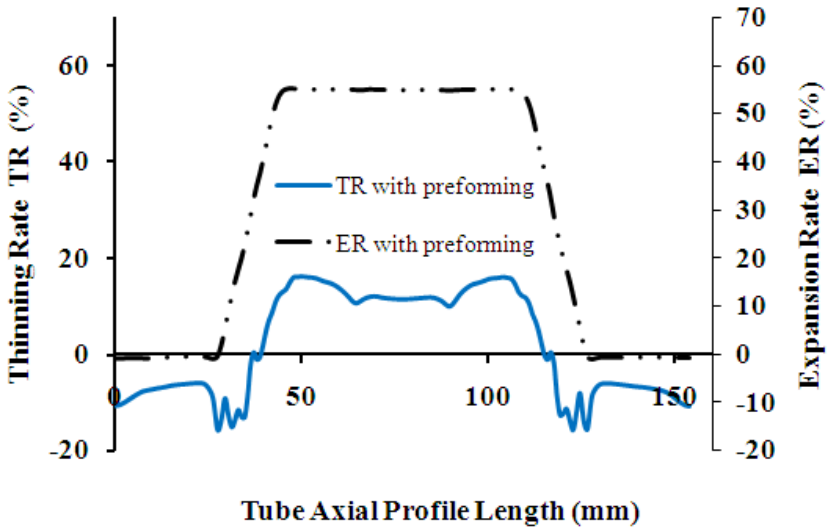

Fig.6- 21 Thinning rate and expansion rate distribution of bulged part of Al 6061

In order to compare the formability improvement with direct THF process, a conventional THF without wrinkle formation is simulated. The tube was bulged to 24-mm diameter.(Fig.6-22) in the direct bulging process where the 26-mm axial feeding

was linearly applied and the internal pressure was linearly ramp from 4 MPa to 13 MPa. Fig.6-24 shows the thinning rate distribution and expansion rate of the bulged part formed with and without preforming. It can be seen that the thinning rate of the formed part are all about 17%, but the expansion rate of the part with preforming is 54% which is much higher than the 37% expansion rate of the part without preforming. Thus, the preforming of the wrinkle formation can significantly increase the formability of the THF process of Al 6061 tubing.

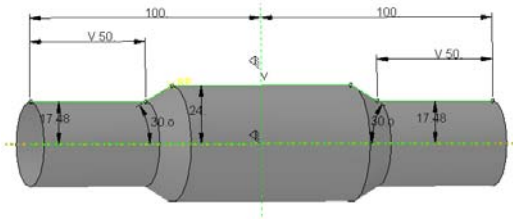

Fig.6- 22 Die for direct THF forming

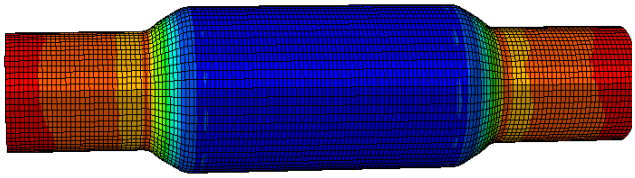

Fig.6- 23 Directly hydroformed part

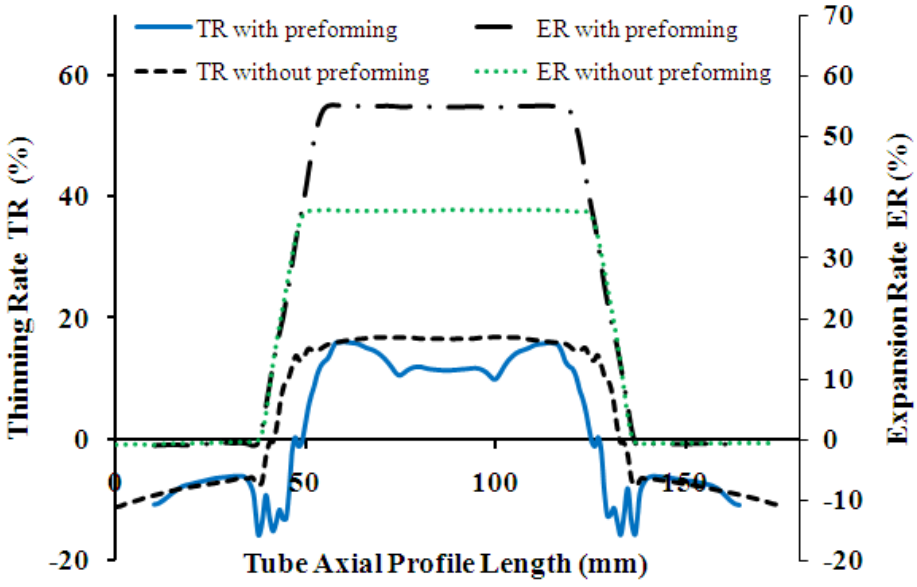

Fig.6- 24 Thinning rate and expansion rate comparison

6.1.3 Formability comparison between SS 304 and Al 6061

Tab.6-6 lists the expansion rate and thinning rate at two strain hardening exponent levels: n=0.577 and n=0.162. It can be seen that the thinning rates obtained from FEA simulations satisfy the maximum thinning rate criterion for SS 304 tube and Al 6061 tube, which are 20% and 17% for SS 304 tube and Al 6061 tube respectively. Tab.6-6 shows that the expansion rate of the bulged part drop from 71 to 54%, when the strain hardening exponent n decreases from 0.577 to 0.162. Thus the expansion rate increases with the strain hardening exponent n.

Tab.6- 6 Comparison of the formability of different n

	Expansion Rate	Thinning Rate
SS 304 n=0.577	71%	20%
Al 6061 n=0.162	54%	17.0%

6.2 The effect of the tube thickness on formability during THF preforming

6.2.1 The effect of the tube thickness on the wrinkle formation characteristics

The effect of tube thickness t on the wrinkle characteristics is investigated by wrinkle evolution analysis on three tube thickness levels, t=0.8 mm, t=1.65 mm and t=2.4 mm. The other tube geometrical variables remain same as that listed in Tab.5-1. The imperfection is set to be 0.5% and the SS 304 tube material is used. The internal pressure is set to be 50% of the yield pressure. Fig.6-25 ~ Fig.6-27 show the effect of tube thickness t on the half wave length λ_c, critical strain ε_c, wrinkle growth height H_b and axial stress σ_x. It can be seen that half wave length, the critical strain, axial stress

increases with the tube thickness t. Fig.6-25 shows that half wave length increases from 7.5 to 13 mm when the thickness changes from 0.8 mm to 2.4 mm. Thus, the thicker the tube is, fewer wrinkles can be observed during the tube compression. Fig.6-26 shows that the effect of the tube thickness t on the wrinkle growth height H_b. The relationship between the tube thickness t and wrinkle height H_b shown in Fig.6-26 are not conclusive. Fig.6-27 shows the axial stress response at different thickness t. It can be seen that the thicker tube has stronger axial rigidity than the thinner tube. More material can be fed into the forming zone for the thicker tube with high axial rigidity, which also indicates better formability of the thicker tube in the THF process.

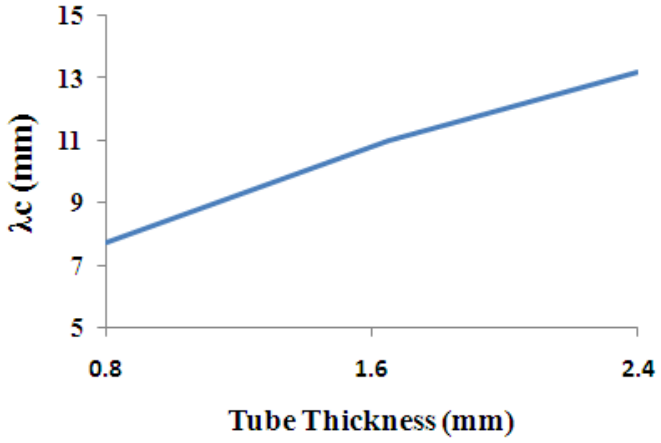

Fig.6- 25 Half wave length Vs tube thickness t

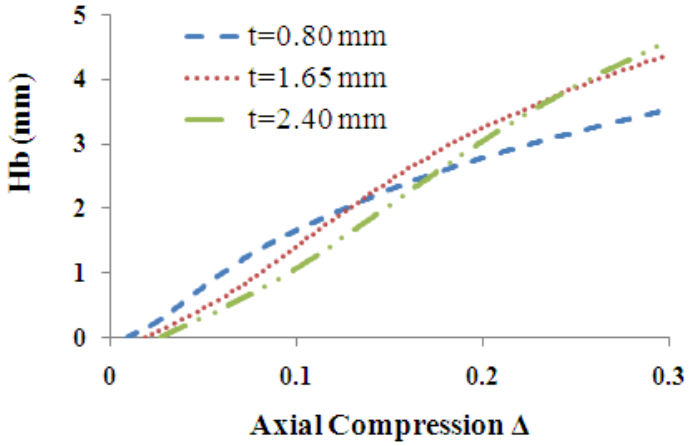

Fig.6- 26 Wrinkle growth height H_b Vs axial compression at different thickness t

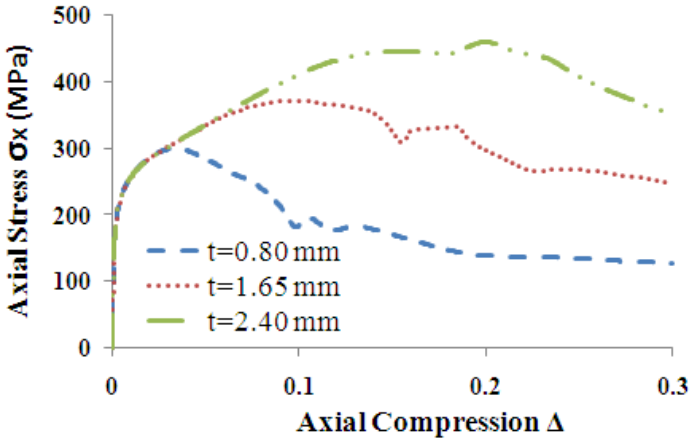

Fig.6- 27 Axial stress Vs axial compression at different thickness

6.2.2 The effect of tube thickness on formability of tube bulging process.

Through the same procedure used in section 6.1.2.1, the analytical model is used to generate the half wave length curve (Fig.6-28), wrinkle growth curve (Fig.6-29) and axial stress response curve (Fig.6-30) to help the designer determine the die size and axial feeding amount of the preforming stage I and II. The internal pressure profile used in the preforming stage are determined through iterative FEA simulations in Abaqus to

make sure that no hoop wrinkle will occur under such pressure profile. Tab.6-7 shows all the process variables determined in the preforming stage 1,2 and final bulging process. Fig.6-31 shows the wrinkle onset in preforming stage 1, wrinkle growth in preforming stage 2 and bulged shape in the final THF process. Fig.6-32 shows the thinning rate distribution and expansion rate distribution on the bulged part. The thinning rate at the bulge is around 20%, In total, 34 mm axial feeding is achieved during the forming of this bulged part which has an expansion rate of 60 %.

Tab.6-8 lists the expansion rate and thinning rate at two thickness levels: t=0.8 and t=1.65. It can be seen that the thinning rates obtained from FEA simulations satisfy the 20% maximum-thinning-rate-criterion for SS 304. Compared to the expansion rate of 71% of the tube at the thickness of t=1.65 mm shown in Fig.6-16, tube of thickness 0.8 mm has 60% expansion rate, which is 10% less than that of the thicker tube of 1.65 mm (Tab.6-8). However, Fig.6-33 shows the thinning distribution comparison which implies that the thinner tube has more uniform thinning distribution.

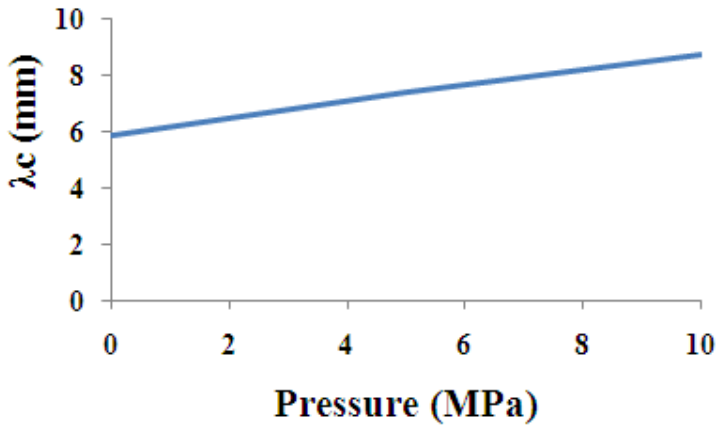

Fig.6- 28 Half wave length Vs internal pressure

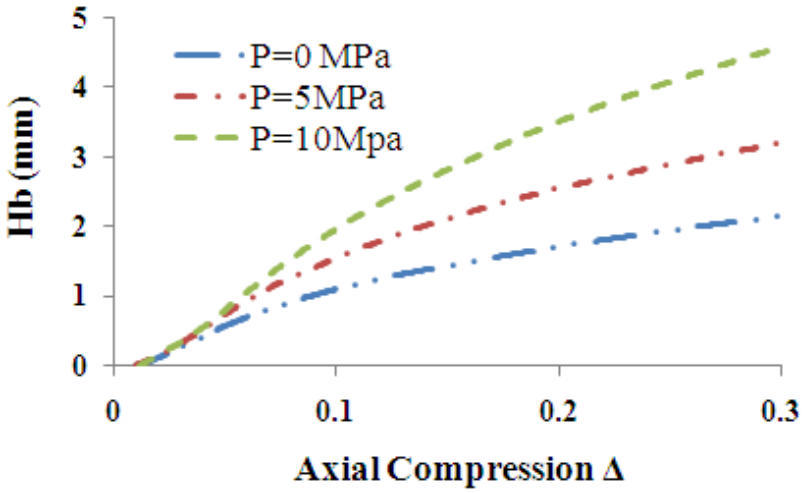

Fig.6- 29 Wrinkle growth height Vs axial compression under different pressure

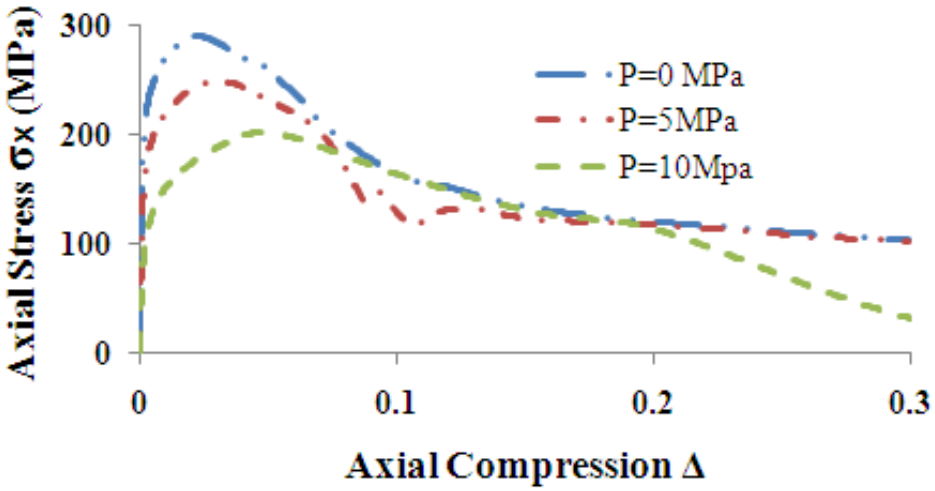

Fig.6- 30 Axial stress Vs axial compression under different pressure

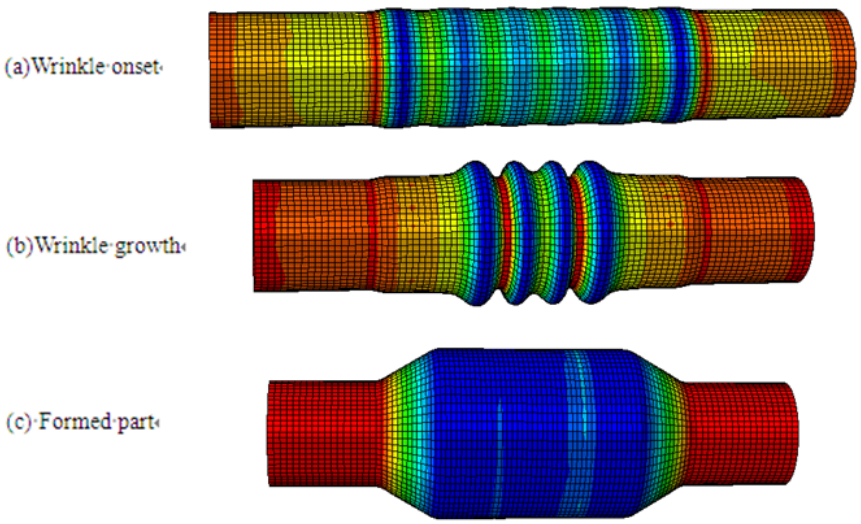

Fig.6- 31 Wrinkle evolution and formed part

Tab.6- 7 Process variables of preforming and final THF process for SS 304 tube of thickness 0.8

Process Variables	Preforming I	Preforming II	Final THF
H_b (mm)	H_{b1}=1.0	H_{b2}=5.5	
Die Radius (mm)	R_1=18.5	R_2=23	R_3=28
Die length (mm)	l_1=17	l_2=66	
Axial Compression	Δ_1=0.056	Δ_2=0.39	
Axial feeding (mm)	f_1=5.6	f_2=21	4
Pressure (MPa)	10	15 to20	20 to 26during feeding 26 to 60 to remove wrinkles
λ_c (mm)	8.5		
Wrinkle number N	$N = 6$		

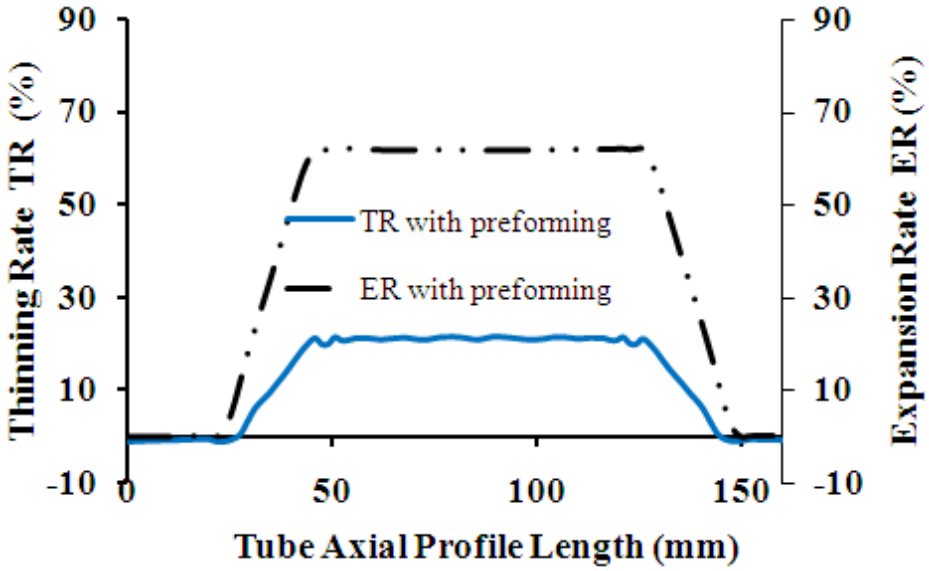

Fig.6- 32 Thinning rate and expansion rate distribution

Tab.6- 8 Formability comparison between different SS 304 tube thickness t

	Expansion Rate	Thinning Rate
Thickness t=0.8	60	20%
Thickness t=1.65	71	20%

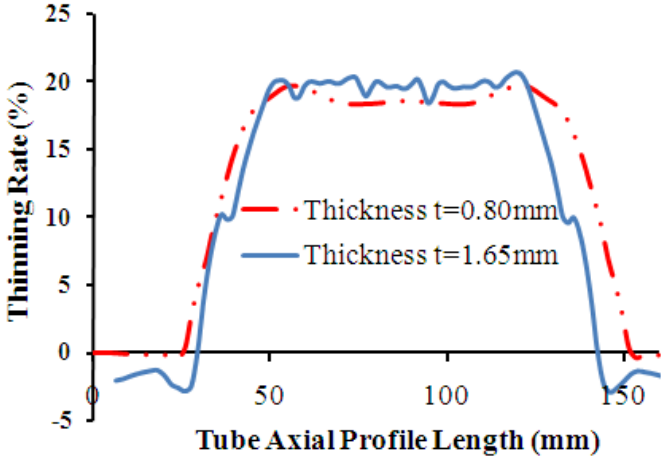

Fig.6- 33 The thinning distribution comparison at different thickness

6.3 The effect of the die cavity length on formability of the tube bulging process

In order to investigate the effect of the die span length on the formability during preforming, a bulged part with 25-mm-radius and 150-mm die span (Fig6-34.c) is used for the preforming and THF process. The expansion rate is about 44%. Fig.6-34 shows the dies of the preforming 1, 2 and final THF process. All the process variables of three stages are listed in Tab.6-9. Fig.6-35 shows the wrinkle evolution and formed part. Fig.6-36 shows the thinning rate and expansion rate distribution.

Tab.6-10 lists the expansion rate and thinning rate at two die-span-length levels: Ls=100 and Ls=150. It can be seen that the thinning rates obtained from FEA simulations satisfy the 17% maximum-thinning-rate-criterion for Al 6061 tube. Compared to the expansion rate of 54% at die span of 100 mm shown in Fig.6-21, 44% of the expansion rate is realized a with die span of 150 mm. Thus, a longer die span can reduce the expansion rate (Tab.6-10).

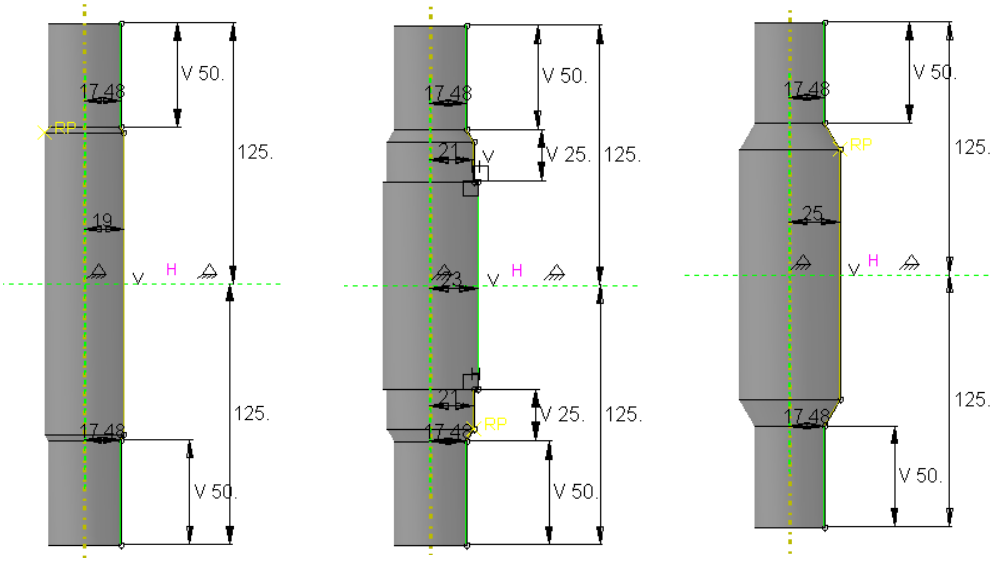

Fig.6- 34 (a) Die of preforming 1 (b) Die of preforming 2 (c) Die of final THf process

Tab.6- 9 Process variables of preforming and final THF process for Al 6061 tube with die span of 150 mm

Process Variables	Preforming I	Preforming II	Final THF
H_b (mm)	H_{b1}=1.5	H_{b2}=5.5	
Die Radius (mm)	R_1=19	R_1=21, R_2=23	R_3=25
Die length (mm)	L_s=150	l_1=25, l_2=100	
Axial Compression	Δ_1=0.10	Δ_2=0.326	
Axial feeding (mm)	f_1=7.5	f_2=23	8
Pressure (MPa)	4.5	4.5 to 7	7 to 9 during feeding 9 to 30 to remove wrinkles
λ_c (mm)	12		
Wrinkle number N	$N = 6$		

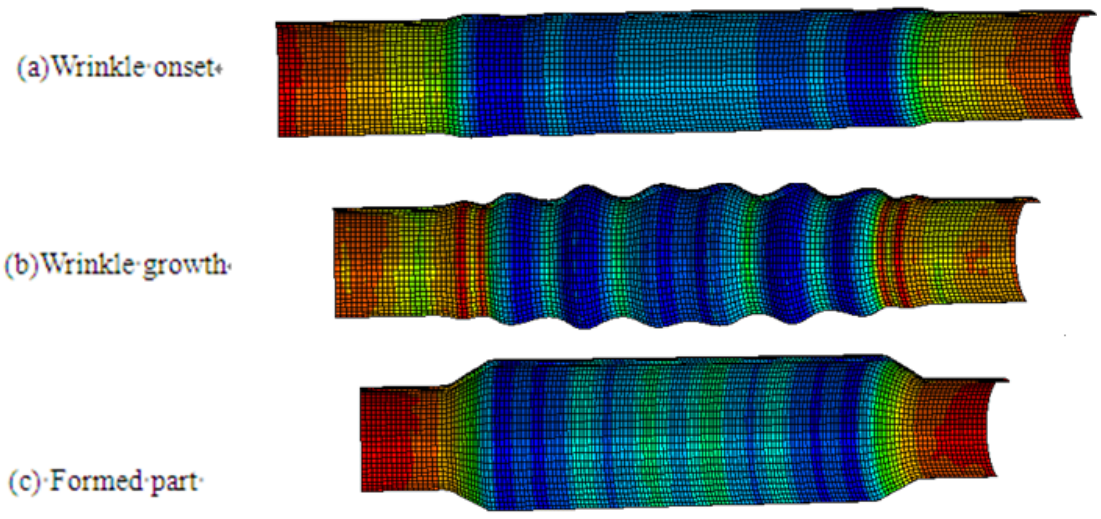

Fig.6- 35 Wrinkle evolution and formed part

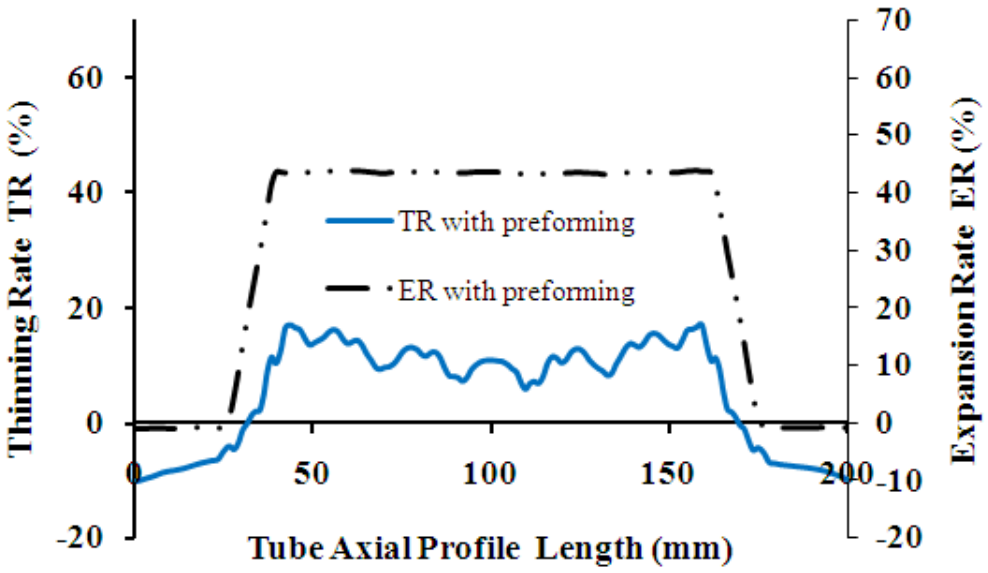

Fig.6- 36 Thinning rate and expansion rate distribution

Tab.6- 10 Formability comparison at different die span

	Expansion Rate	Thinning rate
Die span 100 mm	54%	17.0 %
Die span 150 mm	44%	17.0 %

6.4 Preforming of the SS 304 tubular part with varying cross section

The two-stage preforming scheme was applied to the hydroforming process of the part with varying cross section. The feature of this part consisted of a 25-mm-radius bulge and 30-mm-radius bulge (Fig.6-37). The expansion rates of the smaller bulge and bigger bulge are about 43% and 71%, respectively. Thus, the bigger bulge needs more material to be accumulated in the forming zone. Fig.6-37 shows the preforming die and final THF die. The process parameters determined for the preforming stage and final THF stage are shown in Tab.6-11. The preforming die shape permitted one middle wrinkle on the big

bulge side to grow to a height of 25 mm, while the end bulge and the middle wrinkle on the small bulge side were limited to a height of 21 mm. The loading paths of the preforming stage and final tube bulging stage are shown in Fig.7-4. The element type and coefficient of friction used in the FEA simulation were same as those used in FEA simulation in last section. Fig.6-38 shows the wrinkle evolution and formed part. The maximum thinning rate of the formed part shown is about 21% (Fig. 6-39).

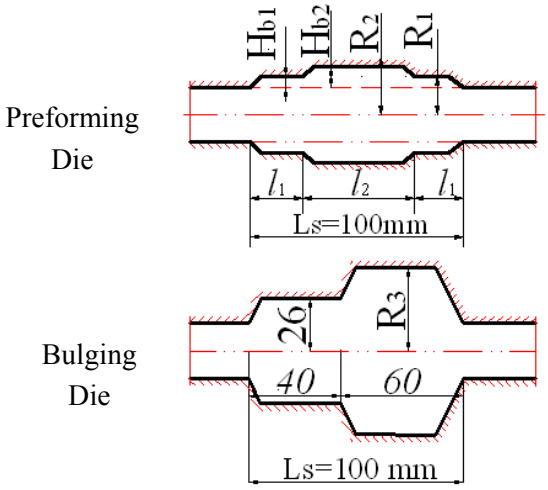

Fig.6- 37 Preforming and bulging die

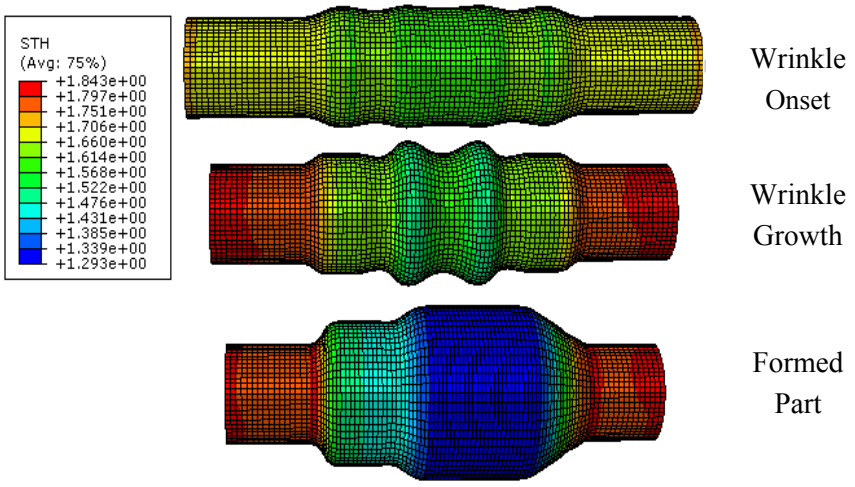

Fig.6- 38 Wrinkle evolution and formed part

Tab.6- 11 Process parameters of preforming and final THF for varying cross section tube

Process Variables	Preforming I	Preforming II	Final THF
H_b (mm)	H_{b1}=3.5	H_{b2}=75	
Die Radius (mm)	R_1=21	R_2=25	R_3=30
Die length (mm)	l_1=25	l_2=50	
Axial compression	Δ_1=0.20	Δ_2=0.51	
Axial feeding (mm)	f_1=20	f_2=8	12
Pressure (MPa)	P=18	45~57.5	57.5~75
λ_c (mm)	12		
Wrinkle number	N=4		

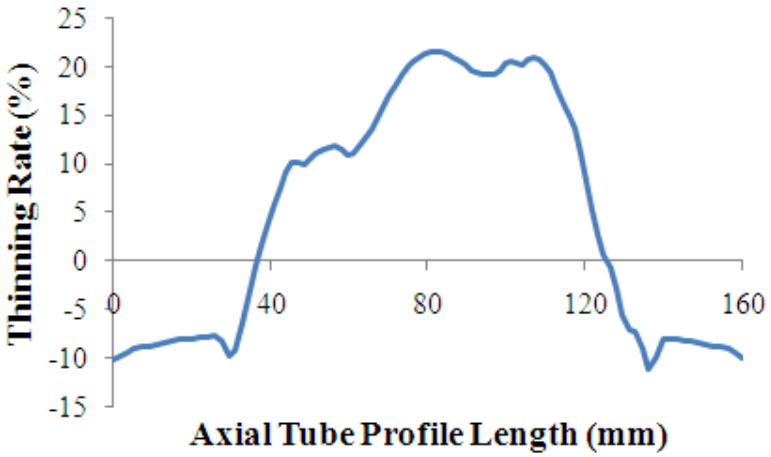

Fig.6- 39 Thinning rate distribution

6.5 The effect of mesh size on the FEA simulation of wrinkle onset

In the FEA simulation of the wrinkle onset and bulging process, the mesh size can affect the accuracy of the simulation results. In this section, an investigation was carried out to study the effect of mesh size on the wrinkle half wave length λ_c and the thinning rate

distribution. The FEA model used for mesh size effect investigation was the same as the one used in section "6.1.2.1". Stainless steel tube (SS 304) with length=200 mm, tube diameter = 34.9 mm and wall thickness = 200 mm, was used. Tab.6-12 shows five different mesh sizes that were investigated.

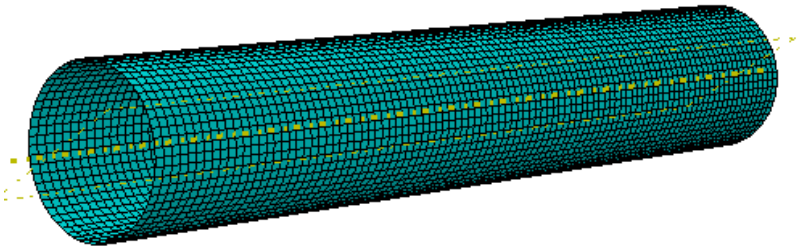

Fig.6- 40 Tube used to study the effect of mesh size

Tab.6- 12 Matrix of the tube mesh size

Number	Element number in axial direction	Element number in hoop direction	One wave length from analytical model	Number of elements in one wave length	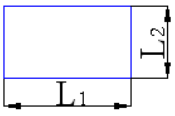 Element size (mm)
1	200	60	24	24	L_1=1, L_2=1.8
2	100	60	24	12	L_1=2, L_2=1.8
3	50	60	24	6	L_1=4, L_2=1.8
4	25	60	24	3	L_1=8, L_2=1.8
5	10	60	24	1.5	L_1=20, L_2=1.8

Fig.6-41 shows the wrinkle onset with different number of elements in one wave length. The loading conditions were set such that four wrinkles will be initiated. It can be seen that there is a minimum number of elements per wave length below which wrinkle will not appear in the FEA simulation. Thus, for the case tested, the minimum number of elements to simulate the onset of wrinkles should be 3.

Number of elements in one wave length	Wrinkle onset
24	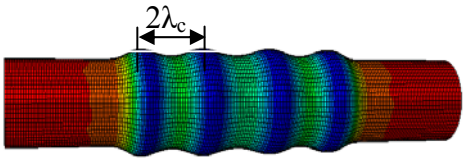
12	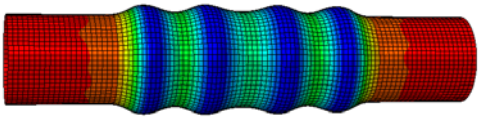
6	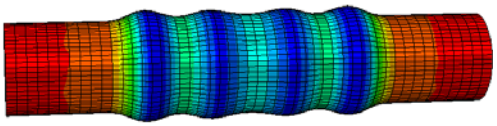
3	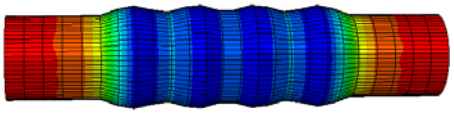
1.5	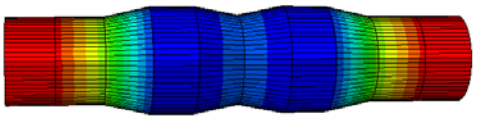

Fig.6- 41 Wrinkle onset with different number of elements in one wave length

Fig.6-42 shows the thinning rate distribution on the bulged part with different number of elements in one wave length. It can be seen that the thinning rate distribution curves

coincide for 24 elements, 12 elements and 6 elements mesh sizes, while the distribution curves for 3 elements and 1.5 elements respectively show different thinning distribution patterns. By considering both the effect of the mesh size on the wrinkle onset and the thinning rate distribution, it can be concluded that the minimum number of elements in one wave length should be 6. It should be noted that the number of elements used in the FEA simulations for the wrinkle onset and bulging processes in previous section were 12.

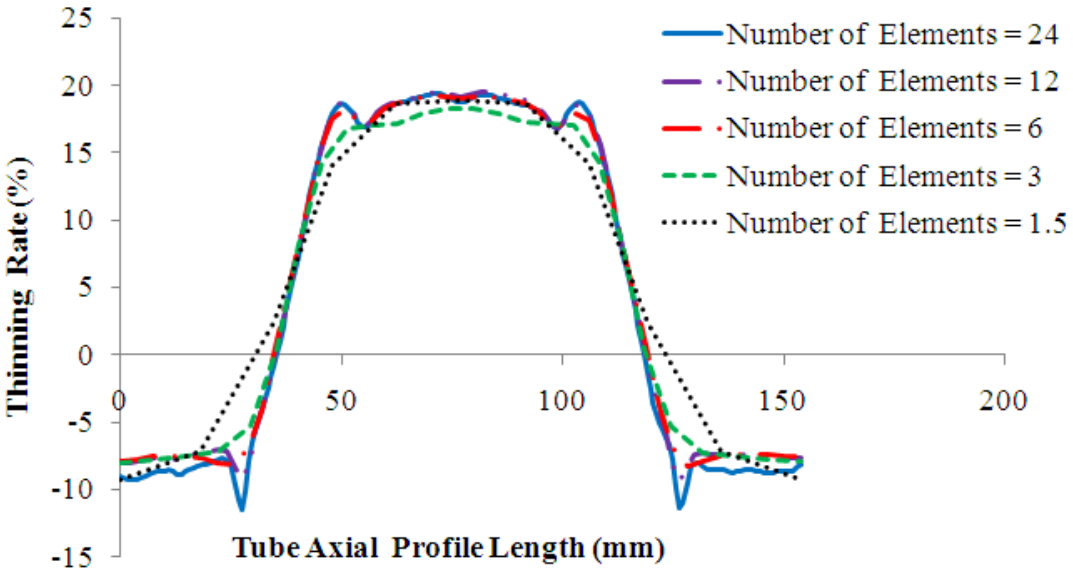

Fig.6- 42 Thinning distribution for different mesh size in one wave length

6.6 Conclusions

The effect of the process variables on the design of preform for THF based on wrinkle formation was investigated. Based on the maximum thinning rate criterion of 20% and 17% for SS 304 tube and AL 6061 tube respectively, expansion rates of 71% and 54%

were achieved for the SS 304 tube and the AL 6061 tube during the bulging test. Therefore the expansion rate of the bulged part increases with the material hardening exponent n. The study also reveals that wall thickness can influence the tube expansion. Expansion rates of 71% and 60% were achieved for 1.65-mm-thick and 0.8-mm-thickness SS 304 tube respectively. It was also found that the expansion rate decreases with increase in the die span length. Expansion rates of 54% and 44% were achieved for 100-mm-long die and 150-mm-long used in Al 6061 tube bulging respectively.

CHAPTER 7: EXPERIMENTAL VERIFICATION OF TWO-STAGE PREFORMING IN THF

In order to verify the two-stage preform scheme, preform die sets for three axisymmetric parts were designed and tube hydroforming experiments were carried out on SS 304 and Al 6061 tubing.

7.1 Experimental setup

THF experiments were carried out using a 150-ton hydroforming test rig (Fig. 7-1). The test setup consists of the upper die, lower die, and two axial cylinders. The upper die is connected to a 150-ton hydraulic press through a 150 ton load cell. The lower die sits on a table. The dies shown in Fig.7-1 consist of steel die inserts and aluminum die housing. The test rig has a maximum fluid pressure capacity of 140 MPa. Stainless steel tubing (SS 304) was used in the experiment. The tube length for all samples was 180 mm. Before testing, the dies and tubular specimens were cleaned with acetone. The tube specimens were hydroformed using Teflon sheets as a lubricant. Teflon sheets 0.12 mm thick were wrapped around the specimens.

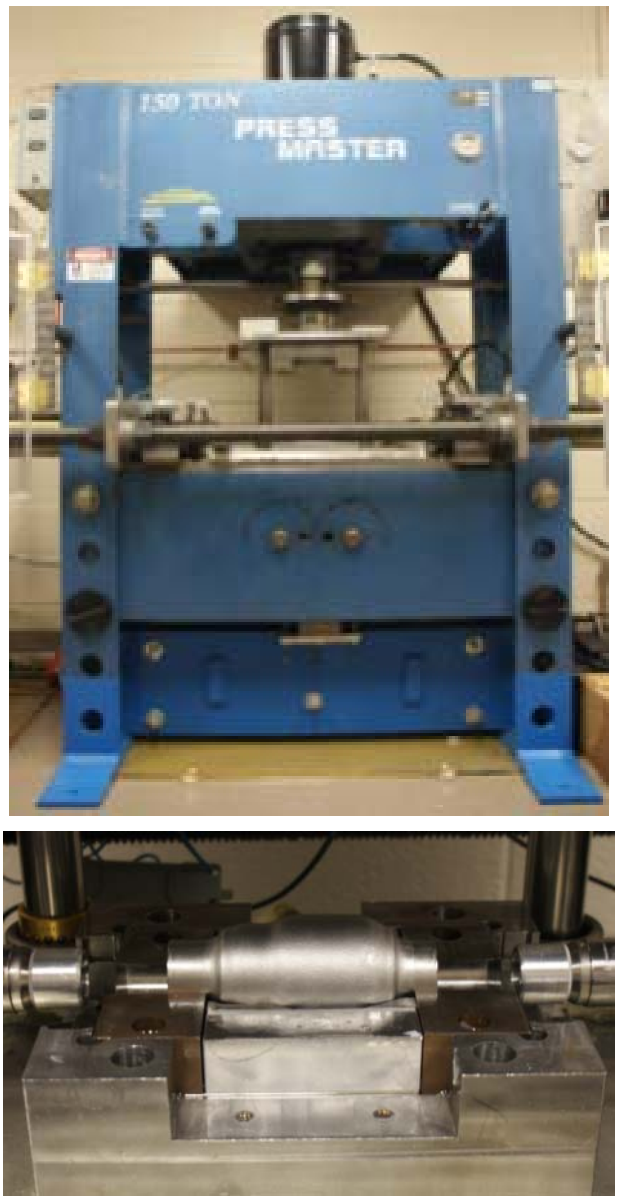

Fig.7- 1 150-ton hydroforming press and Forming die

7.2 Bulging of SS 304 tubing

In the preforming of the tube bulging, the pressure was first ramped up to 18 MPa, where it remained for about 30 s to trigger wrinkle onset when the tube end was compressed by 10 mm (Fig. 7-2). Then the pressure was ramped up to 45 MPa and gradually increased

to 55 MPa to inhibit the hoop wrinkle during wrinkle growth from 30 s to 60 s, while the tube end was continuously compressed another 2 mm (Fig. 7-2). The formed wrinkle is shown in Fig. 7-3a. In the final tube bulging process, the pressure was first ramped up to 55 MPa, then it was gradually increased to 70 MPa to support stable wrinkle growth while the tube end was compressed 10 mm during the first 30 s. Then, the pressure was increased from 70 MPa to 100 MPa to remove the wrinkle and form the part. The final bulged tube with the wrinkles removed is shown in Fig. 7-3b. The expansion rate of this bulged part was 71%. Fig.7-3a, b and Fig.7-4 show the wrinkle shape comparison, formed part comparison, and thinning distribution comparison between the experiment and FEA simulation respectively. It can be found that the experimental results agree well with the FEA simulation results.

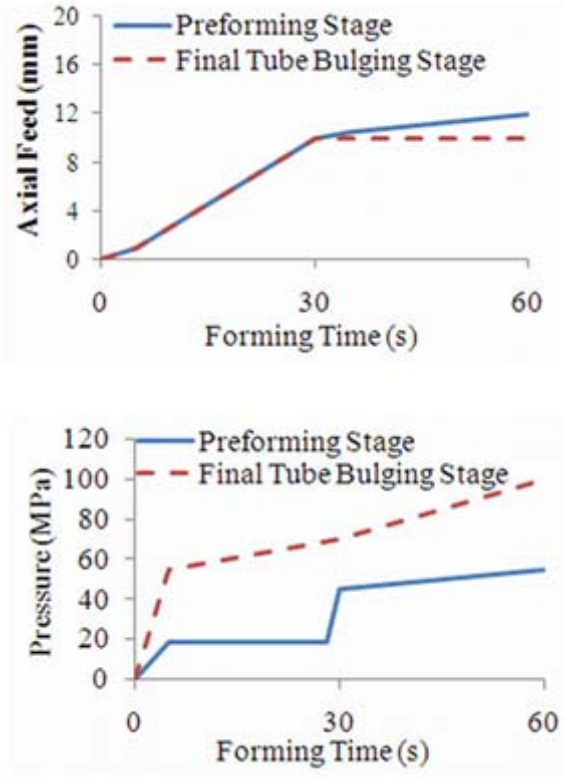

Fig.7- 2 Loading path for hydroforming bulge part

Experiment

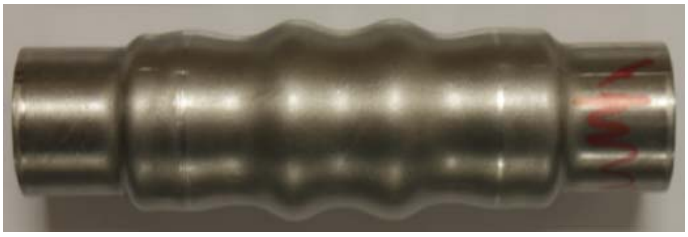

FEA

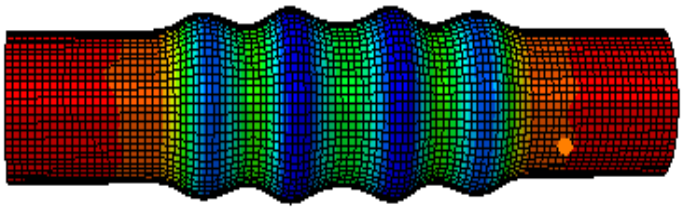

(a)

Experiment

FEA

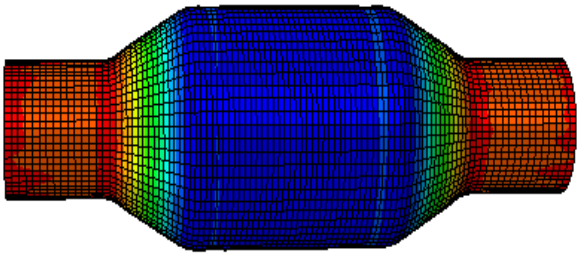

(b)

Fig.7- 3 (a) Wrinkle formation in preforming stage (b) Bulged part

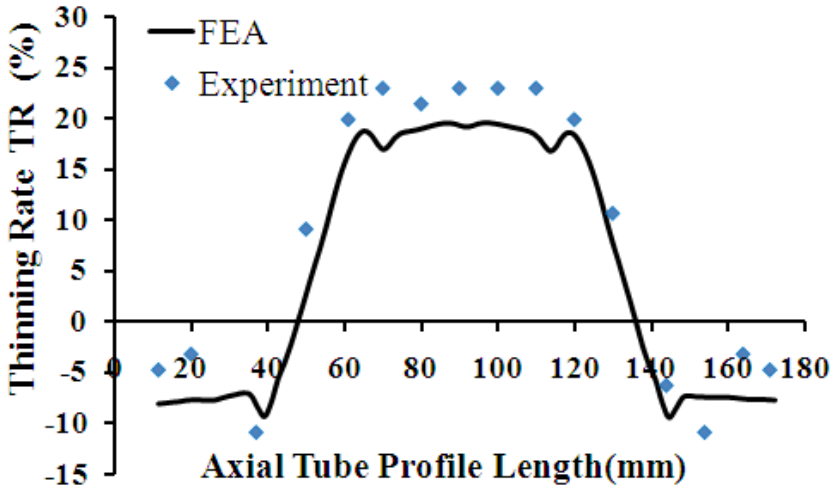

Fig.7- 4 Thinning distribution comparison between FEA simulation and experiment

7.3 THF of SS 304 tubular part with varying cross section

In the preforming of the part with varying cross section, the pressure was held at 18 MPa to trigger wrinkle onset in the first 30 s while the tube was compressed 10 mm along each side (Fig.7-5). Then the pressure was ramped up to 45 MPa and gradually increased to 57.5 MPa to maintain stable wrinkle growth from 30 s to 60 s (Fig. 7-5). The formed wrinkle is shown in Fig. 7-6a. In the final THF, the pressure initially was ramped up to 57.5 MPa and then was gradually increased to 75 MPa in the first 30 s. Due to a bigger bulge at the right side, more material was fed at the right side than to the left side in the first 30 s. From 30 s to 60 s, the pressure was increased from 75 MPa to 100 MPa to remove the wrinkle. The formed final part is shown in Fig. 7-6b. The wrinkle shape comparison and formed part comparison between the experiment and FEA simulation can be found in Fig.7-6a and b respectively, where the experimental results agree well with the FEA simulation results.

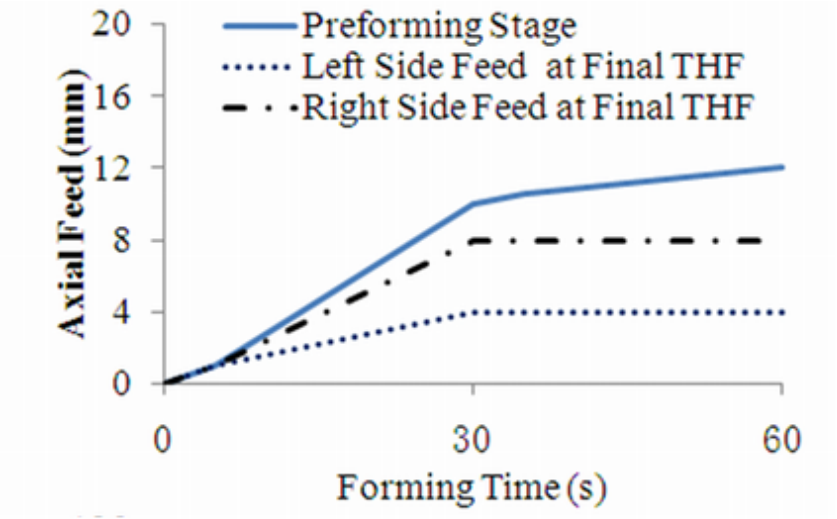

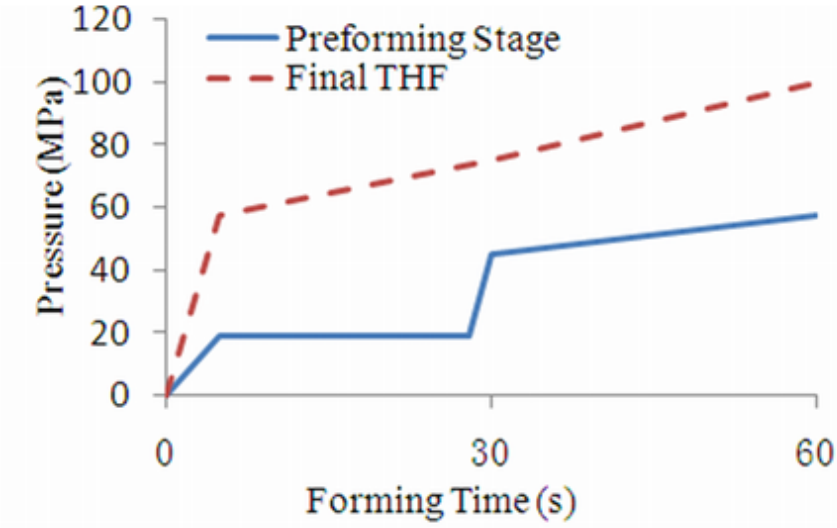

Fig.7- 5 Loading path for hydroforming the part with varying cross section

Experiment

FEA

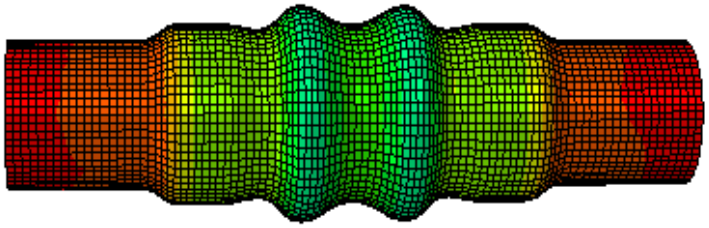

(a)

Experiment

FEA

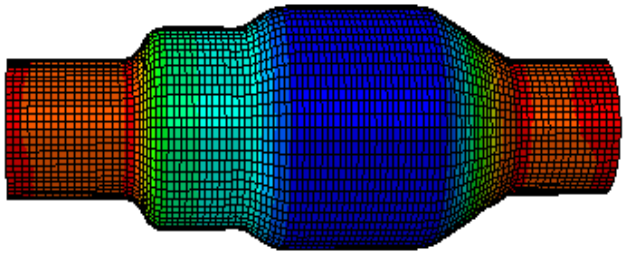

(b)

Fig.7- 6 (a) Wrinkle formation in preforming stage (b) Formed part

7.4 Bulging of Al 6061 tubing

7.4.1 Heat treatment and flow stress measurement for AL 6061 tubing

To improve the formability, AL 6061 T6 tubing was annealed in the Sybron Thernlyne furnace (Fig.7-7) by following the procedures given below.

i. The tubing was heated to 700 F for two hours.
ii. Then it was cooled at 50 F per hour down to 500 F.
iii. Final, the tubing was air cooled.

Fig.7- 7 Sybron thernolyne furnace

In order to measure the flow stress in the low strain range, a compression test was carried using a high resolution 5-ton press. Samples were firstly cut from the annealed Al 6061

material and were machined to a height of 18.41 mm. To ensure minimum friction at the tool work piece interface, Teflon lubricant was used. The experimental data for the compression test can be seen in Tab.7-1. The data was used later to plot a stress-strain curve as shown in Fig.7-9.

Tab.7- 1 Experimental data for the compression test at low strain range

Num	Height (mm)	Height reduction (mm)	Cross Section Area (mm^2)	Force (N)	Strain	Stress (MPa)
1	18.41	0.043	172.87	10252	0.0024	56.8
2	18.41	0.090	172.87	11597	0.0049	64.1
3	18.41	0.136	172.87	12914	0.0074	71.2
4	18.41	0.231	172.87	14928	0.0126	81.9

For the flow stress measurement in the high strain range, another compression test was carried out on a 150-ton press. Four samples were cut from the annealed Al 6061 bar for the flow stress measurement. Then, they were compressed to different heights (Fig.7-8) on the press while the forming loading is recorded. The forming force and geometrical size of compressed samples are listed in Tab.7-2. The data of the flow stress measurement was best fitted using the power law equation with K=152 MPa and n=0.168 as shown in Fig.7-9. Furthermore, the triple piecewise material model was used to fit the experimental data of flow stress measurement. The fitted parameters are listed in Tab.7-3 and the stress-strain curve of the full range is plotted in Fig.7-9. The stress-strain curve of

the annealed Al 6061 tubing was used in the analytical modeling and FEA simulations for two-stage preforming, which was discussed earlier in chapter 6.

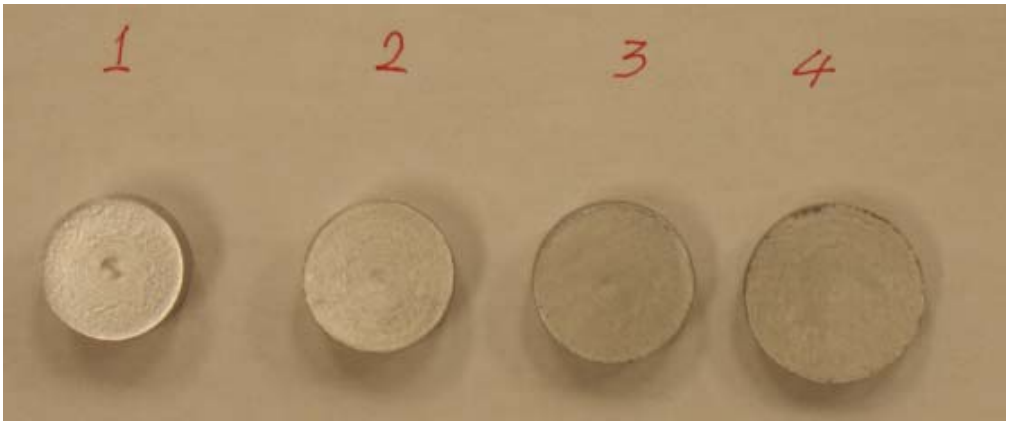

Fig.7- 8 Compressed samples for the flow stress measurement

Tab.7- 2 Experimental data for flow stress determination at high strain range

Sample	H_0(mm)	H_f(mm)	D_0(mm)	D_f(mm)	Load(N)	Strain	Stress (MPa)
1	19.56	17.88	25.4	26.56	56376	0.0896	101
2	19.30	15.62	25.4	28.24	74169	0.2116	118
3	19.53	13.41	25.4	30.65	94649	0.3759	128
4	19.33	11.05	25.4	33.59	123446	0.5593	139

--H_0: initial height, H_f: deformed height, D_0: initial diameter, D_f: deformed diameter.

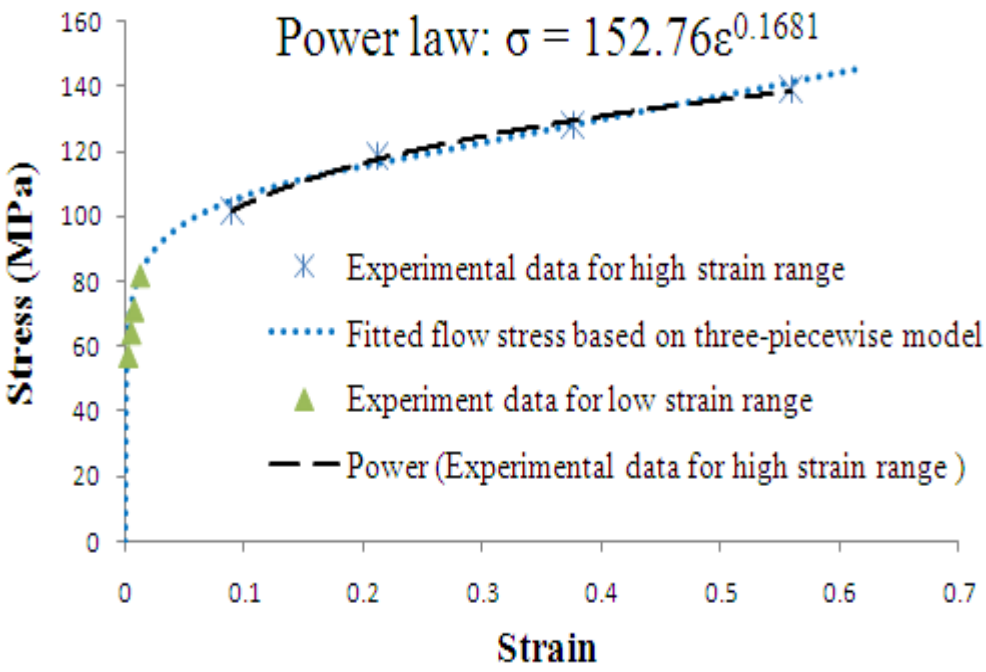

Fig.7- 9 Flow stress of annealed Al 6061

Tab.7- 3 Material properties of annealed Al 6061 tubing based on triple piecewise model

Material Properties	Al 6061
Young's Modulus E (GPa)	69 **[64]**
Yield Stress σ_y (MPa)	55 **[64]**
n*	9
strength coefficient K (MPa)	152
Strain hardening exponent n	0.162
ε_t	0.20
Poisson Ratio v	0.33 **[64]**

7.4.2 Bulging of Al 6061 tubing.

After heat treatment, each tube sample was machined to a length of 180 mm to fit the die. Before testing, the dies and tubular specimens were cleaned with acetone. The tube specimens were bulged using Teflon sheets as a lubricant. Teflon sheets 0.12 mm thick were wrapped around the specimens.

In the preforming stage, the pressure was first ramped up to 4.5 MPa, where it remained for about 30 s to trigger wrinkle onset when the tube end was compressed by 5 mm (Fig. 7-10). Then the pressure was ramped up to 8 MPa and gradually increased to 9 MPa to inhibit the hoop wrinkle during wrinkle growth from 30 s to 60 s, while the tube end was continuously compressed another 5.7 mm (Fig. 7-10). The formed wrinkle is shown in Fig. 7-11a. In the final tube bulging process, the pressure was first ramped up to 10 MPa, then it was gradually increased to 13 MPa to support stable wrinkle growth while the tube end was compressed 7 mm during the first 30 s. Then, the pressure was increased from 13 MPa to 30 MPa to remove the wrinkle and form the part. The final bulged tube with wrinkle removed is shown in Fig. 7-11b. The expansion rate of this bulged part was 54%, which is significantly greater the expansion rate 37% of the direct tube bulging process. The wrinkle shape comparison and formed part comparison between the experiment and FEA simulation can be found in Fig.7-11a and b respectively, where the experimental results agree well with the FEA simulation results.

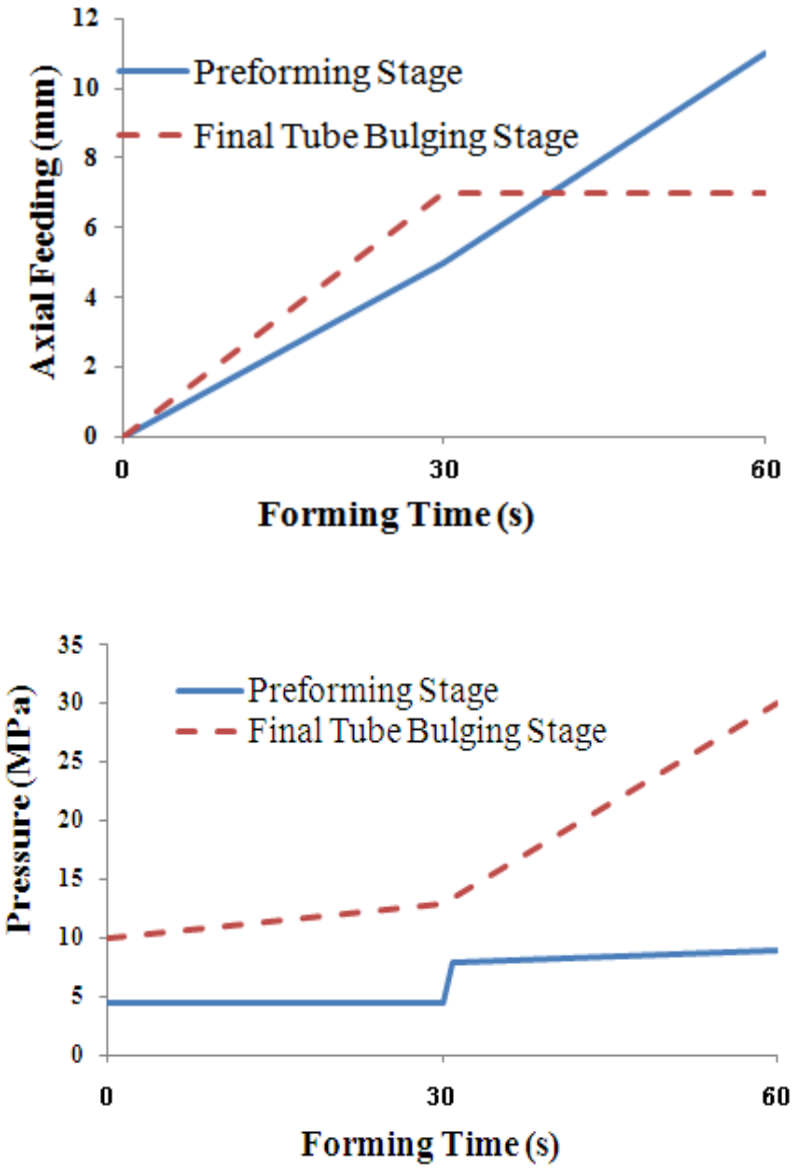

Fig.7- 10 Loading path of hydroforming the bulge

Experiment

FEA

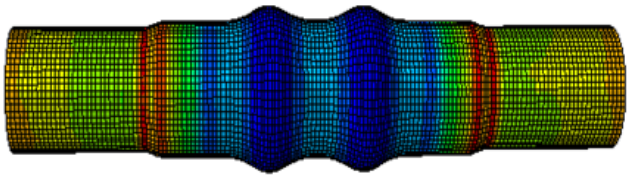

(a)

Experiment

FEA

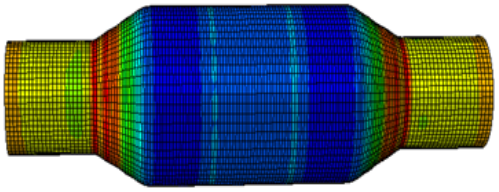

(b)

Fig.7- 11 (a) Wrinkle formation in preforming stage (b) Bulged part

7.5 Conclusions

In order to validate the two-stage preforming scheme, preform die sets for three axisymmetric parts were designed and tube bulging experiments were carried out on SS 304 tubing and Al 6061 tubing, which agreed well with the FEA simulation results.

Through this methodology, expansion rates of 71% and 54% were achieved for SS 304 tubing and Al 6061 tubing respectively. The expansion rates are significantly greater than that of direct tube bulging process, which are 50% and 37% for SS 304 tubing and Al 6061 tubing respectively.

CHAPTER 8: CONCLUDING REMARKS AND FUTURE WORK

8.1 Concluding remarks for preform design for forging and extrusion processes

A new method for preform design based on shape resemblance has been presented. The proposed method is based on constructing a part slightly larger than the desired part and then performing a finite element simulation of the larger part with a reasonably guessed preform. Because the part has been enlarged and most forming defects (i.e. fold, under-fill, flash) usually occur at or close to the boundary, defects will be confined to the enlarged portion. By backwards tracing of material flow on the desired part boundaries, a preform shape can be obtained within a few iterations, which can significantly reduce the computation costs and improve the design efficiency of the forging process. This preform design method can be applied to a variety of axisymmetric forging, extrusion, and upsetting/heading problems. The specific conclusions drawn from this study are:

- The developed preform design methodology has demonstrated that two or three FE iterations are sufficient to converge to a good preform shape for defect-free forming of a given part;
- The case studies presented have shown that this methodology can handle a variety of axisymmetric forging, extrusion, and upsetting/heading problems. All the applications presented in this paper are 2D, but this preform design methodology could be extended to 3D parts. However, 3D parts will require more effort for mapping the track points in the preform design than would 2D parts.

8.2 Concluding remarks for the preform design for tube hydroforming process

A two-stage preforming process based on wrinkle formation was developed for the tube hydroforming process to accumulate material in the forming zone so as to reduce the thinning rate and improve the formability. In preforming stage I, wrinkle onset was triggered. In stage II, the wrinkle grew stably and uniformly to a certain height. Then preformed wrinkles were flattened to conform to the die shape in the final tube hydroforming process. An analytical model based on the post-buckling analysis was used to study the wrinkle evolution characteristics in tube hydroforming. The analytical results offered guidance to the process design of the two-stage preforming process. The two-stage preforming was used in the bulging process of SS 304 tube and Al 6061 tube and led to significantly increased expansion rate, which is verified experimentally. The specific conclusions drawn from this study are:

- The analytical model can accurately predict initiation of wrinkles as verified by both, the finite element analysis and THF experiments. The wrinkle wave length and the number of wrinkles are based on internal pressure, tube size, and tube properties.
- The study has found that uniformity in wrinkle growth is lost soon after the wrinkles have been initiated. i.e., further axial tube compression does not lead to uniform wrinkle growth. Therefore, the current analytical model can only be used to provide information pertaining to wrinkle initiation as a function of pressure, tube size, and tube properties. This information is, however, critical for preform development as it cannot be obtained easily via trial-and-error FEA iterations.
- In order to grow uniform wrinkles to a specific height, die constraining is necessary. Both the finite element simulations and experiments have shown that wrinkles from tube ends will start to grow followed by middle wrinkles as the tube is axially compressed. Therefore, with the aid of finite element analysis and die constraining a

perform die that will accumulate tube material at the die cavity can be determined.

- The effect of the process variable, such as material properties, tube thickness and die span length on the formability of the preforming and THF are investigated. It was found that the expansion rate of the bulged shape increases with the material hardening exponent n and decreases with the tube thickness and die span length.
- Experimental verification of this methodology was carried out for two bulged SS 304 parts and one bulged Al 601 part, where a significant increase in tube expansion rate was achieved as compared to the direct tube hydroforming.

8.3 Future work

8.3.1 Preform design for forging process based on geometrical resemblance

In this work, the preform design based on geometrical resemblance was applied to the 2D axisymmetric parts, but it could be extended to 3D parts. However, 3D parts will require more effort for mapping the track points in the preform design than would 2D parts. Further study is also needed to investigate the influence of the initial preform guess and variations in the construction of the larger part on the effective strain distribution and forming load.

8.3.2 Preform design for tube hydroforming process based on wrinkle formation

In this work, a two-stage preforming scheme based on wrinkle formation was developed for tube hydroforming process and the influence of the process variables on the formability of tube bulging process were investigated. Future work can focus on the following aspects.

1) Optimize of the loading path of the two-stage preforming
2) Investigate the influence of pressure pulsation on the formability of the tube bulging with two-stage preforming
3) Optimize the preforming die shape to better control the wrinkle growth in the preforming stage.

REFERENCES

[1].Vemuri, K. R., Oh, S. I., and Altan, T. A knowledge-base system to automate blocker design. Int. J. Mach. Tools Mf, 1988, 29(4), 505–518.

[2] Bariani, P. and Knight, W. A. Computer-aided cold forging process design: a knowledge-based system approach to forming sequence generation. Annls CIRP,1988, 37, 243.

[3] Osakada, K., Yang, G. B., Nakamura, T., and Mori, K.Expert system for coldforging process based on FEM simulation. Annls CIRP, 1990, 39, 249–252.

[4]Kim, H. and Altan, T. Computer-aided part and processing-sequence design in cold forging. J. Mater. Process. Technol., 1992, 33, 57–74.

[5] Kim, H. S. and Im, Y. T. Expert system for multi-stage cold forging process design with a redesigning algorithm. J. Mater. Process. Technol., 1995, 54, 271–285.

[6]Tisza, M. Expert systems for metal forming. J. Mater.Process. Technol., 1995, 53, 423–432.

[7]Kim, H. S. and Im, Y. T. Multi-stage cold forging process design with a searching algorithm. Trans. NAMRC, 1996, 24, 161.

[8] Kim, H. and Altan, T. Cold forging of steel-practical examples of computerized part and process design. J.Mater. Process. Technol., 1996, 59, 122.

[9] Osakada, K., Kado, T., and Yang, G. B. Application of AI-technique to planning of cold forging. Annls CIP, 1998, 37(1), 239–242.

[10] Caporalli, A., Gileno, L. A., and Button, S. T. Expert system for hot forging design. J. Mater. Process. Technol., 1998, 80–81, 131–135.

[11] Kim, H. S. and Im, Y. T. An expert system for cold forging process design based on a depth-first search. J. Mater. Process. Technol., 1999, 95, 262–274.

[12] Song, J. H. and Im, Y. T. Development of a computeraided-design system of cold forward extrusion of a spur gear. J. Mater. Process. Technol., 2004, 153, 821.

[13] Song, J. H. and Im, Y. T. The applicability of process design system for forward extrusion of spur gears. J. Mater. Process. Technol., 2007, 184, 411–419.

[14] Bakhshi-Jooybari, M., Pillinger, I., Dean, T. A., and Hartley, P. Development of product and process comparison criteria for an intelligent knowledge-based system for forging die design. Proc. IMechE, Part B: J. Engineering Manufacture, 1996, 210(B7), 565–578.

[15] Park, J. J., Rebelo, N., and Kobayashi, S. A new approach to preform design in metal forming with the finite element method. Int. J. Mach. Tool Des. Res., 1983, 23, 71–79.

[16] Kobayashi, S., Oh, S. I., and Altan, T. Metal forming and finite element method, 1989 (Oxford University Press, New York).

[17] Kim, N. and Kobayashi, S. Preform design in H-shape cross section axisymmetric forging by finite element method. Int. J. Mach. Tools Mf., 1990, 30, 243–268.

[18] Zhao, G., Wright, E., and Grandhi, R. V. Forging preform design with shape complexity control in simulating backward deformation. Int. J. Mach. Tools Mf., 1995, 35, 1225–1239.

[19] Zhao, G., Wright, E., and Grandhi, R. V. Computer aided preform design in forging using the inverse die contact tracking method. Int. J. Mach. Tools Mf., 1996, 36, 755–769.

[20] Chang, C. C. and Bramley, A. N. Forging preform design using a reverse simulation approach with the upper bound finite element procedure. Proc. IMechE, Part C: J. Mechanical Engineering Science, 2000, 214 (C1), 127–136. DOI: 10.1243/0954406001522868.

[21] Badrinarayanan, S. and Zabaras, N. A sensitivity analysis for the optimal design of metal forming processes. Computer Methods in Appl. Mechanics Engng, 1996,129, 319–348.

[22] Fourment, L. and Chenot, J. L. Optimal design for nonsteady-state metal forming process-I: Shape optimization method. Int. J. Numer. Methods Engng, 1996, 39,33–50.

[23] Zhao, G., Wright, E., and Grandhi, R. V. Preform die shape design in metal forming using an optimization method. Int. J. Numer. Methods Engng, 1997, 40, 1213–1230.

[24] Srikanth, A. and Zabaras, N. Shape optimization and preform design in metal forming process. Computer Methods in Appl. Mech. Engng, 2000, 190, 1859–1901.

[25] Zabaras, N., Ganapathysubramanian, S., and Li, Q. A continuum sensitivity method for the design of multistage metal forming processes. Int. J. Mech. Sci., 2003,45, 325–358.

[26] Vieilledent, D. and Fourment, L. Shape optimization of axisymmetric preform tools in forging using a direct differentiation method. Int. J. Numer. Meth. Engng, 2001, 52, 1301–1321.

[27] Castro, C. F., Sousa, L. C., Antonio, C. A. C., and Cesarde Sa, J. M. A. An efficient algorithm to estimate optimal preform die shape parameters in forging. Engng Comput.,2001, 18, 1057–1077.

[28] Castro, C. F., Antonio, C. A. C., and Sousa, L. C. Optimization of shape and process parameters in metal forging using genetic algorithms. J. Mater. Process Technol., 2004, 146, 356–364.

[29] Thiyagarajan, T. and Grandhi, R. V. 3D preform shape optimization in forging using reduced basis techniques. Engng Optimization, 2005, 37, 797–811.

[30] Hong, J. T., Lee, S. R., Park, C. H., and Yang, D. Y. Iterative preform design technique by tracing the material flow along the deformation path application to piston forging. Engng Computing, 2006, 23, 16–31.

[31] Nagpal, V. Process design and finite element analysis software for metal forming. Fastener Tech. Int. J., October2009, 30—31.

[32] Bramfitt, B. L. and Hingwe, A. K. Annealing of steel. ASM Handbook, 1991, Vol 4, p. 46 (ASM International, Materials Park, Ohio).

[33] Karadeniz, E. Influence of different initial microstructure on the process of spheroidization in cold forging. Mater. Des., 2008, 29, 251–256.

[34]M. Ahmetoglu, T. Altan – 'Tube hydroforming: state-of-the-art and future trends', Journal of Materials Processing Technology, 98 (2000), p. 25-33

[35] Yang Jae-Bong, Jeon Byung-Hee, Oh Soo-Ik. Design sensitivity analysis and optimization of the hydroforming process. J Mater Process Technol 2001;113:666–72.

[36] Genlin JC, Labergere C. Numerical control strategies for the hydroforming of thin walled metallic tubes, Numisheet 2002, October 21–25, Jeju Island, Korea; 2002. p. 499–504.

[37] Strano Matteo, Jirathearanat Suwat, Shr Shiuan-Guang, Altan Taylan. Virtual process development in tube hydroforming. J Mater Process Technol 2004;146:130–6.

[38] Aue-U-Lan Yingyot, Ngaile Gracious, Altan Taylan. Optimizing tube hydroforming using process simulation and experimental verification. J Mater Process Technol 2004;146:137–43.

[39] Aydemir A, de Vree JHP, Brekelmans WAM, Geers MGD, Sillekens WH, Werkhoven RJ (2005) An adaptive simulation approach designed for tube hydroforming processes. J Mater Process Technol 159:303–310 doi:10.1016/j.jmatprotec.2004.05.018

[40] S. Fuchizawa, Influence of strain hardening exponent on the deformation of thin-walled tube of finite length subjected to hydrostatic external pressure, Adv. Technol. Plasticity 1 (1984) 297±302.

[41] S. Fuchizawa, Influence of plastic anisotropy on deformation of thinwalled tubes in

bulge forming, Adv. Technol. Plasticity 2 (1987) 727±732.

[42] T. Altan, H. Palaniswamy and Y. Aue-u-lan. Tube and Sheet Hydroforming-Advances in Material Modeling, Tooling and Process Simulation. Advanced Materials Research Vols. 6-8 (2005) pp 1-12

[43] Gracious Ngaile, Stefan Jae ger, Taylan Altan-“ Lubrication in tube hydroforming (THF) Part I. Lubrication mechanisms and development of model tests to evaluate lubricants and die coatings in the transition and expansion zones”, Journal of Materials Processing Technology 146 (2004),P. 108–115

[44] Gracious Ngaile, Stefan Jaeger, Taylan Altan-“ Lubrication in tube hydroforming (THF) Part II. Performance evaluation of lubricants using LDH test and pear-shaped tube expansion test”, Journal of Materials Processing Technology 146 (2004),P. 116–123

[45] Hwang, Y M "Process fusion: tube hydroforming and crushing in a square die". Proceedings of the Institution of Mechanical Engineers. Part B, Journal of engineering manufacture (0954-4054), 218 (2),p. 169.

[46] Jeong Kim, Li-Ping Lei and Beom-Soo Kang. "Preform design in hydroforming of automobile lower arm by FEM". Journal of materials processing technology (0924-0136), 138 (1-3),p. 58.

[47**]** Yuan, SJ; Wang, XS; Yuan, WJ"Effect of wrinkling behavior on formability and thickness distribution in tube hydroforming". *Journal of materials processing technology.* 177. (2006). 668 - 671

[48**]** Shijian Yuan , Xiaosong Wang, Gang Liu, Z.R. Wang."Control and use of wrinkles in tube hydroforming". Journal of Materials Processing Technology. 182 (2007) 6–11

[49**]** Lihui Lang Huili Li Shijian Yuan, J. Danckert and K.B. Nielsen. (03/01/2009). "Investigation into the pre-forming's effect during multi-stages of tube hydroforming of aluminum alloy tube by using useful wrinkles". Journal of materials processing technology (0924-0136), 209 (5),p. 2553.

[50**]** Xiaosong Wang and YinXue Yao ." Wrinkling behavior in hydroforming of

unsymmetrical tubular part ". International journal of modern physics. B, Condensed matter physics, statistical physics, applied physics (0217-9792), 23 (6-7),p. 1937.

[51**]** K. Mori, A.U. Patwari, S. Maki, Improvement of formability by oscillation of internal pressure in pulsating hydroforming of tube, Annals of the CIRP 53 (1) (2004) 215–218

[52**]** K. Mori, T. Maeno, S. Maki. Mechanism of improvement of formability in pulsating hydroforming of tubes. International Journal of Machine Tools & Manufacture 47 (2007) 978–984

[53] Takayuki Hama, Motoo akawa, iroshi Fukiharu and Akitake Makinouchi. "Simulation of Hammering Hydroforming by Static Explicit FEM" . ISIJ International, Vol. 44 (2004), No. 1, pp. 123–128

[54] M Loh-Mousavi, M Bakhshi-Jooybari, K-I Mori, and K Hyashi. "Improvement of formability in T-shape Hydroforming of tubes by pulsating pressure" Proc. IMechE Vol. 222 Part B: J. Engineering Manufacture . P1139-1146

[55] R. HILL, A general theory of uniqueness and stability in elastic-plastic solids. J. Mech. Phys. Solids 6, 236 (1958).

[56] Batterman SC. Plastic buckling of axially compressed cylindrical shells. AIAA Journal 1965;3:316–25.

[57] Lee,L.H.N "Inelastic buckling of initially imperfect cylindrical shells subject to axial compression.'' J. Aerospace Sci.29,87-95(1962)

[58] Tvergaard V. Plastic buckling of axially compressed circular cylindrical shells. Thin Walled Structures 1983;1:139–63.

[59] Bardi, F.C., Kyriakides, S. and Yun, H.D. (2006). Plastic buckling of circular tubes under axial compression. Part I :Experiment. Int. J. Mech. Sci. 48 (2006) 830–841

[60] Bardi, F.C., Kyriakides, S. and Yun, H.D. (2006). Plastic buckling of circular tubes under axial compression. Part II analysis. Int. J. Mech. Sci. 48, 842–854.

[61] J.A. Paquette, S. Kyriakides. (2006) Plastic buckling of tubes under axial compression and internal pressure. International Journal of Mechanical Sciences 48, 855–867

[62] Stelios Kyriakides. Edmundo Corona .Mechanics of Offshore Pipelines Vol. I Buckling and Collapse

[63] Y. Aue-u-lan et.al. including T. Altan, "Warm forming magnesium, aluminum tubes - A high temperature process for light weight alloys" Tube and Pipe Journal, September 2006, p.36

[64] http://asm.matweb.com/search/SpecificMaterial.asp?bassnum=MA6061O

APPENDICES

APPENDIX A: ANALYTICAL MODEL FOR PREDICTING TUBE WRINKLES

Plastic buckling can be modeled based on two theories, "J_2 flow theory" and "J_2 deformation theory". But the prediction of analytical model based on the "J_2 deformation theory" matches the experiment results better than the "J_2 flow theory". Thus, the "J_2 deformation theory" is used here to predict the plastic wrinkling of the circular cylinder which is subject to axial compression and internal pressure. In this work, the wrinkle analytical model, which is discussed next, is from the references **[59-62].**

1. Kinematics

The thin-walled circular cylindrical shell (Fig.A-1) with mid-surface radius *R* and wall thickness *t* are considered here.

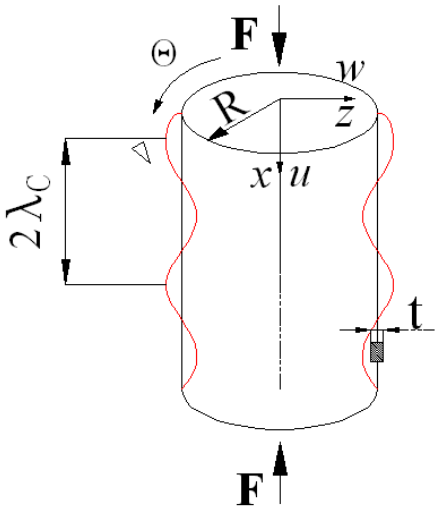

Fig.A- 1 Wrinkled tube and it's size

The strain at any point on the shell is defined as:

$$\varepsilon_{\alpha\beta} = \left(\varepsilon^0_{\alpha\beta} + z\kappa_{\alpha\beta}\right) \Big/ (A_\alpha A_\beta) \qquad (\alpha, \beta = 1, 2) \tag{A1}$$

Where: $A_1 = 1, A_2 = 1 + \dfrac{z}{R}$

If only the axisymmetric wrinkle mode is considered，the membrane and bending strains in terms of displacements ***(u, w)*** are defined as:

$$\begin{aligned} \varepsilon^0_{xx} &= u_{,x} + \frac{1}{2} w_{,x}{}^2 \\ \varepsilon^0_{\theta\theta} &= \frac{w}{R} \\ \kappa_{xx} &= -w_{,xx} \end{aligned} \tag{A2}$$

The membrane and bending moment intensities are given by:

$$\begin{aligned} N_{xx} &= \int_{-t/2}^{t/2} (1 + \frac{z}{R}) \sigma_{xx} dz \\ N_{\theta\theta} &= \int_{-t/2}^{t/2} \sigma_{\theta\theta} dz \\ M_{xx} &= \int_{-t/2}^{t/2} (1 + \frac{z}{R}) \sigma_{xx} z dz \end{aligned} \tag{A3}$$

2. Equilibrium equation

The equilibrium equation is established through the principle of virtual work as:

$$\int_s (N_{xx}\delta\varepsilon^0_{xx} + N_{\theta\theta}\delta\varepsilon^0_{\theta\theta} + M_{xx}\delta\kappa^0_{xx}) ds = p\delta w \tag{A4}$$

3. Constitutive equations

In the wrinkling prediction, the deformation process of the cylinder is modeled based on the "J_2 flow theory", while the wrinkle onset checking is based on "J_2 deformation theory". Thus, both constitutive equations of the deformation and flow theory are presented here.

The constitutive equation of "J_2 deformation theory":

$$\begin{Bmatrix} d\varepsilon_x \\ d\varepsilon_\theta \end{Bmatrix} = \frac{1}{E_s} \begin{vmatrix} 1+q(2\sigma_x-\sigma_\theta)^2 & -v_s+q(2\sigma_x-\sigma_\theta)(2\sigma_\theta-\sigma_x) \\ -v_s+q(2\sigma_x-\sigma_\theta)(2\sigma_\theta-\sigma_x) & 1+q(2\sigma_\theta-\sigma_x)^2 \end{vmatrix} \begin{Bmatrix} d\sigma_x \\ d\sigma_\theta \end{Bmatrix} \quad (A5)$$

$$E_s = \frac{\sigma_e}{\varepsilon_e}$$

$$v_s = \frac{1}{2} + \frac{E_s}{E}(v - \frac{1}{2})$$

Where: $$q = \frac{1}{4\sigma_e^{\,2}}(\frac{E_s}{E_t} - 1)$$

The constitutive equation of "J_2 flow theory":

$$\begin{Bmatrix} d\varepsilon_x \\ d\varepsilon_\theta \end{Bmatrix} = \frac{1}{E} \begin{vmatrix} 1+Q(2\sigma_x-\sigma_\theta)^2 & -v+Q(2\sigma_x-\sigma_\theta)(2\sigma_\theta-\sigma_x) \\ -v\ +q(2\sigma_x-\sigma_\theta)(2\sigma_\theta-\sigma_x) & 1+Q(2\sigma_\theta-\sigma_x)^2 \end{vmatrix} \begin{Bmatrix} d\sigma_x \\ d\sigma_\theta \end{Bmatrix} \quad (A6)$$

Where: $$Q = \frac{1}{4\sigma_e^{\,2}}(\frac{E}{E_t} - 1)$$

4. The onset of plastic buckling

Equation (A7) gives the critical condition for the plastic axisymmetric wrinkle onset. Once the critical axial stress σ_c is satisfied, the plastic wrinkle will start and half

wave-length λ_c of the wrinkle can be computed as (A8)

$$\sigma_c = \left(\frac{C_{11}C_{22} - C_{12}}{3} \right)^{1/2} (\frac{t}{R}) \tag{A7}$$

$$\lambda_c = \pi \left(\frac{C_{11}{}^2}{12(C_{11}C_{22} - C_{12}{}^2)} \right)^{1/4} (Rt)^{1/2} \tag{A8}$$

Where $C_{\alpha\beta}$ is the element of the inverse of the constitutive matrix in equation (A5).

5. Wrinkling evolution and collapse

The post buckling response of the wrinkled cylinder can be studied by introducing a small initial imperfection corresponding to the critical buckling mode as follows;

$$\overline{w} = -tw_o \cos(\frac{\pi x}{\lambda_c}) \tag{A9}$$

In this model, the interested domain is limited to just one half of the axial wave length λ_c. In the presence of an initial imperfection, the strain is given by:

$$\varepsilon_{\alpha\beta} = \varepsilon_{\alpha\beta}(u, v, w + \overline{w}) - \varepsilon_{\alpha\beta}(0, 0, \overline{w}) \tag{A10}$$

Assuming the displacement after wrinkle onset is:

$$u = b_0 x + \sum_{i=1}^{Nu} b_i \sin(\frac{i\pi x}{\lambda_c})$$
$$w = a_0 + \sum_{i=1}^{Nw} a_i \sin(\frac{i\pi x}{\lambda_c}) \tag{A11}$$

Substitute (A11) into equilibrium equation (A4):

$$\int_0^{\lambda_c} (N_{xx}\varepsilon^0_{xx,i} + N_{\theta\theta}\varepsilon^0_{\theta\theta,i} + M_{xx}\kappa^0_{xx,i})dx\delta q_i = P\int_0^{\lambda_c} w,_i dx\delta q_i$$

(i=1,2,……Nw+Nu+1)

(A12)

Where:

$$(\bullet),_i = \frac{\partial(\bullet)}{\partial q_i} \quad \text{and} \quad q = \left[a_0, a_1, ..., a_{Nw}, b_1, b_2, ...b_{Nu}\right].$$

b_0 is the average axial strain which is prescribed incrementally. Due to the arbitrariness of δq_i, equation (A21) can be transformed to:

$$\int_0^{\lambda_c} (N_{xx}\varepsilon^0_{xx,i} + N_{\theta\theta}\varepsilon^0_{\theta\theta,i} + M_{xx}\kappa^0_{xx,i})dx - P\int_0^{\lambda_c} w,_i dx = 0$$

$$i = 1, 2, ..., Nw + Nu + 1 \tag{A13}$$

In order to obtain the displacement coefficient $q = \left[a_0, a_1, ..., a_{Nw}, b_1, b_2, ...b_{Nu}\right]$, the equation (A13) is solved by prescribing the average axial strain incrementally.

Assuming total axial feeding of ***f***, tube length ***L***, the average axial strain can be expressed as:

$$b_0 = -\frac{f}{L} \tag{A14}$$

Assuming that the displacement coefficient ***q**** represents the converged solution of the equation (A13) corresponding to $\boldsymbol{b_0}$ and ***dq*** is the required increment for current solution corresponding to $\boldsymbol{db_0}$, the instantaneous constitutive equation is given as:

$$\begin{Bmatrix} dN_{xx} \\ dN_{\theta\theta} \\ dMxx \end{Bmatrix} = \int_{-t/2}^{t/2} \begin{vmatrix} (1+\frac{z}{R})C_{11} & C_{12} & z(1+\frac{z}{R})C_{11} \\ C_{21} & \frac{1}{(1+\frac{z}{R})}C_{22} & ZC_{21} \\ z(1+\frac{z}{R})C_{11} & zC_{12} & z^2(1+\frac{z}{R})C_{11} \end{vmatrix} dz \begin{Bmatrix} d\varepsilon_{xx}{}^0 \\ d\varepsilon_{\theta\theta}{}^0 \\ d\kappa_{xx} \end{Bmatrix} \tag{A15}$$

Where $C_{\alpha\beta}$ is the element of the inverse of the constitutive matrix of equation (A6).

Substitute (A15) into (A13) and solve the nonlinear equation to obtain $\boldsymbol{dq}$, then the displacement coefficient q can be expressed:

$$q = q^* + dq \tag{A16}$$

Thus, the displacement coefficient $\boldsymbol{q}$ corresponding to each average axial strain b0 can be obtained by iterating the solution scheme above .Accordingly, the axial stress σx , stress resultant N_x, N_θ and moment M_x can be computed once the displacement coefficient $\boldsymbol{q}$ is obtained.

APPENDIX B: SOFTWARE MODULE FOR WRINKLE EVOLUTION PREDICTION IN THF PROCESS

1. Introduction of the program function, menu and user interface

Based on the analytical model aforementioned, a software module was developed to compute the evolution process of wrinkles in the tube hydroforming process by using the Fortran language. This program can compute all the state variables of the wrinkle evolution process such as such critical axial stress σ_c , critical strain ε_c , half wave length λ_c, axial stress σ_x, hoop stress σ_θ, axial stress resultant N_x, hoop stress resultant N_θ, and wrinkle height H_b, once the required process variables are defined. Fig.B-1 shows the program menu bar. It has five menus as listed below:

- Process variables: for user to input the process variables such as loading path and material properties.
- Solution setting: for user to define the settings related to solution accuracy
- Solve: start the computation
- Pressure Set solution: compute the wrinkle evolution under different pressure

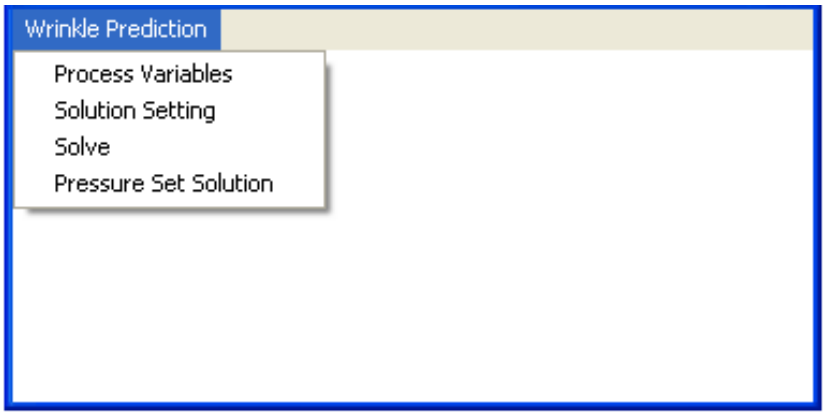

Fig.B- 1 Program menu

2. Input and output description of the program

In order to compute the wrinkle evolution, user needs to define the process variables prior to solving. By clicking the menu "P**rocess Variables**", user can enter the "**process variable input dialogue**" box shown as Fig.B-2. There are four sets of process variables:

- Tube geometry size: Tube outer diameter D, tube thickness t and tube length L
- Material (Small Strain): Young's Modulus E, Yield stress σ_y (Sigma Y), strain hardening related factor n and Poisson ratio V.
- Material(Large Strain): material strength K and strain hardening exponent n*
- Loading Path: internal pressure P and axial compression amount

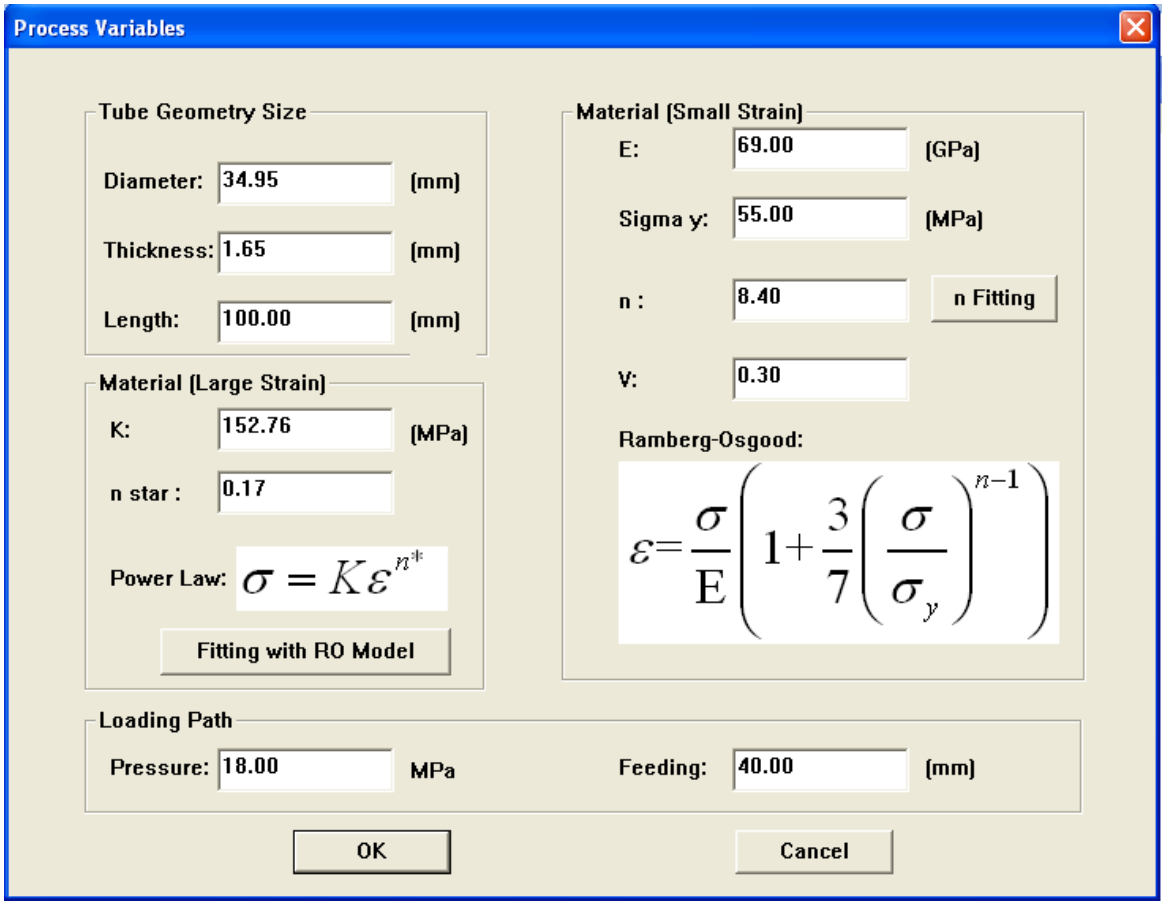

Fig.B- 2 Process variables dialogue

In the dialogue box, there are two buttons, **"Fitting with RO Model"** and **"n Fitting"**. These two buttons are designed for user to fit the material property data in the small strain range with data in large strain range. When only the power law data, young's modulus E, and yield stress data are available, user can click the button **"n Fitting"** to find n of the RO model best fitted with the power law model. When both power law data and RO model data are available, user can click button **"Fitting with RO Model"** to connect these two curves with a best fitted line segment. After user finishes the fitting, a file of the full range of the flow stress is output and stored in the computer with name "RO-flow-stress.txt", which allows user to plot flow stress in the excel.

Another input prior to solving is the **"solution setting".** By clicking menu **"solution setting"**, user can enter the solution setting dialogue box shown in Fig.B-3. In this dialogue box, user can define the parameters relevant to solution accuracy as listed below:

- Imperfection factor: W_0
- The number of the sinusoidal function (Ai) used to define to the radial displacement of wrinkles
- The number of the cosine function (Bi) used to define to the axial displacement of the wrinkles
- Total incremental steps to solve the problem

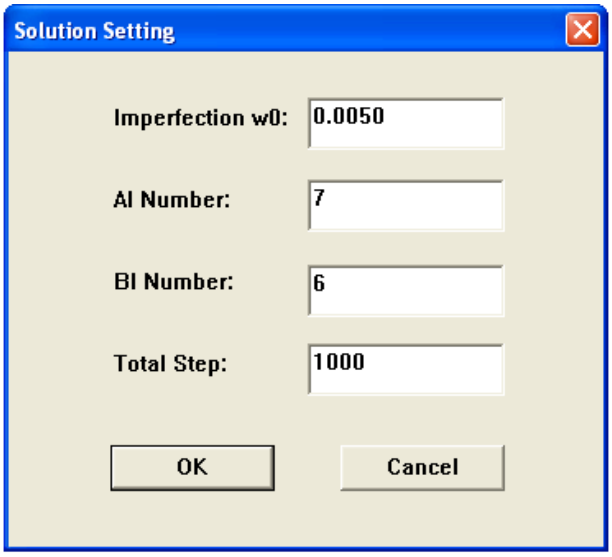

Fig.B- 3 Solution setting dialogue box

After the user clicks the menu **"Solve"**, the program starts to compute the wrinkle evolution incrementally. Once it finishes the computation, the program will output all the state variables into three files as described below:

- File 1 **"Wrinkle_evolution_shape.txt"**. It contains the variables such as displacement function coefficient, critical strain ε_c , half wave λ_c and wrinkle height H_b of each increment step.
- File 2 **"Wrinkle_evolution_stress_resultant.txt"**. It contains stress resultant on 16 integration points along the half-wave-length region of each increment step
- File 3 **"Wrinkle_evolution_stress.txt"**. It contains stress on 16 X 5 integration points.

Once user runs the analytical model with different pressure conditions by clicking menu **"Pressure Set solution"**, all the outputs will be stored in the file **"Pressure_set_solution.txt"** and user can use excel to process it. It contains half wave length λ_c, axial stress resultant N_x and wrinkle height H_b at three pressure levels: zero, half yield pressure and yield pressure.

3. The procedures of how to run the program

The procedures to run the analytical model program are listed below:

i. Click the menu **"Process variables"** to enter the dialogue and input the process variables, such as loading path and material properties.

ii. Click the menu **"Solution setting"** to define the settings related to solution accuracy

iii. Click the menu **"Solve"** to start the computation of the analytical model.

iv. If necessary, click the menu **"Pressure Set solution"** to compute the wrinkle evolution under different pressure

v. Open the output files mentioned in last section using excel to process all the state variables interested.

4. How to process the output data

In excel, user can open text files by importing data files with space to delimit the text line. Next, how to process the data in the files of **"Wrinkle_evolution_shape.txt"**, **"Wrinkle_evolution_stress_resultant.txt"**, **"Wrinkle_evolution_stress.txt"** and **"Pressure_set_solution.txt"** will be discussed.

Once the file "**Wrinkle_evolution_shape.txt"** is opened in excel, data of half wave length, wrinkle height Hb and displacement functions can be obtained. The columns inside the file are explained below:

- Column with heading"B0": axial compression ratio of the tube
- Column with heading "dB": axial compression increment of each step
- Column with heading from "dA" and "dB": increment of displacement function coefficient Ai (i=1…7) and Bi (i=1...6)
- Column with heading "A" and "B": displacement function coefficient Ai (i=1…7)

and Bi (i=1...6)

- Column with heading " Ex_Cr": critical strain
- Column with heading "Sx_Cr": critical stress
- Column with heading "HB0": wrinkle height

The wrinkle height curve can be obtained by plotting "HB0" column against "B0" column as shown below:

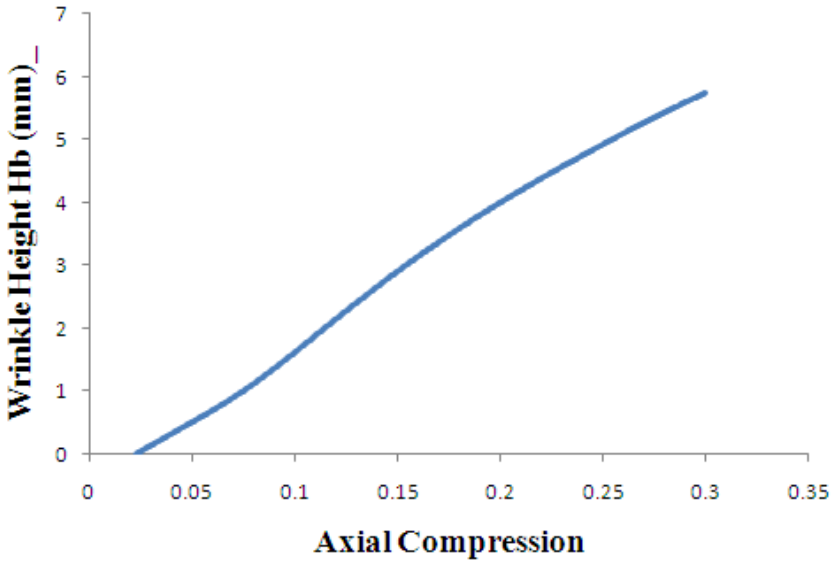

Fig.B- 4 Wrinkle height curve

Once the "**Pressure_set_solution.txt"** is opened in excel, data of stress resultant on sixteen points along the axial direction in the half wave length can be obtained. The columns inside the file are explained below:

- Column with heading"B0": axial compression ratio of the tube
- Column with heading "dB": axial compression increment of each step
- Column with heading "Nx": axial stress resultant
- Column with heading "Ns": hoop stress resultant

- Second row with number from 1 to 16 means sixteen integration points along axial direction.
- The rigidity curve can be obtained by plotting “Nx” column with number “1” below it against “B0” column as shown below:

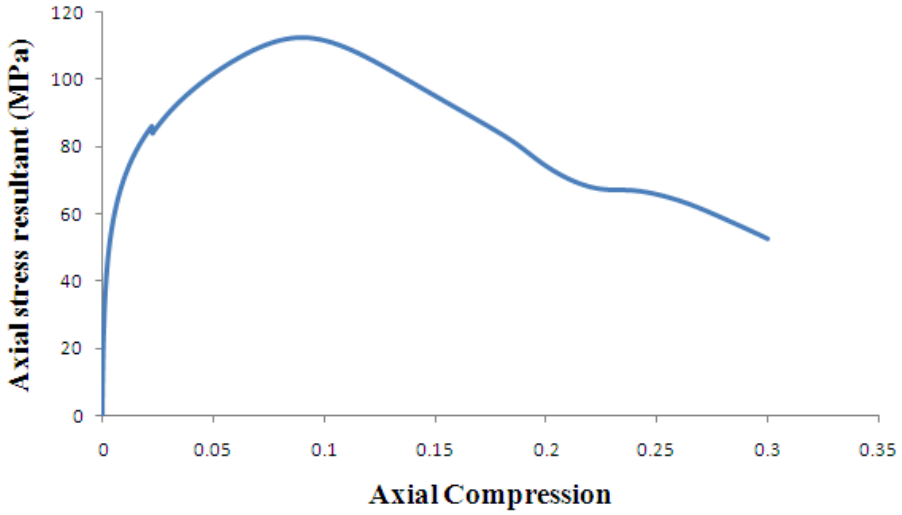

Fig.B- 5 Tube axial rigidity curve

Once the file **“Wrinkle_evolution_stress.txt”** is opened in excel, data of stress on all integration points can be obtained. The columns inside the file are explained below:

- Column with heading”B0”: axial compression ratio of the tube
- Column with heading ”dB”: axial compression increment of each step
- Column with heading from “L1” to”L5”: stress on five layers from tube inner surface to outer surface.
- Second row with number from 1 to 16 means 16 integration points along axial direction.

Once the file **“Wrinkle_evolution_stress.txt”** is opened in excel, data of the half wave length, wrinkle number, wrinkle height and axial stress resultant at three pressure levels: zero pressure, half yielding pressure and yielding pressure can be obtained. The columns

inside the file are explained below:

- Column with heading “Pressure”: three pressure levels
- Column with heading “Lmd”:half wave length
- Column with heading “wrinkle Number”: wrinkle number along the tube axial length
- Column with heading “P1_B0” , “P2_B0” and “P3_B0”: axial compression rate at three pressure levels
- Column with heading “P1_Hbo”, “P2_Hb0” and “P3_Hb0”: wrinkle height at three pressure levels
- Column with heading “P1_Stress”, “P2_Stress” and “P3_Stress”: axial stress resultant at three pressure levels

The curve of half wave length, wrinkle number, and wrinkle height at three pressure levels: zero pressure, half yielding pressure and yielding pressure can be plotted as shown in Fig.B-6, Fig.B-7 and Fig.B-8 respectively.

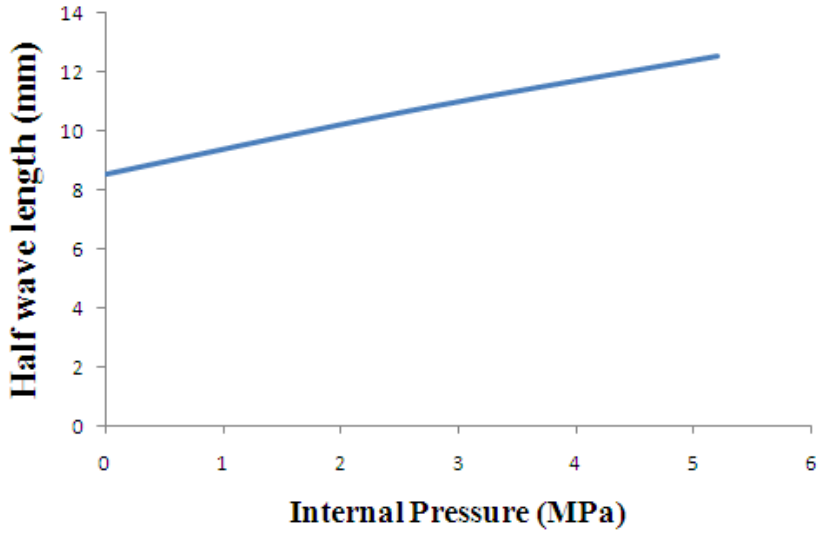

Fig.B- 6 Half wave length at three pressure levels

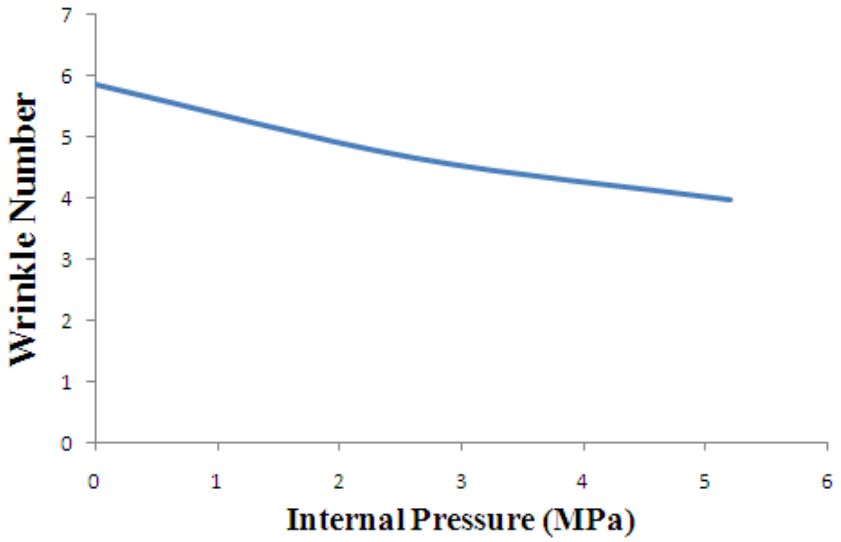

Fig.B- 7 Wrinkle number at three pressure levels

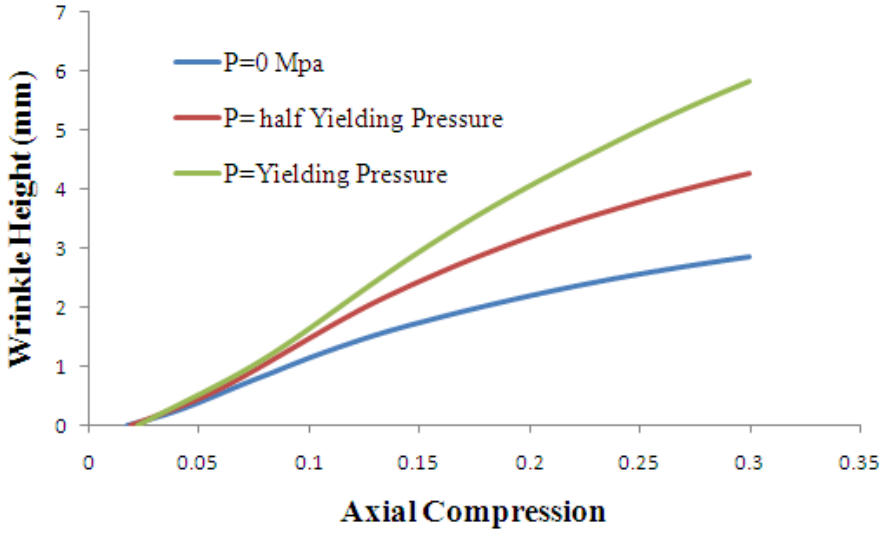

Fig.B- 8 Wrinkle height at three pressure levels

PUBLICATIONS

[1] Chen Yang and Gracious Ngaile, “Preform design for forging and extrusion processes based on geometrical resemblance” Proc. IMechE Vol. 224 Part B: J. Engineering Manufacture. P.1409-1423

[2] Chen Yang and Gracious Ngaile, Preform design for forging and extrusion processes based on geometrical resemblance, Proceedings of ASME International Manufacturing Science and Engineering Conference , Vol.1, pp.583-591, October 2009, West Lafayette, IN, USA .

[3] Chen Yang and Gracious Ngaile. Preform design in Tube Hydroforming. Accepted in Journal of Manufacturing Science and Engineering-Transactions of the ASME.

[4] Chen Yang and Gracious Ngaile. Preform design in tube hydroforming. Proceedings of the 9th International Conference on Technology of Plasticity, September 2011, Aachen, Germany.